

## High-silica Zeolites as Novel Adsorbents for the Removal of Organic Micro-pollutants in Water Treatment

Jiang, Nan

**DOI**

[10.4233/uuid:d4e7d2a8-aed1-48c8-98c3-eb61f18dde0b](https://doi.org/10.4233/uuid:d4e7d2a8-aed1-48c8-98c3-eb61f18dde0b)

**Publication date**

2019

**Document Version**

Final published version

**Citation (APA)**

Jiang, N. (2019). *High-silica Zeolites as Novel Adsorbents for the Removal of Organic Micro-pollutants in Water Treatment*. [Dissertation (TU Delft), Delft University of Technology].  
<https://doi.org/10.4233/uuid:d4e7d2a8-aed1-48c8-98c3-eb61f18dde0b>

**Important note**

To cite this publication, please use the final published version (if applicable).  
Please check the document version above.

**Copyright**

Other than for strictly personal use, it is not permitted to download, forward or distribute the text or part of it, without the consent of the author(s) and/or copyright holder(s), unless the work is under an open content license such as Creative Commons.

**Takedown policy**

Please contact us and provide details if you believe this document breaches copyrights.  
We will remove access to the work immediately and investigate your claim.

**High-silica Zeolites as Novel Adsorbents for the  
Removal of Organic Micro-pollutants  
in Water Treatment**



# **High-silica Zeolites as Novel Adsorbents for the Removal of Organic Micro-pollutants in Water Treatment**

**Dissertation**

For the purpose of obtaining the degree of doctor  
at Delft University of Technology  
by the authority of the Rector Magnificus Prof.dr.ir. T.H.J. van der Hagen  
chair of the Board for Doctorates  
to be defended publicly on

**Tuesday 10 December 2019 at 10:00 o'clock**

by

**Nan JIANG**

Master of Science in Municipal Engineering,  
Harbin Institute of Technology,

Born in Suihua, China

This dissertation has been approved by the promotor.

Composition of the doctoral committee:

Rector Magnificus,	Chairperson
Prof.dr.ir. L.C. Rietveld	Delft University of Technology, promotor
Dr.ir. S.G.J. Heijman	Delft University of Technology, promotor

Independent members:

Prof.dr.ir. J.P. van der Hoek	Delft University of Technology
Prof.dr.-ing. Habil. T. Wintgens	RWTH Aachen, Germany
Prof.dr. M. Yang	Chinese Academy of Science, China
Dr.ir. D. de Ridder	Evides
Dr. R. Shang	Veolia Biothane
Prof.dr.ir. T.J. Heimovaara	Delft University of Technology, reserve member

This research study was financed by the Surcharge for Top Consortia for Knowledge and Innovation (TKIs) of the Ministry of Economic Affairs. Nan Jiang acknowledges the China Scholarship Council and Lamminga Fund for providing her scholarship.

Printed by: Gildeprint - the Netherlands

ISBN: 978-94-6323-961-5

Copyright © 2019 by Nan Jiang

Email: [hitjiangnan@gmail.com](mailto:hitjiangnan@gmail.com)

All rights reserved. No part of the material protected by this copyright may be reproduced or utilized in any form or by any means, electronic or mechanical, including photocopying, recording, or by any information storage and retrieval system, without the written permission from the copyright owner.

# Contents

<b>Chapter 1</b>	Introduction	<b>1</b>
<b>Chapter 2</b>	High-silica zeolites for adsorption of organic micro-pollutants in water treatment: A review	<b>7</b>
<b>Chapter 3</b>	Adsorption of triclosan, trichlorophenol and phenol by high-silica zeolites: Adsorption efficiencies and mechanisms	<b>43</b>
<b>Chapter 4</b>	The adsorption mechanisms of organic micropollutants on high-silica zeolites causing S-shaped adsorption isotherms	<b>69</b>
<b>Chapter 5</b>	Adsorption of pharmaceuticals on high-silica zeolites affected by natural organic matters	<b>93</b>
<b>Chapter 6</b>	Conclusions and outlook	<b>119</b>
	Summary	<b>127</b>
	Bibliography	<b>131</b>
	Acknowledgement 致谢	<b>151</b>
	Curriculum vitae	<b>155</b>



# **CHAPTER 1**

## **INTRODUCTION**



## 1 The occurrence of organic micro-pollutants

Various pharmaceutically active compounds, pesticides and personal care products, known as organic micro-pollutants (OMPs), are present in drinking water sources and in wastewater treatment plant (WWTP) effluent. Drinking water of impaired quality, contaminated with a high level of OMPs, significantly threatens public health (Kolpin et al., 2002; Pal et al., 2010; Stackelberg et al., 2004). Therefore, the level of OMPs in drinking water is strictly regulated in most countries (Australian Government National Health and Medical Research Council 2011; United States Environmental Protection Agency 2009; World Health Organization 2011). On the other hand, current WWTPs are not designed for OMP removal, giving rise to environmental pollution by OMPs that are discharged to the receiving water body. In response, in some countries, stricter regulations on OMP discharge with the WWTP effluent have been set (Swiss Federal Council 1998).

A range of physical and chemical treatment technologies are found to be effective in reducing the level of OMPs in water, such as membrane filtration, adsorption and (advanced) oxidation (Bal and Dhagat 2001; Klavarioti et al., 2009; Siegrist and Joss 2012). Nanofiltration (NF) and reverse osmosis (RO) membranes reject a large range of OMPs, although the removal of OMPs seems to be incomplete and traces may still be detected in the permeate of NF and RO installations (Verliefde et al., 2007). A drawback of using NF/RO is its high costs and the generation of a waste stream that still contains OMPs. As an alternative, advanced oxidation can efficiently eliminate OMPs in an aqueous environment by inherently changing their structure (Esplugas et al., 2007; Wols and Hofman-Caris 2012). However, the risk of toxic by-product formation arises due to incomplete degradation of OMPs and reactions with other compounds, such as bromide and humic acids in the water (von Gunten 2003b). In contrast, advanced water treatment with activated carbon typically decreases toxic effects (Guzzella et al., 2002; Magdeburg et al., 2014), since compounds are adsorbed onto the material and thus removed from water.

## 2 Adsorption in drinking water treatment

### 2.1 Adsorption principles

Adsorption is a phase transfer process that is widely used to remove (organic) substances from fluid phases (Ali and Gupta 2006; Worch 2012). In water treatment, adsorption is defined as the process where solutes, dissolved in water (adsorbates), are removed onto solid surfaces (adsorbents). Adsorption is a dynamic process, where solute adsorption can happen simultaneously with desorption (Figure 1). When the rate of adsorption is equal to the rate of desorption, the system reaches equilibrium. For specific adsorbent and solute, the equilibrium at constant temperature is determined by:

- Solute concentration in water. In water with single solute, the solute loading on adsorbents increases with the increase of solute concentration.
- Competing solutes. When competing solutes are present in water, they can replace the adsorbed solute. The loading of adsorbed solutes on adsorbents will thus decrease (Ruthven 1984).

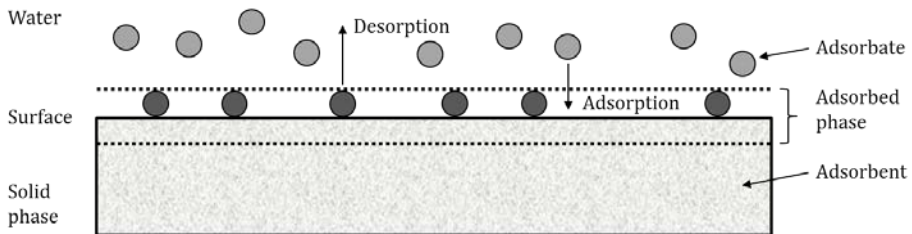


**Figure 1** The adsorption equilibrium in water.

### 2.2 Applications of activated carbon in water treatment

In drinking water treatment, activated carbon is the most widely used adsorbent to remove undesirable odour, taste, colour, and OMPs. Currently, activated carbon adsorption is applied in all Dutch drinking water treatment plants with surface water sources.

Activated carbon can adsorb a broad spectrum of OMPs in water, due to the well-developed pores and high-degree of surface reactivity (Delgado et al., 2012; Mailler et al., 2015). Activated carbon contains pores with a large range of sizes: Micropores, mesopores

and macropores with diameters of  $< 2$  nm,  $2 - 50$  nm and  $> 50$  nm, respectively. OMPs are mainly adsorbed in the micropores, while mesopores and macropores act as the diffusion routes for OMPs (Ebie et al., 2001). The functional groups and the charges on the carbon surface will affect the affinity of OMPs for activated carbon (Karanfil and Kilduff 1999; Li et al., 2002; Newcombe et al., 1993).

Used activated carbon with toxic residues need to be decomposed or disposed. Saturated activated carbon in granular form can be regenerated off-site by heating. Adsorbed OMPs will decompose and desorb from carbon during regeneration at a temperature of up to  $1000^{\circ}\text{C}$  (Tipnis and Harriott 1986). Normally, thermal regeneration cause 4 - 10% carbon loss (Hutchins 1973). Powdered activated carbon is also dosed in water to remove OMPs. However, powdered activated carbon cannot be regenerated, leaving undesired toxic residues, which need further treatment before re-entering the environment.

OMP adsorption onto activated carbon can be hampered by the competition with natural organic matter (NOM) in water (Pelekani and Snoeyink 1999; Zietzschmann et al., 2014b). Due to a large variation in pore sizes in the activated carbon, NOM is able to compete with the OMPs which increases the regeneration frequency for activated carbon (Hepplewhite et al., 2004; Newcombe et al., 2002). Besides competition, the relatively large NOM molecules are also known to block pores in the activated carbon. Pore access is thus restricted for solutes and the effective adsorption surface is reduced (Hung et al., 2005; Li et al., 2003a). To avoid their costly regeneration/replacement and the negative effect of NOM on OMP adsorption, a sound alternative for activated carbon is urgently needed.

### 3 High-silica zeolites

Zeolites are highly structured porous minerals with pore diameters that are too small for NOM molecules to enter (Auerbach et al., 2003; Baerlocher et al., 2007), thus avoiding the negative influence of NOM that is observed for activated carbon (Hung et al., 2005). Besides, high-silica zeolites have hydrophobic surfaces (Lobo 1997), which could prevent water competition with OMP adsorption from water. Higher adsorption efficiencies of zeolites as compared to activated carbon have been reported for, e.g. methyl tertiary-butyl ether (MTBE) (Abu-Lail et al., 2010; Gonzalez-Olmos et al., 2013; Li et al., 2003b; Rossner and Knappe 2008) and various nitrosamines (de Ridder et al., 2012). Moreover, zeolites

are stable in oxidative conditions, which potentially guarantees the quality and quantity during oxidative regeneration processes (Liu et al., 2014a; Zhang et al., 2014), being a potential for regeneration and operated on-site in the water treatment plant. High-silica zeolites are thus expected to be potential alternative adsorbents for activated carbon in drinking water treatment.

Compared to the studies on activated carbon, only a few studies have been conducted on high-silica zeolites for OMP removal from water. Numerous OMPs with a variety of properties are present in drinking water sources (Luo et al., 2014; Schwarzenbach et al., 2006), while zeolite research has mainly focused on specifically adsorbing OMPs (Anderson 2000; Damjanovic et al., 2010; de Ridder et al., 2012; Rakic et al., 2010; Rossner et al., 2009). There is limited insight in the adsorption mechanisms where zeolites need to adsorb a broad range of OMPs. In addition, more studies are needed for adsorption mechanisms of multi OMPs on specific high-silica zeolites in the presence of NOM.

## **4 Thesis research framework**

Therefore, the objective of this research is to obtain further knowledge on the adsorption mechanisms of high-silica zeolites for a broad spectrum of OMPs, in order to establish an alternative adsorption technology in the current drinking water treatment by the application of high-silica zeolites.

To meet the objective stated above, the following research questions were proposed. The individual research questions were addressed in the chapters of the thesis as listed below:

**Research question 1: What is the current understanding of OMP adsorption on high-silica zeolites?**

**Chapter 2** reflects a literature study focusing on the available knowledge on the adsorption of OMPs on high-silica zeolites. The physiochemical properties of high-silica zeolites relating to OMP adsorption were introduced. By reviewing the present publications, the already-known OMP adsorption mechanisms on high-silica zeolites was summarized. From there, the feasibility of high-silica zeolites for water treatment was identified, based on the existing knowledge.

**Research question 2: What are the OMP adsorption mechanisms on high-silica zeolites?**

**Chapter 3** describes the adsorption efficacies and mechanisms of OMPs with a variety of properties on different high-silica zeolites in the batch experiments. The OMP adsorption efficacies were related to the characteristics of OMPs, e.g. molecular sizes and water affinities, as well as the properties of high-silica zeolites, e.g. porous structures and surface properties. On this basis, the dominant adsorption mechanisms were concluded. The featured adsorption mechanisms of high-silica zeolites were highlighted by comparing high-silica zeolites from this study with other commonly used adsorbents, e.g. activated carbon and clays described in literature.

In **Chapter 4**, a Monte Carlo (MC) simulation is represented to better understand the adsorption mechanisms of OMPs on high-silica zeolites. The main focus was on the occurrence of S-shaped adsorption isotherms, which were firstly observed during OMP adsorption on high-silica zeolites. MC simulation, providing the necessary atomistic resolution, could support the experiments in order to promote a deeper understanding of the governing adsorption mechanisms of OMPs on high-silica zeolites.

**Research question 3: How does NOM affect OMP adsorption on high-silica zeolites?**

In **Chapter 5**, the effect of NOM on OMP adsorption on high-silica zeolites is described. The OMP adsorption efficiencies in water without and in the presence of NOM were compared for high-silica zeolites with different porous structures. The effect of OMP characteristics, e.g. hydrophobicity/hydrophilicity, charge and molecular sizes, on the adsorption efficacies of OMPs in the presence of NOM were studied. The mechanisms of NOM affecting OMP adsorption on high-silica zeolites were discussed in this chapter.

The general conclusions and outlook are given in **Chapter 6**.

## **CHAPTER 2**

# **HIGH-SILICA ZEOLITES FOR ADSORPTION OF ORGANIC MICRO-POLLUTANTS IN WATER TREATMENT: A REVIEW**

This chapter is based on: Jiang, N., Shang, R., Heijman, S.G., & Rietveld, L.C. (2018). High-silica zeolites for adsorption of organic micro-pollutants in water treatment: A review. *Water research*, 144, 145-161.

## Abstract

High-silica zeolites have been found to be effective adsorbents for the removal of organic micro-pollutants (OMPs) from impaired water, including various pharmaceuticals, personal care products, industrial chemicals, etc. In this review, the properties and fundamentals of high-silica zeolites are summarised. Recent research on mechanisms and efficiencies of OMP adsorption by high-silica zeolites are reviewed to assess the potential opportunities and challenges for the application of high-silica zeolites for OMP adsorption in water treatment. It is concluded that the adsorption capacities are well-related to surface hydrophobicity/hydrophilicity and structural features, e.g. micropore volume and pore size of high-silica zeolites, as well as the properties of OMPs. By using high-silica zeolites, the undesired competitive adsorption of background organic matter (NOM) in natural water could potentially be prevented. In addition, oxidative regeneration could be applied on-site to restore the adsorption capacity of zeolites for OMPs and prevent the toxic residues from re-entering the environment.

## 1. Introduction

Organic micro-pollutants (OMPs) have become a worldwide issue of increasing environmental concern (Petrie et al., 2015; Schwarzenbach et al., 2006). In the aquatic environment including drinking water sources and water bodies, OMPs are widely present at trace concentrations ranging from several ng L<sup>-1</sup> to a few µg L<sup>-1</sup> (Gracia-Lor et al., 2011; Hughes et al., 2013; Joss et al., 2008). The discharge of OMPs can be attributed to the diffuse sources of pesticides used in agriculture, industrial wastewater effluent, municipal wastewater effluent, etc (Eggen et al., 2014; Gerecke et al., 2002; Lefebvre and Moletta 2006; Michael et al., 2013). The occurrence of OMPs does not only raise toxicological concerns in the aquatic environment (Alan et al., 2008; Santos et al., 2010), but also threatens public health if present in drinking water (Kolpin et al., 2002; Pal et al., 2010; Reemtsma et al., 2016; Stackelberg et al., 2004).

Adsorption of OMPs by porous materials, typically activated carbon, is known as one of the most effective processes for OMP removal and is thus widely deployed (Ahmaruzzaman 2010; Alsbaiee et al., 2016; Stackelberg et al., 2007). Activated carbon adsorbs a broad spectrum of OMPs (Delgado et al., 2012; Karanfil and Kilduff 1999; Rossner et al., 2009;

Snyder et al., 2007) due to the well-developed pore structure, large surface area and high degree of surface reactivity (Dias et al., 2007; Marsh et al., 1997; Moreno-Castilla 2004). However, used adsorbents, with their resultant toxic residues, need to be either decomposed or disposed (Omorogie et al., 2016). To restore the adsorption capacity of used activated carbon and prevent the toxic residues from re-entering the environment, thermal regeneration of activated carbon has been a common practice. During the thermal regeneration process, OMPs that are adsorbed by activated carbon are eliminated by vaporization, pyrolysis and gasification (Sabio et al., 2004; Suzuki et al., 1978; Van Vliet 1991). Nevertheless, the regeneration processes considerably influence the pore structure and chemical functional groups in the activated carbon, which then deteriorates their OMP adsorption performance (Cooney et al., 1983; Martin and Ng 1984). Thermal regeneration of activated carbon could also cause carbon loss of up to 10% in mass (Hutchins 1973; Tipnis and Harriott 1986). New activated carbon has to be purchased and added into the process. Moreover, the OMP adsorption efficiency of activated carbon might be lowered by the co-existence of natural organic matter (NOM) with OMPs, which will reduce the operational period between activated carbon regeneration events (Narbaitz and Cen 1997; Pelekani and Snoeyink 1999; Schork and Fair 1988; Zietzschmann et al., 2014b).

As a feasible alternative, zeolites are crystalline aluminosilicates with orderly distributed and uniformly sized micropores (with a pore diameter less than 2nm) (Li and Yu 2014). Owing to the featured porous properties and chemical composition (Table 1), zeolites can act as molecular sieves and catalysts which are used in the fields of air-pollution remediation, removal of volatile organic compounds, gas separation and catalytic conversion of biomass, etc (Alonso et al., 2017; Ennaert et al., 2016; Li et al., 2017; Perego et al., 2017; Shi et al., 2017; Sun and Wang 2014; Zhang et al., 2016). Based on the unique structural characteristics, framework types of zeolites are defined (refer to Section 2). To date, 235 zeolite frameworks have been assigned at the Structure Commission of the International Zeolite Association (IZA-SC) (Baerlocher and McCusker 2017).

The properties of zeolites vary by the proportion of silica and aluminium content, namely the silica to aluminium ratio (Si/Al ratio). Low-silica zeolites with a Si/Al ratio less than 2 have excellent ion exchange capacity. In the field of water treatment, low-silica zeolites can therefore be applied for softening (Wajima 2012) (Table 1), removal of ammonium (Burgess et al., 2004; Farkas et al., 2005; Kwakye-Awuah et al., 2014), and removal of



heavy metals e.g. zinc (Cerjan Stefanović et al., 2007; Katsou et al., 2010a; Purna Chandra Rao et al., 2006), nickel (Álvarez-Ayuso et al., 2003; Çoruh and Ergun 2009; Katsou et al., 2010b), copper (Ursini et al., 2006) and cadmium (Terbouche et al., 2011).

**Table 1.** Basic physicochemical properties and the featured application for water treatment of zeolite and activated carbon.

	Zeolite	Activated carbon
<b>Porous structure</b>	Uniformed micropores <sup>a</sup>	Micropores (< 2 nm), mesopores (2 – 50 nm) and macropores (> 50nm) <sup>d</sup>
<b>Chemical composition</b>	Si, Al, O and cations <sup>a</sup>	C, H, N, S and O <sup>d</sup>
<b>Surface area</b>	300 – 2300 m <sup>2</sup> g <sup>-1</sup> <sup>b</sup>	800 – 1500 m <sup>2</sup> g <sup>-1</sup> <sup>d</sup>
<b>Featured application for water treatment</b>	Water hardness control ingredients in detergents <sup>c</sup>	Adsorbents for removal of colour, odour, taste and other undesirable organics in the industrial and municipal treatment plants <sup>d</sup>

<sup>a</sup> (McCusker and Baerlocher 2001)

<sup>b</sup> Computational Characteristic molecule diameter of 0.6 nm. (First et al., 2011)

<sup>c</sup> (Maesen and Marcus 2001)

<sup>d</sup> (Bansal and Goyal 2005)

High-silica zeolites (Figure 1) with Si/Al ratios up to several thousands are industrially manufactured by replacing the aluminium contents with silica (Burton 2018; Burton et al., 2005). The hydrophobicity of these zeolites provides favourable characteristics for OMP adsorption in aqueous solutions (Maesen 2007; Tsitsishvili 1973). Currently, high-silica zeolite powders have been proven to be effective adsorbents for the removal of OMPs from water, including pharmaceuticals, personal care products and industrial chemicals, based on information provided only by batch tests (Damjanovic et al., 2010; Rakic et al., 2010; Rossner et al., 2009). However, the application of high-silica zeolite granules in full-scale water treatment has not been realized yet.

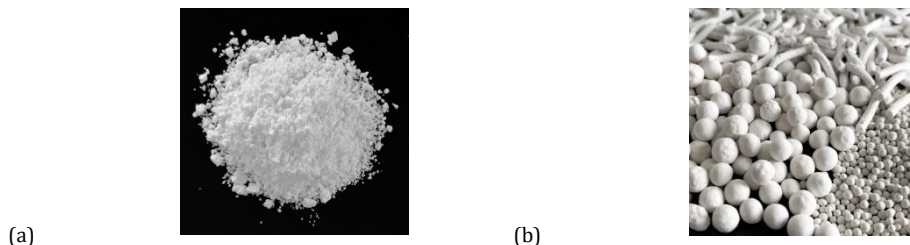


**Figure 1.** Commercial high-silica zeolite (a) powders; (b) granules with cylindrical and spherical shapes.

As a type of aluminosilicate crystal, zeolites are stable in oxidative conditions, which potentially guarantees the regeneration of zeolites by (advanced) oxidation without compromising their surface properties and pore structure (Liu et al., 2014a; Zhang et al., 2014). Combining zeolite adsorption and oxidation regeneration can restore the adsorption capacity of zeolites in situ and degrade or mineralize OMPs (Zhang et al., 2014). Concentrated toxic residues from the adsorption process will be thus minimized by oxidation. Therefore, effective oxidative regeneration of zeolites without impairing the quality and quantity of adsorbents could be a key advantage over activated carbon as a benchmark technology.

In this review, the literature on high-silica zeolites for OMP adsorption from water is reviewed, including the fundamentals of the zeolite frameworks, the physicochemical properties and their relation to OMP adsorption. The adsorption mechanisms of high-silica zeolite powders are elaborated by considering the properties of zeolites and variety of OMPs. Examples of the application of high-silica zeolite granules are presented. Finally, the potential opportunities and challenges of applying high-silica zeolites to water treatment are discussed.

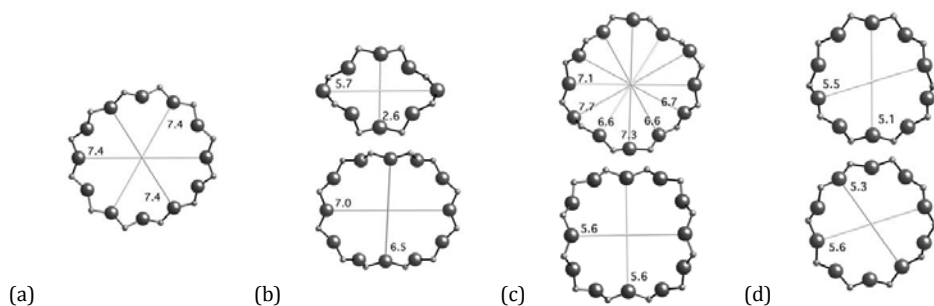
## 2. Physicochemical properties of high-silica zeolites

Zeolites have a 3-dimensional structure constructed by  $\text{TO}_4$  tetrahedra, where the T atom is either a  $\text{Si}^{4+}$  or  $\text{Al}^{3+}$  atom located in the centre of an oxygen tetrahedron. Since each  $\text{Al}^{3+}$  atom introduces one negative charge, the same number of cations can associate loosely with the tetrahedral-coordinated  $\text{Al}^{3+}$  to neutralize the entire framework. The ratio of  $\text{Si}^{4+}$

and  $\text{Al}^{3+}$  in the framework, known as the silica-to-alumina ratio, is commonly written as either  $\text{SiO}_2/\text{Al}_2\text{O}_3$  mole ratio or Si/Al mole ratio by different authors. In this review, the Si/Al ratio is used to describe the hydrophobicity of zeolite surface, which is two times of the  $\text{SiO}_2/\text{Al}_2\text{O}_3$  mole ratio (McCusker and Baerlocher 2001).

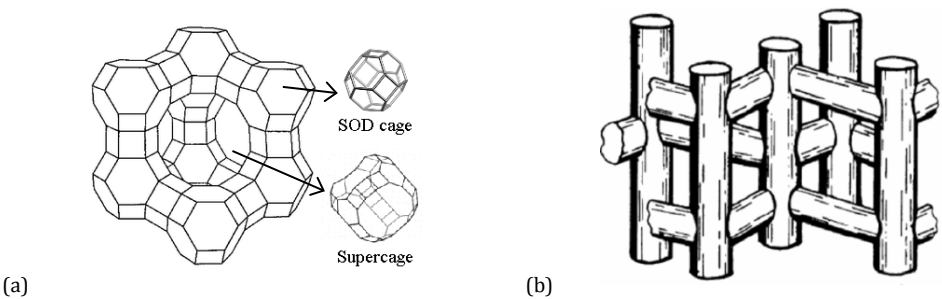
The framework of zeolites describes the connectivity of the tetrahedrally coordinated atoms (T-atoms) without reference to elemental composition. The framework type exclusively defines the structural properties of zeolites including pore opening, cage and channel structure (McCusker and Baerlocher 2001).

- The pore opening of zeolites, composed by T atoms and the connected oxygen atoms, is the entry of a cage or a channel which will decide the entering of OMPs. The pores with more T atoms/oxygen atoms have larger sizes. The pore opening could be described as an  $n$ -ring, e.g. 8-, 10-, and 12-rings, where  $n$  represents the number of T or oxygen atoms.



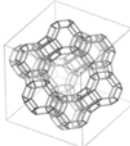
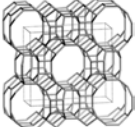
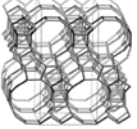
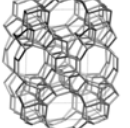
**Figure 2.** Examples of pore opening of zeolites (Baerlocher et al., 2007). (a) 12-ring opening in FAU zeolites, (b) 8-ring & 12-ring opening in MOR zeolites, (c) 12-ring opening in BEA zeolites, (d) 10-ring opening in MFI zeolites (framework type codes of the zeolites, referring to Table 2).

- The pore space of zeolites is parcelled into cages and/or channels. Cages, also called cavities, are the polyhedral units in zeolites, while channels in zeolites are composed by linked polyhedral units. The channels of zeolites vary from straight to sinusoidal forms or from wide to narrow. Many adsorption-related properties of zeolites, e.g. surface area and pore volume, are decided by the features of the cages and channels.



**Figure 3.** Examples of cages and channels of zeolites (a) Schematic representation showing cages in FAU type zeolites (Baerlocher et al., 2007), (b) 'hollow-tube' representation showing channels in MFI zeolites (Rhodes 2010) (FAU and MFI are framework type codes of the zeolites, referring to Table 2)

**Table 2.** Key properties of four commonly used frameworks of zeolites.

Framework		Ring number and pore opening size <sup>a</sup>		Framework density <sup>a</sup>	Accessible Area (m <sup>2</sup> g <sup>-1</sup> ) <sup>b</sup>	Maximum diameter of a sphere <sup>b</sup>	
Type	Structure <sup>a</sup>	Å×Å	Å×Å	T atoms (Å <sup>3</sup> ) <sup>-1</sup>		can be included (Å)	can diffuse along (Å×Å×Å)
FAU		12 ring 7.4×7.4		12.7	1211.42	11.24	7.35*7.35*7.35
MOR		12 ring 6.5×7.4	8 ring 2.6×5.7	17.2	1010.22	6.70	1.57*2.95*6.45
BEA		12 ring 6.6×6.7	12 ring 5.6×5.6	15.1	1220.45	6.68	5.95*5.95*5.95
MFI		10 ring 5.1×5.5	10 ring 5.3×5.6	17.9	834.41	6.36	4.70*4.46*4.46

<sup>a</sup> (Baerlocher et al., 2007)

<sup>b</sup> The accessible area is the area of that surface visited by the centre of the water molecule in the idealised framework model. Accessible area and maximum diameter of a sphere were calculated by Mike Treacy, Arizona State University, using his codes "TOTOPOL" and "DelaneyDonkey." (Foster et al., 2006).

The structural features of high-silica zeolites are mostly determined by their framework types. A framework type represents a unique structure of channels and cages that will highly affect the adsorption efficiency of OMPs. FAU, MOR, MFI and BEA types of high-silica zeolites were selected for review, because they are the most commercially available and have been commonly studied for OMP adsorption. Their structural features are summarized in Table 2.

All selected framework types contain a high accessible area (from 834 to 1220 m<sup>2</sup> g<sup>-1</sup> in Table 2) for the adsorption of both water and organic compounds. The framework density is related to the pore volume such that zeolites with a lower framework density have a higher pore volume (Meier and Baerlocher 1999). The pore volume of zeolites would follow the opposite order of framework density, namely FAU > BEA > MOR > MFI (Table 2). The effect of pore volume on OMP adsorption will be discussed in section 3.1.

The properties of high-silica zeolites with the same framework type and Si/Al ratio vary. Theoretically, ideally crystalized zeolites with the same framework type and Si/Al ratio show identical properties. However, high-silica zeolites are synthesised from low-silica zeolites by dealuminating, which would bring defects to the framework (Yu et al., 2007). Therefore, the micropore volume of high-silica zeolites with the same framework types could vary (Yonli et al., 2012). Their actual surface area is usually less than what would be found in the ideal framework (Dubinin 1967). In addition, mesopores in zeolites, generated during the dealumination process, account for a small portion of the entire surface area of zeolites, mainly as external surface area (Yonli et al., 2012). As a result, the adsorption efficiency of the “same type” high-silica zeolites is similar but to some extent different due to the variation in properties.

### 3. Adsorption mechanisms and factors affecting the adsorption of OMPs by high-silica zeolite powders

In aqueous solutions, the overall adsorption efficiency of OMPs by high-silica zeolite powders is represented in Equation 2-1 (Israelachvili 2015):

$$W_{ozw} = W_{oz} + W_{ww} - W_{ow} - W_{zw} \quad \text{Equation 1}$$

where  $W_{ij}$  is the work to separate two phases,  $i$  and  $j$ , and the subscripts  $z$ ,  $o$  and  $w$  refer to zeolite, OMP and water, respectively.  $W_{ozw}$  is the work of adhesion of the OMP to zeolites in water, e.g. the adsorption energy of the OMP by the zeolite in aqueous solution, which will decide the adsorption efficiency. Water cohesion ( $W_{ww}$ ) describes the interaction between water molecules. In the discussion, water cohesion is regarded as a constant parameter with negligible effect on adsorption efficiency. The OMP adsorption efficiency by high-silica zeolites will depend on the OMP-zeolite interaction ( $W_{oz}$ ), zeolite-water interactions, ( $W_{zw}$ ) and OMP-water interactions ( $W_{ow}$ ), which will include the effect of structural features, surface hydrophobicity and existing adsorption sites of high-silica zeolites as well as characteristics of OMPs.

### 3.1 Structural features and framework types of high-silica zeolites

The adsorption of OMPs primarily takes place in the micropores of the high-silica zeolites. In many studies, the adsorption saturations were observed and the isotherms were fitted by the Langmuir model (Table 4), which indicate the occurrence of monolayer adsorption in micropores (Sing 1985). In some cases, mesopores could still provide additional accommodation for OMPs (Martucci et al., 2012). For example, when adsorption takes place in the presence of high concentrations of organic solutions ( $\text{g L}^{-1}$ ), a strong adsorption driving force at the high equilibrium concentration may lead to pore filling in the mesopores, which will increase the adsorption capacity. During the pore filling process, both adsorption and absorption may occur (Damjanovic et al., 2010).

The adsorption capacity of zeolites can thus be well-correlated to their microporous volume. Several studies found that FAU and BEA zeolites with larger micropore volumes showed a higher adsorption capacity for OMPs (Koubaisy et al., 2012; Reungoat et al., 2007; Yonli et al., 2012). As an example, FAU zeolite was found to have a higher adsorption capacity for nitrobenzene than BEA, MFI and MOR type zeolites (Reungoat et al., 2007). Compared to MFI type zeolites, BEA also has a higher adsorption capacity for phenol, dichlorophenol and nitrobenzene since the BEA type framework possesses a higher micropore volume (Damjanovic et al., 2010; Koubaisy et al., 2008; Reungoat et al., 2007).

The pore opening size of zeolites determines the diffusivity and accessibility of the OMPs during the adsorption process. OMPs with a molecular size smaller than the pore opening size of zeolites can easily diffuse inside zeolite powders due to negligible steric hindrance

(Roque-Malherbe et al., 1995; Rungsirisakun et al., 2006). Certain OMP molecules, e.g. carbamazepine, may form molecular chains of enlarged size due to the molecular interactions. The molecular chain of carbamazepine could enter the FAU zeolite, which has a large pore opening size, but could not enter the MOR and MFI zeolites, which have narrow channel openings (Martucci et al., 2012). The adsorption of OMPs is minimal when the size of OMPs are larger than the pore opening size of zeolites. Zeolites would then behave as molecular sieves, resulting in the exclusion of OMPs from the framework of zeolites (Rouquerol et al., 2013).

Multiple studies showed that OMPs with environmentally relevant concentrations, ranging from  $\text{ng L}^{-1}$  to  $\mu\text{g L}^{-1}$ , were preferably adsorbed by high-silica zeolites with pore sizes closely similar to the molecular size of OMPs, so-called close-fit theory (de Ridder et al., 2012; Rossner et al., 2009). A common explanation is that the closely fitted pores may lead to strong interactions between OMPs and high-silica zeolites (de Ridder et al., 2012; Erdem-Senatalar et al., 2004; Rossner et al., 2009). Giaya and Thompson (2002a; 2002b) also suggested that the structure of water clusters might be disrupted in the well-fitted pores, which would promote the affinities for OMPs. For example, all seven tested N-nitrosamine compounds (MW: 74 – 158  $\text{g mol}^{-1}$ , estimated stokes diameter 2.6 - 4.0 Å) with an initial concentration of 15  $\mu\text{g L}^{-1}$  could not be removed by FAU zeolites, while MOR and MFI with small pore sizes (see Table 2) removed five N-nitrosamines from the seven tested compounds. MOR and MFI zeolites, possessing comparable pore opening and channel sizes as N-nitrosamine compounds, were thus suitable for their removal at these low concentration ranges (de Ridder et al., 2012). In another study, Rossner et al. (2009) compared the removal of 25 emerging OMPs (MW: 151 - 791  $\text{g mol}^{-1}$ , estimated spherical diameter: 6.5 – 9.5 Å) from lake water with initial concentrations less than 1  $\mu\text{g L}^{-1}$  by MFI, MOR and FAU zeolites. A total of 15 OMPs were either partially or completely removed by MOR zeolites, while FAU could only remove 3 OMPs to an acceptable level. Two types of zeolites with relatively small pore openings, MFI zeolites with 10-ring pores and MOR zeolites with 12- & 8-ring pores, were proven to be effective for the adsorption of these low molecular weight OMPs at low concentrations. It was found that the molecular size of these OMPs was similar to the pore opening size or channel size of MFI and MOR zeolites.

### 3.2 Surface hydrophobicity and Si/Al ratio of high-silica zeolites

Surface hydrophobicity is defined as the absence of 'strong sorption' of polar compounds, particularly water (Olson et al., 2000). Highly hydrophobic zeolites could prevent water uptake (Damjanovic et al., 2010; de Ridder et al., 2012). Thus, the pore blockage by water clusters could be inhibited, resulting in more pores of zeolites available for OMP diffusion and adsorption (de Ridder et al., 2012; Guvenc and Ahunbay 2012).

The chemical composition of zeolites strongly influences the hydrophobicity and zeolite-water interaction. Bolis et al., (2006) proposed that water molecules can interact with Al sites of zeolite framework. In addition, the hydrophobicity can be influenced by a small number of Si-OH species, which are located at the defects in the zeolites, since Si-OH species could adsorb water by forming stable adducts.

For zeolites with the same framework type, the hydrophobicity increases with decreasing aluminium content, thus zeolites with higher Si/Al ratios are more hydrophobic (Chen 1976; Eberly Jr et al., 1971; Nakamoto and Takahashi 1982; Olson et al., 1980). It can be concluded that zeolites with higher Si/Al ratios (examples found in Table 3) exhibit a higher adsorption capacity than the zeolites of the same framework with a low Si/Al ratio (Anderson 2000; Damjanovic et al., 2010; Grieco and Ramarao 2013; Li et al., 2003b; Reungoat et al., 2007; Yonli et al., 2012). In the case of  $\alpha$ -endosulfan and tris-2-chloroethyl phosphate adsorption, the zeolites with a higher Si/Al ratio, regardless of their slightly lower surface area, have a higher adsorption capacity for OMPs (Table 3). The adsorption of nicotine using zeolites, however, is an exception. Rakic et al., (2010) reported a higher adsorption capacity of nicotine on BEA zeolite with a lower Si/Al ratio. The results were driven by specific adsorption site interactions, which will be further explored in section 3.4.

When the Si/Al ratio is high enough, the hydrophobicity of zeolites is no longer of significant importance because the effect of water competition and water cluster hindering has become negligible. Gonzalez-Olmos et al., (2013) found that by increasing the Si/Al ratio from 800 to 1366, MFI zeolites did not improve their adsorption capacity of MTBE, and even a slight decrease was observed when the surface area of zeolites increased from 265 to 330 m<sup>2</sup> g<sup>-1</sup>. In addition, the adsorption capacities for 4-chlorophenol increased by 28% when the Si/Al ratio increased from 504 to 2252, but there was little effect after further increase in the Si/Al ratio (Shu et al., 1997). For nitrobenzene, the adsorption capacity of



BEA and MFI zeolites were also related to its Si/Al ratio for those with a low Si/Al ratio. However, the adsorption capacity of zeolites became independent of the Si/Al ratio for ratios over 800 in this case (Reungoat et al., 2007).

**Table 3.** The maximum adsorption capacities from the Langmuir isotherm by adjustment to the properties of zeolites for the adsorption of OMPs on high-silica zeolites.

Adsorbate	Q <sub>L</sub> (mg g <sup>-1</sup> ) <sup>a</sup>	Si/Al ratio	BET surface area (m <sup>2</sup> g <sup>-1</sup> )	C <sub>0</sub> (mg L <sup>-1</sup> ) <sup>b</sup>	Framework type of zeolite	Reference
Nitrobenzene	75.6	84	531	600	BEA	(Reungoat et al., 2007)
	95.0	196	700	600	BEA	
	83.9	80	300	600	MFI	
	118.7	200	300	600	MFI	
	147.6	800	300	600	MFI	
	135.7	1800	300	600	MFI	
α-endosulfan	500.0	43	789	10-30	FAU	(Yonli et al., 2012)
	666.6	51	830	10-30	FAU	
	833.3	68	825	10-30	FAU	
	763.4	72	546	10-30	BEA	
	787.4	126	594	10-30	BEA	
	793.7	220	528	10-30	BEA	
Phenol	28.2	30	392	~2820	MFI	(Damjanovic et al., 2010)
	31.0	80	425	~2820	MFI	
	38.5	280	400	~2820	MFI	
Tris-2-chloroethyl phosphate	76.6	50	680	10	BEA	(Grieco and Ramarao 2013)
	103,0	600	620	10	BEA	
Methyl tert-butyl ether	6.5	472	385	1-100	MFI	(Gonzalez-Olmos et al., 2013)
	15.2	800	265	1-100	MFI	
	14.1	1366	330	1-100	MFI	
Nicotine	240	50	741	4.9	BEA	(Rakic et al., 2010)
	60	172	650	4.9	BEA	

<sup>a</sup> Q<sub>L</sub> is the maximum adsorption capacity of high-silica zeolites estimated from Langmuir isotherm.

<sup>b</sup> C<sub>0</sub> is the initial concentration of OMPs in the experiments.

Since the hydrophobicity of high-silica zeolites is well-related to Al content, the adsorption capacity could be strongly-correlated to the Al content (Al%) (Khalid et al., 2004), which can be expressed by:

$$\text{Al}\% = \frac{\text{Al}}{\text{Si} + \text{Al}} * 100\% = \frac{1}{1 + \text{Si}/\text{Al ratio}} * 100\% \quad \text{Equation 2}$$

For high-silica zeolites with the same framework, Al% of high-silica zeolites has a negative linear correlation with the adsorption capacity of various OMPs (Figure 4). Therefore, Al% may serve as an indicator of adsorption capacity in the high Si/Al ratio range.

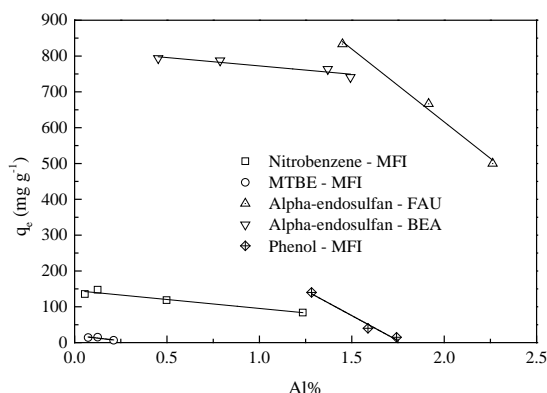


**Figure 4.** The effect of Al% for the adsorption capacity of various OMPs. Data source: nitrobenzene (Reungoat et al., 2007), MTBE (Gonzalez-Olmos et al., 2013), alpha-endosulfan (Yonli et al., 2012) and phenol (Damjanovic et al., 2010)

In place of Si/Al ratio and Al content, hydrophobicity index (HI) was applied to represent hydrophobicity of zeolites by Yonli et al., (2012). The value of HI could be determined by:

$$\text{HI} = \frac{X_{\text{toluene}}}{X_{\text{water}}} \quad \text{Equation 3}$$

where  $X_{\text{toluene}}$  represents toluene adsorption capacity ( $\text{g g}^{-1}$ ) and  $X_{\text{water}}$  represents water adsorption capacity ( $\text{g g}^{-1}$ ). For the FAU and BEA zeolites, there was a linear increase of  $\alpha$ -endosulfan adsorption efficiency with the increase of HI.

The increased adsorption efficiency of OMPs by high-silica zeolites with the same framework could thus be related to the hydrophobicity of high-silica zeolites, which, in its turn, could be predicted by Si/Al ratio, Al content and HI index. However, the hydrophobicity of zeolites with different framework types should not be compared only by reference to Si/Al ratio but also by the structural features of the zeolites. For example, MFI zeolites are more hydrophobic than FAU zeolites with the same Si/Al of 80 because the smaller confinement pore space of MFI zeolites disrupts the interactions of water molecules such that water can hardly stay inside the pores (Damjanovic et al., 2010; de Ridder et al., 2012; Giaya and Thompson 2002b). In this case, the adsorption efficiency of OMPs by high-silica zeolites is then better determined by framework type.

### 3.3 Characteristics of OMPs

The effects of surface charge and the ionization form of the OMPs on the adsorption efficiency of high-silica zeolites have been studied (Bautista-Toledo et al., 2005; Janos et al., 2003). High-silica zeolites have a limited number of cations and negative charges around Al sites, while most of the framework structures remain neutral (no ionized sites). The preferential adsorption of neutral OMP species by high-silica zeolites was observed (Fukahori et al., 2011; Grieco and Ramarao 2013; Koubaissy et al., 2012; Simon et al., 2015; Tsai et al., 2006). For example, the neutral aromatic compounds, e.g. nitroaniline and chlorophenol, were preferentially adsorbed onto FAU zeolite compared to the ionic compounds (Koubaissy et al., 2011). Fukahori et al., (2011) reported that sulfa drugs in neutral form could be more readily adsorbed onto FAU zeolites than those in cationic and anionic forms, based on the hydrophobic interactions.

When OMPs in anionic forms are dominant under alkaline conditions, a reduction of adsorption capacity has been observed (Chen et al., 2015; Koubaissy et al., 2011). Since high-silica zeolites employ a large amount of electron-rich oxygen sites and very few negative sites, repulsion forces between the anionic form of the OMPs and the zeolite surface arise (Fukahori et al., 2011; Koubaissy et al., 2011; Koubaissy et al., 2012). The removal mechanism of cationic OMPs by adsorbents has been regarded as ion exchange. As high-silica zeolites possess few exchangeable ions, the removal capacity of cationic OMPs by high-silica zeolites might be less than that of the low-silica zeolites, e.g. natural zeolites (Margeta et al., 2013). Since the ionization of OMPs is affected by the relationship between

pH value in an aqueous solution and the  $pK_a$  value of OMPs, the pH of the solution should therefore be taken into consideration in the adsorption process.

Previous studies have shown that the decreased interactions between OMP and water will enhance OMP-zeolite interaction, and a strong correlation between the adsorption capacity and hydrophobicity of OMPs has been observed (Fukahori et al., 2011; Koubaissy et al., 2011; Koubaissy et al., 2008). It was found that hydrophilic N-Nitrosodimethylamine (NDMA) and N-Nitrosomethylethylamine (NEMA) were not adsorbed by MFI nor MOR zeolites, while less hydrophilic N-nitrosamines with comparable sizes to NDMA and NEMA were adsorbed to a larger extent (de Ridder et al., 2012). Similar results were reported by Zhu et al., (2001). The interaction between neutral OMP molecules and water can be described by the octanol-water coefficient ( $K_{ow}$ ). When the effect of OMP charge is considered, the interaction could be expressed by the distribution coefficient,  $\log D$ , which is calculated from  $K_{ow}$ ,  $pK_a$  of OMPs and pH of the aqueous solution. Neglecting the interaction between OMPs and octanol, OMPs with higher  $K_{ow}$  and  $\log D$  are more hydrophobic and less soluble in water (Gschwend 2016).

### **3.4 Adsorption forces and possible adsorption sites of high-silica zeolites**

Much effort has been dedicated to determining adsorption forces and locations of adsorbed OMPs, which would give further insight into how high-silica zeolites interact with OMPs. The adsorption of OMPs by high-silica zeolites is a physical process attributed mainly to Van der Waals forces (Blasioli et al., 2014). Aside from the Van der Waals forces, acid-base forces exist between the functional groups of OMPs and the specific sites of zeolites, so-called “adsorption sites.” The heterogeneity of the adsorption sites has been indicated from the results of adsorption heats during OMP adsorption by high-silica zeolites (Damjanovic et al., 2010; Rakic et al., 2010). From simulation results of a Monte Carlo study and Rietveld’s analysis, MFI and FER zeolites were proved to employ different types of sites for OMPs adsorption (DeJaco et al., 2016).

Two typical adsorption sites of high-silica zeolites, oxygen and acidic sites, have been identified in literature. Oxygen atoms in the framework of zeolites widely exist as oxygen sites. OMPs with hydrogen on the aromatic ring and amino groups show an acidic character and have an affinity for oxygen sites (Blasioli et al., 2014; Koubaissy et al., 2011).

The results of Blasioli et al. (2014) indicate that sulfamethoxazole interacts with FAU and MOR zeolites by weak H-bonds.

A limited number of Brønsted and Lewis acidic sites in high-silica zeolites are known to interact with OMPs with nucleophilic groups, e.g. sulphur or chlorine atoms (Bolis et al., 2006; Damjanovic et al., 2010; Nikolakis 2005; Phung and Busca 2015). The specific interaction may lead to chemisorption and higher adsorption energy (Batonneau-Gener et al., 2010). Acidic sites may thus promote the adsorption of certain OMPs on high-silica zeolites. Rakic et al., (2010) reported a higher adsorption capacity of nicotine on BEA zeolite with a lower Si/Al ratio and more acidic sites. Nicotine is an organic base with basic nitrogen atoms acting as an amine (de Lucas et al., 1998). The adsorption mechanism could be explained by the neutralisation of nicotine by the acidic sites on the zeolites.

## **4. Potential applications of high-silica zeolites for water treatment**

### **4.1 Adsorption of OMPs by high-silica zeolites**

The efficiency of high-silica zeolites for OMP adsorption and their isotherm fitting constants are summarised in Table 4. Results are collected from batch-scale experiments applying high-silica zeolite powders.

In this section, we first discuss the adsorption of specific OMPs, including MTBE, nitrosamines, phenol and phenolic compounds, which were studied at high equilibrium concentrations, e.g. mg L<sup>-1</sup>. Afterwards, OMP adsorption at environmentally relevant concentrations, e.g. ng L<sup>-1</sup> and µg L<sup>-1</sup>, is discussed in the sub-sections “OMP mixtures” and “Prediction of adsorption on high-silica zeolites at environmentally relevant concentrations”. A few studies on the application of high-silica zeolite granules in column-scale experiments will be discussed at the end of this section.

#### *MTBE*

Methyl tertiary-butyl ether (MTBE) is a widely used fuel additive with a good aqueous solubility, 51,000 mg L<sup>-1</sup> at 25 °C. MTBE is frequently found in surface water and groundwater (Achten et al., 2002; Squillace et al., 1996). Various types of zeolites can adsorb MTBE from water, e.g. BEA, MFI and MOR zeolites (Knappe and Campos 2005; Li et

al., 2003b). At the equilibrium concentration of 1 mg L<sup>-1</sup>, MOR zeolites with a Si/Al ratio of 180 exhibited an adsorption capacity of 22 mg g<sup>-1</sup>, while the capacity of carbonaceous resins and activated carbon were 15.6 mg g<sup>-1</sup> and 14.0 mg g<sup>-1</sup>, respectively (Davis and Powers 2000; Erdem-Senatarlar et al., 2004; Melin 1999). BEA zeolites had a capacity of 8 mg g<sup>-1</sup>, and MTBE adsorption was negligible on the FAU at the equilibrium concentration of 1 mg L<sup>-1</sup> since the pore opening and cage size were much larger than the size of MTBE (Erdem-Senatarlar et al., 2004). High-silica zeolites with closely fitted pores for MTBE, e.g. MFI and MOR types, are more effective adsorbents for MTBE removal than BEA and FAU zeolites at the equilibrium concentration range 0.1 – 1000 µg L<sup>-1</sup> (Knappe and Campos 2005).

### *Nitrosamines*

Nitrosamines are a group of disinfection by-products with a molecular weight less than 200 g mol<sup>-1</sup>. Most of them are classified as probable human carcinogens and have been detected in both water sources and drinking water (Mitch et al., 2003; Zhao et al., 2008). At initial concentrations of 5 mg L<sup>-1</sup>, the NDMA adsorption capacity of MFI zeolites was 0.196 mg g<sup>-1</sup>, which was 4 – 7 times greater than the tested FAU and MOR zeolites (He and Cheng 2016). MFI and MOR zeolites were able to adsorb five species of N-nitrosamines, namely N-Nitrosomorpholine (NMOR), N-Nitrosopiperidine (NPIP), N-Nitrosodiethylamine (NDEA), N-Nitrosodi-n-propylamine (NDPA) and N,N-Dibutyl nitrosamine (NDBA) at an initial concentration of 15 µg L<sup>-1</sup>, while activated carbon showed a lower nitrosamine removal (de Ridder et al., 2012). Zhu et al. (2001) reported that MFI zeolites had an adsorption capacity of 9.2 mg g<sup>-1</sup> for NDMA and 16.7 mg g<sup>-1</sup> for N-nitrosopyrrolidine (NPYR) at the equilibrium concentration ~ 480 mg L<sup>-1</sup>, which was also higher than the capacity of FAU zeolites. To minimize the formation of N-nitrosamines, high silica zeolites could also be applied to remove the secondary and tertiary amines, which are nitrosamines formation precursors. More than 90% of the nitrosamines' precursors could be removed by MOR zeolites when the dosage of zeolites was 100 mg L<sup>-1</sup> in laboratory reagent water. To remove N-nitrosamine precursors, MOR zeolites were reported to be more effective than the tested activated carbon (Wu et al., 2015).

### *Phenol and phenolic compounds*

Different types of zeolites were applied for adsorption of phenol and phenolic compounds. Khalid et al. (2004) demonstrated that pure silica BEA zeolite (no Al content) employed the best performance among all tested zeolites, i.e. MOR, BEA and FAU zeolites as well as activated carbons at a phenol equilibrium concentration  $<1.6 \text{ g L}^{-1}$ . The FAU zeolites had the fastest kinetics for phenol adsorption among other studied adsorbents: activated carbon, activated alumina and silica gel (Roostaei and Tezel 2004). From the experimental results of the nitrophenolic compounds' adsorption, FAU type zeolites and pure silica BEA zeolites possessed a much higher capacity than MFI. The highest capacity for nitrophenolic compounds (ortho-nitrophenol) was  $240 \text{ mg g}^{-1}$  at an equilibrium concentration of  $50 \text{ mg L}^{-1}$ , achieved by FAU zeolites (Koubaissy et al., 2008). However, Zhang et al. (2014) studied the adsorption of 2,4,6-trichlorophenol (TCP) by FAU zeolites and found that the adsorption capacity reached  $3.06 \text{ mg g}^{-1}$  at an equilibrium concentration of  $30 \text{ mg L}^{-1}$ , much less than the capacity of granular activated carbon with a capacity of  $\sim 500 \text{ mg g}^{-1}$  (Nelson and Yang 1995).

**Table 4.** The application of high-silica zeolites for OMP adsorption, the isotherm information and experimental conditions.

Adsorbate	Framework type of zeolite (Si/Al ratio)	Isotherm type	Isotherm constants		Freundlich isotherm fitting constants*		Experimental conditions	Ref.
					$K_F$	$n$	$(\mu\text{g g}^{-1})(\text{L } \mu\text{g}^{-1})^n$	
Methyl tert-butyl ether (MTBE)	MFI(1366)	Freundlich	$K_F(\text{mg kg}^{-1})(\text{L mg}^{-1})^n$	$n$	-	61.73	0.95	1-2 g zeolites were dosed in MTBE solution with concentration 1-100mg L <sup>-1</sup> . The fitted concentration range for MFI zeolites was 0.01 – 0.79mg L <sup>-1</sup> and 0.01-32 mg L <sup>-1</sup> for BEA and FAU zeolites.
			43700	0.95				
	MFI(800)	Freundlich	$K_F(\text{mg kg}^{-1})(\text{L mg}^{-1})^n$	$n$	-	99.43	0.88	
			43400	0.88				
	MFI(472)	Freundlich	$K_F(\text{mg kg}^{-1})(\text{L mg}^{-1})^n$	$n$	-	6.97	1.07	
			11300	1.07				(1)
	BEA(400)	Freundlich	$K_F(\text{mg kg}^{-1})(\text{L mg}^{-1})^n$	$n$	-	2.79	0.98	
			2430	0.98				
	FAU(400)	Freundlich	$K_F(\text{mg kg}^{-1})(\text{L mg}^{-1})^n$	$n$	-	0.13	1.15	
			363	1.15				
	FAU(40)	Freundlich	$K_F(\text{nmol g}^{-1})(\text{L nmol}^{-1})^n$	$n$	-	0.07	0.87	
			0.0179	0.87				
	MFI(12.5)	Freundlich	$K_F(\text{nmol g}^{-1})(\text{L nmol}^{-1})^n$	$n$	-	0.12	1.03	
N-Nitrosodimethylamine (NDMA)			0.1734	1.03				(2)
	MFI(25)	Freundlich	$K_F(\text{nmol g}^{-1})(\text{L nmol}^{-1})^n$	$n$	-	0.25	0.92	
			0.1119	0.92				
	MFI(40)	Freundlich	$K_F(\text{nmol g}^{-1})(\text{L nmol}^{-1})^n$	$n$	-	0.80	0.95	
			0.4588	0.95				
	MFI(130)	Freundlich	$K_F(\text{nmol g}^{-1})(\text{L nmol}^{-1})^n$	$n$	-	1.40	0.89	
			0.4447	0.89				
	MFI(80)	Freundlich	$K_F(\mu\text{g g}^{-1})(\text{L } \mu\text{g}^{-1})^n$	$n$	-	17	1.04	
N-Nitrosomorpholine (NMOR)			17	1.04				(3)



N-Nitrosomorpholine (NMOR)	MOR(200)	Freundlich	$K_F(\mu\text{g g}^{-1})(\text{L } \mu\text{g}^{-1})^n$	n	-	2	1.70	1.70	was 15 $\mu\text{g L}^{-1}$ . The adsorbent concentration varied between 10 and 200 $\text{mg L}^{-1}$ .
N-Nitrosopiperidine (NPiP)	MFI(80)	Freundlich	$K_F(\mu\text{g g}^{-1})(\text{L } \mu\text{g}^{-1})^n$	n	-	491	1.11	1.11	
N-Nitrosopiperidine (NPIP)	MOR(200)	Freundlich	$K_F(\mu\text{g g}^{-1})(\text{L } \mu\text{g}^{-1})^n$	n	-	187	0.99	0.99	
N-Nitrosodiethylamine (NDEA)	MFI(80)	Freundlich	$K_F(\mu\text{g g}^{-1})(\text{L } \mu\text{g}^{-1})^n$	n	-	303	1.65	1.65	
N-Nitrosodiethylamine (NDEA)	MOR(200)	Freundlich	$K_F(\mu\text{g g}^{-1})(\text{L } \mu\text{g}^{-1})^n$	n	-	43	0.65	0.65	
N-Nitrosodi-n-propylamine (NDPA)	MFI(80)	Freundlich	$K_F(\mu\text{g g}^{-1})(\text{L } \mu\text{g}^{-1})^n$	n	-	$9.04 \times 10^4$	$1.20 \times 10^4$	1.20	
N-Nitrosodi-n-propylamine (NDPA)	MOR(200)	Freundlich	$K_F(\mu\text{g g}^{-1})(\text{L } \mu\text{g}^{-1})^n$	n	-	1574	0.91	0.91	
Phenol	BEA(43)	Sips	$Q_s(\text{mol g}^{-1})$	$K_s(\text{L mol}^{-1})^{\beta_s}$	$\beta_s$	0.012	1.20	1.20	
	MFI(15)	Sips	$Q_s(\text{mol g}^{-1})$	$K_s(\text{L mol}^{-1})^{\beta_s}$	$\beta_s$	4.03	0.65	0.65	
	MFI(40)	Sips	$Q_s(\text{mol g}^{-1})$	$K_s(\text{L mol}^{-1})^{\beta_s}$	$\beta_s$	0.71	0.93	0.93	
	MFI(140)	Sips	$Q_s(\text{mol g}^{-1})$	$K_s(\text{L mol}^{-1})^{\beta_s}$	$\beta_s$	$3.70 \times 10^{-5}$	1.73	1.73	
Bisphenol-A	MOR(180)	Redlich-peterson	$K_R(\text{L } \mu\text{g}^{-1})$	$a_R(\text{L } \mu\text{g}^{-1})^{\beta_R}$	$\beta_R$	19275.24	0.23	0.23	100 mg dry zeolite was dosed in 1.5 ml water with an appropriate amount of 0.03 mol $\text{L}^{-1}$ phenol solution. The equilibrium concentrations at 303K were achieved after 1h of stirring.
			0.735	1.0	0.59				
Trichlorophenol	FAU(60)	Freundlich	$K_F(\text{mg g}^{-1})(\text{L } \mu\text{g}^{-1})^n$	n	-	0.09	0.43	0.43	0.5g $\text{L}^{-1}$ dry zeolite was dosed in bisphenol-A solution with concentration 10-30 $\text{mg L}^{-1}$ .
			$1.80 \times 10^{-3}$	0.43					
									1 g of zeolite was added to 50mL of TCP solution with deionised water at different concentrations (10, 25, 50,

75, and 100 mg L <sup>-1</sup> ).						
2-nitrophenol	FAU(200)	Fowler-Guggenheim	Q <sub>FG</sub> (mg g <sup>-1</sup> ) 102	K <sub>FG</sub> (L g <sup>-1</sup> ) 3.3	ω (KJ mol <sup>-1</sup> J) -4	0.34 1.00
4-nitrophenol	FAU(200)	Fowler-Guggenheim	Q <sub>FG</sub> (mg g <sup>-1</sup> ) 110	K <sub>FG</sub> (L g <sup>-1</sup> ) 3.6	ω (KJ mol <sup>-1</sup> J) -4.2	0.39 1.00
2,4-dichlorophenol	FAU(200)	Fowler-Guggenheim	Q <sub>FG</sub> (mg g <sup>-1</sup> ) 190	K <sub>FG</sub> (L g <sup>-1</sup> ) 20	ω (KJ mol <sup>-1</sup> J) -3.7	3.80 1.00
3,4-dichlorophenol	FAU(200)	Fowler-Guggenheim	Q <sub>FG</sub> (mg g <sup>-1</sup> ) 185	K <sub>FG</sub> (L g <sup>-1</sup> ) 18	ω (KJ mol <sup>-1</sup> J) -3.6	3.33 1.00
2-nitroaniline	FAU(200)	Fowler-Guggenheim	Q <sub>FG</sub> (mg g <sup>-1</sup> ) 220	K <sub>FG</sub> (L g <sup>-1</sup> ) 13	ω (KJ mol <sup>-1</sup> J) -5.7	2.86 1.00
4-nitroaniline	FAU(200)	Fowler-Guggenheim	Q <sub>FG</sub> (mg g <sup>-1</sup> ) 212	K <sub>FG</sub> (L g <sup>-1</sup> ) 5.7	ω (KJ mol <sup>-1</sup> J)	1.21 1.00

For each equilibrate isotherm, 100 mg of the adsorbent was added to 200 mL of solution to equilibrate for 24 h (total equilibrium) in a batch equipment. The initial concentrations of adsorbates in water and buffer ranged from 1 to 500 mg L<sup>-1</sup> at 298 K at constant pH.

-5.4						
3,4-dichloroaniline	FAU(200)	Fowler-Guggenheim	$Q_{FG}$ (mg g <sup>-1</sup> ) 190	$K_{FG}$ (L g <sup>-1</sup> ) 31.5	$\omega$	1.00
					(KJ mol <sup>-1</sup> ) 5.98	
-3.8						
3,-dichloroaniline	FAU(200)	Fowler-Guggenheim	$Q_{FG}$ (mg g <sup>-1</sup> ) 192	$K_{FG}$ (L g <sup>-1</sup> ) 34.8	$\omega$	1.00
					(KJ mol <sup>-1</sup> ) 6.68	
-3.7						
2,4-dichloroaniline	FAU(200)	Fowler-Guggenheim	$Q_{FG}$ (mg g <sup>-1</sup> ) 220	$K_{FG}$ (L g <sup>-1</sup> ) 40.4	$\omega$	1.00
					(KJ mol <sup>-1</sup> ) 8.89	
-3.7						
2,4-dinitrophenol	FAU(200)	Fowler-Guggenheim	$Q_{FG}$ (mg g <sup>-1</sup> ) 280	$K_{FG}$ (L g <sup>-1</sup> ) 13	$\omega$	1.00
					(KJ mol <sup>-1</sup> ) 3.64	
-2.7						
2-nitrophenol	FAU(200)	Fowler-Guggenheim	$Q_{FG}$ (mg g <sup>-1</sup> ) 240	$K_{FG}$ (L g <sup>-1</sup> ) 13.4	$\omega$	1.00
					(KJ mol <sup>-1</sup> ) 3.22	
-4.2						
Sulfamethoxazole	FAU(400)	-	$Q_M$ (mg g <sup>-1</sup> ) 296	-	-	The concentration of sulfamethoxazole solution was 202.3 μM. Zeolite: sulfamethoxazole solution (8)
Sulfamethoxazole	MOR(400)	-	$Q_M$ (mg g <sup>-1</sup> ) 52	-	-	

Sulfamethoxazole	MFI(1000)	-	Q <sub>m</sub> (mg g <sup>-1</sup> ) 96	-	-	-	ratio of 1 mg :2 mL Suspensions of FAU or MOR in sulfamethoxazole solution were shaken for 30 min, whereas MFI for 24 h.
Sulfamethoxazole	FAU(200)	Langmuir	Q <sub>L</sub> (mg g <sup>-1</sup> ) 481	K <sub>L</sub> (L mg <sup>-1</sup> ) 0.89	-	423.55	0.99
Sulfathiazole	FAU(200)	Langmuir	Q <sub>L</sub> (mg g <sup>-1</sup> ) 444	K <sub>L</sub> (L mg <sup>-1</sup> ) 0.11	-	48.78	0.99
Sulfamerazine	FAU(200)	Langmuir	Q <sub>L</sub> (mg g <sup>-1</sup> ) 307	K <sub>L</sub> (L mg <sup>-1</sup> ) 0.42	-	128.29	0.99
Sulfamethizole	FAU(200)	Langmuir	Q <sub>L</sub> (mg g <sup>-1</sup> ) 268	K <sub>L</sub> (L mg <sup>-1</sup> ) 0.64	-	170.22	0.99
Sulfadimidine	FAU(200)	Langmuir	Q <sub>L</sub> (mg g <sup>-1</sup> ) 253	K <sub>L</sub> (L mg <sup>-1</sup> ) 0.75	-	188.06	0.99
2-nitrophenol	FAU(200)	Langmuir	Q <sub>L</sub> (mg g <sup>-1</sup> ) 267.2	K <sub>L</sub> (L mg <sup>-1</sup> ) 0.753	-	199.39	0.99
	MFI(1800)	Langmuir	Q <sub>L</sub> (mg g <sup>-1</sup> ) 135.7	K <sub>L</sub> (L mg <sup>-1</sup> ) 0.174	-	23.56	0.99
	MFI(800)	Langmuir	Q <sub>L</sub> (mg g <sup>-1</sup> ) 147.6	K <sub>L</sub> (L mg <sup>-1</sup> ) 0.148	-	21.81	0.99
	MFI(200)	Langmuir	Q <sub>L</sub> (mg g <sup>-1</sup> ) 118.7	K <sub>L</sub> (L mg <sup>-1</sup> ) 0.104	-	12.33	0.99
	MFI(80)	Langmuir	Q <sub>L</sub> (mg g <sup>-1</sup> ) 83.9	K <sub>L</sub> (L mg <sup>-1</sup> ) 0.022	-	1.85	0.99
	BEA(98)	Langmuir	Q <sub>L</sub> (mg g <sup>-1</sup> ) 95.0	K <sub>L</sub> (L mg <sup>-1</sup> ) 0.021	-	1.99	0.99
	BEA(42)	Langmuir	Q <sub>L</sub> (mg g <sup>-1</sup> ) 75.6	K <sub>L</sub> (L mg <sup>-1</sup> ) 0.019	-	1.44	0.99
Coumaric acid	FAU(14.5)	Langmuir	Q <sub>L</sub> (mg g <sup>-1</sup> )	K <sub>L</sub> (L mg <sup>-1</sup> )	-	9.36	0.97

5 mg zeolite was dosed in a sulfa drug solution (10 mg L<sup>-1</sup>, 50 mL in Millipore (9) water). pH was adjusted using sulfuric acid and sodium hydroxide

100 mg zeolites was added to 200 mL of solution with the initial concentrations of adsorbates in water and buffer ranging from 1 to 500 mg L<sup>-1</sup> (10)

50 mg of zeolites and 10 mL (11)

		108	5.8	of aqueous solution of hydroxycinnamic acids with the same initial concentrations from 10 to 500 mg L <sup>-1</sup> were placed in 50 mL glass flask	
Ferulic acid	FAU(25)	Langmuir	Q <sub>i</sub> (mg g <sup>-1</sup> ) 68.0	K <sub>i</sub> (L mg <sup>-1</sup> ) 11.3	- 688.49 0.95
	BEA(88)	Langmuir	Q <sub>i</sub> (mg g <sup>-1</sup> ) 122.0	K <sub>i</sub> (L mg <sup>-1</sup> ) 82	- 6465.47 0.82
	FAU(14.5)	Langmuir	Q <sub>i</sub> (mg g <sup>-1</sup> ) 137.0	K <sub>i</sub> (L mg <sup>-1</sup> ) 1.33	- 179.34 0.99
Cinnamic acid	FAU(25)	Langmuir	Q <sub>i</sub> (mg g <sup>-1</sup> ) 131.6	K <sub>i</sub> (L mg <sup>-1</sup> ) 1.2	- 155.67 0.99
	BEA(88)	Langmuir	Q <sub>i</sub> (mg g <sup>-1</sup> ) 138.9	K <sub>i</sub> (L mg <sup>-1</sup> ) 144.0	- 11045 0.76
	FAU(25)	Langmuir	Q <sub>i</sub> (mg g <sup>-1</sup> ) 65.8	K <sub>i</sub> (L mg <sup>-1</sup> ) 8.44	- 509.57 0.96
Erythromycin	BEA(88)	Langmuir	Q <sub>i</sub> (mg g <sup>-1</sup> ) 108.7	K <sub>i</sub> (L mg <sup>-1</sup> ) 153.33	- 9028.18 0.75
	FAU(400)	Langmuir	Q <sub>i</sub> (mg g <sup>-1</sup> ) 42	K <sub>i</sub> (L mg <sup>-1</sup> ) 2.1	- 86.08 0.98
	MOR(400)	Langmuir	Q <sub>i</sub> (mg g <sup>-1</sup> ) 26	K <sub>i</sub> (L mg <sup>-1</sup> ) 1.3	- 33.28 0.99
Levofloxacin	FAU(400)	Langmuir	Q <sub>i</sub> (mg g <sup>-1</sup> ) 45	K <sub>i</sub> (L mg <sup>-1</sup> ) 1.4	- 61.96 0.99
	MOR(400)	Langmuir	Q <sub>i</sub> (mg g <sup>-1</sup> ) 27	K <sub>i</sub> (L mg <sup>-1</sup> ) 0.15	- 4.04 0.99
	MFI(1000)	Langmuir	Q <sub>i</sub> (mg g <sup>-1</sup> ) 16	K <sub>i</sub> (L mg <sup>-1</sup> ) 0.10	- 1.60 0.99
Carbamazepine	FAU(400)	Langmuir	Q <sub>i</sub> (mg g <sup>-1</sup> ) 100	K <sub>i</sub> (L mg <sup>-1</sup> ) 3.1	- 299.30 0.98
	MOR(400)	Langmuir	Q <sub>i</sub> (mg g <sup>-1</sup> ) 32	K <sub>i</sub> (L mg <sup>-1</sup> ) 0.46	- 14.64 0.99

The adsorption experiments were made up of dual solute, i.e. water and one of the studied drugs over the zeolites. The equilibrium concentration of each solute was 0 - 5mg L<sup>-1</sup>.

(12)

	MFI(1000)	Langmuir	$Q_L(\text{mg g}^{-1})$ 26	$K_L(\text{L mg}^{-1})$ 0.52	-	13.43	0.99
	FAU(34)	Langmuir	$Q_L(\text{mg g}^{-1})$ 833	$K_L(\text{L g}^{-1})$ 0.923	-	0.77	1.00
	FAU(26)	Langmuir	$Q_L(\text{mg g}^{-1})$ 667	$K_L(\text{L g}^{-1})$ 0.577	-	0.38	1.00
	FAU(22)	Langmuir	$Q_L(\text{mg g}^{-1})$ 500	$K_L(\text{L g}^{-1})$ 0.345	-	0.17	1.00
$\alpha$ -endosulfan	BEA(110)	Langmuir	$Q_L(\text{mg g}^{-1})$ 794	$K_L(\text{L g}^{-1})$ 0.490	-	0.39	1.00
	BEA(63)	Langmuir	$Q_L(\text{mg g}^{-1})$ 787	$K_L(\text{L g}^{-1})$ 0.410	-	0.32	1.00
	BEA(36)	Langmuir	$Q_L(\text{mg g}^{-1})$ 763	$K_L(\text{L g}^{-1})$ 0.247	-	0.19	1.00
	BEA(33)	Langmuir	$Q_L(\text{mg g}^{-1})$ 741	$K_L(\text{L g}^{-1})$ 0.205	-	0.15	1.00
Tris-2-chloroethyl phosphate (TCEP)	BEA(50)	Langmuir	$Q_L(\text{mg g}^{-1})$ 76.649	$K_L(\text{L } \mu\text{g}^{-1})$ 0.0078	-	0.55	0.96
	BEA(300)	Langmuir	$Q_L(\text{mg g}^{-1})$ 103.00	$K_L(\text{L } \mu\text{g}^{-1})$ 0.0030	-	0.30	0.98
						The respective zeolite dosage was added to a 200 mL aliquot of 10 mg L <sup>-1</sup> TCEP solution. The zeolites were dosed by values of 0-0.09 mmol TCEP g <sup>-1</sup> zeolite. The solution pH was adjusted using HCl or NaOH to 4.8.	
Nicotine	BEA(43)	Sips	$Q_s(\text{mol g}^{-1})$ 0.001	$K_s(\text{L mol}^{-1})^{\beta_s}$ 18739.8	$\beta_s$ 1.14	1.14	1.13
	MFI(40)	Sips	$Q_s(\text{mol g}^{-1})$ 0.0007	$K_s(\text{L mol}^{-1})^{\beta_s}$ 325.1	$\beta_s$ 0.34	3551.40	0.20
						100 mg dry zeolites were dosed in 1.5 ml water with an appropriate amount of 0.03 mol L <sup>-1</sup> nicotine solution. The equilibrium	

concentrations at 30 °C were achieved after 1h of stirring.						
Dimethylamine (DMA)	LTA	Freundlich	$K_F(\text{nmol g}^{-1})(\text{L nmol}^{-1})^n$	n	-	Zeolites (~100 mg) were added into 40 mL glass vials containing 30 mL of DMA solutions at varying concentrations (18 - 740 µg L <sup>-1</sup> )
	FAU(40)	Freundlich	334.1	0.86	1486.27	0.86
	MFI(40)	Freundlich	$K_F(\text{nmol g}^{-1})(\text{L nmol}^{-1})^n$	n	-	1.14
Metformine			10011.3	1.14	2026.28	1.14
			$K_F(\text{nmol g}^{-1})(\text{L nmol}^{-1})^n$	n	-	0.77
			2439.61	0.77	27829.15	0.77
Lidocaine	MFI(80)	Freundlich	$K_F(\mu\text{g g}^{-1})(\text{L } \mu\text{g}^{-1})^n$	n	-	0.70
			1122	0.70	1122	0.70
	MOR(200)	Freundlich	$K_F(\mu\text{g g}^{-1})(\text{L } \mu\text{g}^{-1})^n$	n	-	0.60
Lincomycine			630	0.60	630	0.60
			$K_F(\mu\text{g g}^{-1})(\text{L } \mu\text{g}^{-1})^n$	n	-	0.84
			133	0.84	133	0.84
Ifosfamide	MOR(200)	Freundlich	$K_F(\mu\text{g g}^{-1})(\text{L } \mu\text{g}^{-1})^n$	n	-	0.55
			5012	0.55	5012	0.55
			$K_F(\mu\text{g g}^{-1})(\text{L } \mu\text{g}^{-1})^n$	n	-	1.18
Cyclophosphamide			2339	1.18	2339	1.18
			$K_F(\mu\text{g g}^{-1})(\text{L } \mu\text{g}^{-1})^n$	n	-	0.68
			145	0.68	145	0.68
Iofosfamide	MOR(200)	Freundlich	$K_F(\mu\text{g g}^{-1})(\text{L } \mu\text{g}^{-1})^n$	n	-	0.70
			8	0.70	8	0.70
			$K_F(\mu\text{g g}^{-1})(\text{L } \mu\text{g}^{-1})^n$	n	-	0.88
			459	0.88	459	0.88
			$K_F(\mu\text{g g}^{-1})(\text{L } \mu\text{g}^{-1})^n$	n	-	0.81
			51	0.81	51	0.81
	MFI(80)	Freundlich	$K_F(\mu\text{g g}^{-1})(\text{L } \mu\text{g}^{-1})^n$	n	-	0.90
			22	0.90	22	0.90

The initial concentration of each of the pharmaceuticals was 2 µg L<sup>-1</sup>. The adsorbent concentration varied between 2.5 and 1000 mg L<sup>-1</sup>

1

MOR(200)	Freundlich	$K_F(\mu\text{g g}^{-1})(\text{L } \mu\text{g}^{-1})^n$ 132	n 0.82	-	132	0.82
Carbamazepine	MOR(200)	Freundlich	$K_F(\mu\text{g g}^{-1})(\text{L } \mu\text{g}^{-1})^n$ 31	n 0.80	-	31
	MFI(80)	Freundlich	$K_F(\mu\text{g g}^{-1})(\text{L } \mu\text{g}^{-1})^n$ 63	n 1.18	-	63
Sulfamethoxazole	MOR(200)	Freundlich	$K_F(\mu\text{g g}^{-1})(\text{L } \mu\text{g}^{-1})^n$ 36	n 0.91	-	36
	MFI(80)	Freundlich	$K_F(\mu\text{g g}^{-1})(\text{L } \mu\text{g}^{-1})^n$ $9.20 \times 10^{-5}$	n 0.40	-	$9.20 \times 10^{-5}$
Gemfibrozil	MOR(200)	Freundlich	$K_F(\mu\text{g g}^{-1})(\text{L } \mu\text{g}^{-1})^n$ 597	n 0.39	-	597
Naproxen	MOR(200)	Freundlich	$K_F(\mu\text{g g}^{-1})(\text{L } \mu\text{g}^{-1})^n$ 1054	n 0.41	-	1054
Phenazon	MOR(200)	Freundlich	$K_F(\mu\text{g g}^{-1})(\text{L } \mu\text{g}^{-1})^n$ 230	n 0.48	-	230
Ketoprofen	MOR(200)	Freundlich	$K_F(\mu\text{g g}^{-1})(\text{L } \mu\text{g}^{-1})^n$ 52	n 0.55	-	52
Clofibric acid	MOR(200)	Freundlich	$K_F(\mu\text{g g}^{-1})(\text{L } \mu\text{g}^{-1})^n$ 52	n 0.55	-	52

The adsorption isotherm equation in Table 2-4 were expressed as below: Langmuir,  $q_e = \frac{Q_L K_L C_e}{1 + K_L C_e}$ ; Sips,  $q_e = \frac{K_S Q_S C_e^{1/S}}{1 + K_S C_e^{1/S}}$ ; Redlich-Peterson,  $q_e = \frac{K_R C_e}{1 + a_R C_e^b}$ ; Freundlich,  $q_e = K_F C_e^n$ ; Fowler-Guggenheim,  $K_{FG} C_e = \frac{\theta}{1-\theta} \exp\left(\frac{2\theta\omega}{RT}\right)$ , Where  $\theta = \frac{q_e}{Q_{FG}}$ .  $C_e$  is the equilibrium concentration.  $q_e$  is equilibrium adsorption capacity.  $Q_M$  is the maximum amount of OMPs adsorbed by high-silica zeolites.

\* The Freundlich isotherm constants were recalculated by the isotherm data given in the literature. The fitting concentration range was 0.01 – 70  $\mu\text{g L}^{-1}$ .

- (1) (Gonzalez-Olmos et al., 2013); (2) (He and Cheng 2016); (3) (de Ridder et al., 2012); (4) (Damjanovic et al., 2010); (5) (Tsai et al., 2006); (6) Zhang et al. (2014); (7) (Koubaissy et al., 2011); (8) (Blasioli et al., 2014); (9) (Fukahori et al., 2011); (10) (Reungoat et al., 2007); (11) (Simon et al., 2015); (12) (Martucci et al., 2012); (13) (Yonli et al., 2012); (14) (Grieco and Ramarao 2013); (15) (Rakic et al., 2010); (16) (He and Cheng 2016).



*OMP mixtures*

High-silica zeolites were also tested for the adsorption of OMP mixtures. For example, MFI and MOR type zeolites were tested for the removal of 16 pharmaceuticals in both demineralised and surface water. When the initial concentration of each pharmaceutical was  $2 \mu\text{g L}^{-1}$ , MOR zeolites with a Si/Al ratio of 400 either completely or considerably removed 15 species from the mixed solution (de Ridder et al., 2012). Rossner et al. (2009) investigated the removal of a 25 OMP mixture with concentrations between 200 and  $900 \text{ ng L}^{-1}$  in lake water by two high-silica zeolites i.e. MOR and FAU zeolites, activated carbon and a carbonaceous resin. Activated carbon was able to remove most of the tested compounds, while only 15 compounds were either completely or partially removed with the MOR zeolite and 3 compounds (fluoxetine, oxybenzone, and triclosan) with the FAU zeolite. It was demonstrated that effective adsorbents for the removal of a broad spectrum of OMPs from water should exhibit heterogeneity in pore size and shape.

*Prediction of adsorption on high-silica zeolites at environmentally relevant concentrations*

The adsorption by high-silica zeolites varied with the equilibrium concentration of OMPs. When the concentration of OMPs in the experiment was high (ranges of  $\text{mg L}^{-1}$ ), the adsorption limit could be predicted by the adsorption isotherm models such as Langmuir and Sips (Martucci et al., 2012; Yonli et al., 2012). The estimated maximum adsorption capacity of OMPs by high-silica zeolites was then in the range of 16 to  $833 \text{ mg g}^{-1}$  (Table 4). The adsorption isotherms of OMPs at environmentally realistic concentration range ( $\mu\text{g L}^{-1}$  and  $\text{ng L}^{-1}$ ) follow the Freundlich isotherm, since no concentration independent plateau is observed from these isotherms. The maximum adsorption capacity of zeolites cannot be predicted at these concentrations (de Ridder et al., 2012; Gonzalez-Olmos et al., 2013).

To compare the adsorption efficiency of OMPs in various conditions, the constants for the Freundlich isotherm model were also determined for the high concentration experiments, translating them to environmentally relevant concentrations ranging from  $0.01$  to  $70 \mu\text{g L}^{-1}$ . In addition, the values of the Freundlich isotherm constant  $K_F$  given with different units were unified, since they are unit dependent. The recalculated isotherm constants are listed in Table 4, including the  $K_F$  with a unit of  $(\mu\text{g g}^{-1})(\text{L } \mu\text{g}^{-1})^n$  and the  $n$  value. When  $n$  was around 1, the higher adsorption capacity was implied by the higher  $K_F$  value.

By referring to the results in Table 4, the adsorption isotherms from the one-solute solution had, in most cases,  $n$ -values of around 1 where the adsorption capacity linearly increased with the increase in equilibrium concentration of OMPs. The  $n$  value varied in multi-solute solutions with competition adsorption. Favourable adsorption was indicated by high  $n$  value ( $n > 1$ ), while the adsorption of OMPs was unfavoured when  $n$  was below 1 (Freundlich 1906).

The recalculated results could be utilized as an overview of OMP adsorption efficiency. For instance, high-silica zeolites achieved great adsorption efficiency in the following cases where the  $K_F$  value exceeded  $10,000 (\mu\text{g g}^{-1})(\text{L } \mu\text{g}^{-1})^n$ : the adsorption of bisphenol-A by MOR zeolite, dimethylamine by MFI zeolite and hydroxycinnamic acids by BEA zeolite. Conversely, high-silica FAU zeolites showed limited adsorption for 2,4,6-trichlorophenol (TCP) with low value of  $K_F$  ( $0.09 (\mu\text{g g}^{-1})(\text{L } \mu\text{g}^{-1})^n$ ) and  $n$  (0.43). Reference to the recalculated isotherm information can thus guide the selection of suitable high-silica zeolites for the adsorption of specific OMPs at environmentally relevant concentrations. Moreover, high-silica zeolites showed possibilities for the adsorption of OMPs which were hardly adsorbed by activated carbon. For example,  $K_F$  for sulfametoxazole adsorption by FAU(200) was  $423.55 (\mu\text{g g}^{-1})(\text{L } \mu\text{g}^{-1})^n$  (Table 4,  $n=0.99$ ) (Fukahori et al., 2011) which was much higher than the reported value of  $K_F$  in literature for powder activated carbon of  $1.10 (\mu\text{g g}^{-1})(\text{L } \mu\text{g}^{-1})^n$  ( $n=1$ ) (Nam et al., 2014).

#### *OMP adsorption by high-silica zeolite granules*

In practice, adsorbents are frequently used in the form of a column with a packed granular bed, in order to eliminate the need for post filtration to remove powder adsorbents. The use of columns also allows for easier regeneration. The performance of column adsorption can be examined by breakthrough curves which describe the OMP concentration in the column effluent changing in time. When the adsorbents in the column become saturated, a drastic increase of the effluent concentration appears, indicating the so-called breakthrough.

High-silica MFI zeolite granules with grain sizes 0.5 and 1.0 mm were applied for the adsorption of MTBE (Rossner and Knappe 2008). For MFI zeolite granules, co-adsorption of NOM had a small effect on the MTBE adsorption uptake but a more pronounced effect on MTBE adsorption kinetics. The adsorbent usage rate was estimated assuming an influent

MTBE concentration of  $100 \mu\text{g L}^{-1}$  in river water, an empty bed contact time (EBCT) of 15min and an effluent MTBE concentration of  $10 \mu\text{g L}^{-1}$ . Based on experimental data, a coconut-shell-based GAC column was predicted to have a useful life of 33 days while the MFI zeolite column was predicted to have a useful life of 175 days.

Abu-Lail et al. (2010) evaluated the performance of zeolite granules from FAU, BEA, MOR and MFI types for the removal of MTBE in batch-scale experiments. Compared with other tested zeolite granules, MFI zeolite granules (Si/Al ratio 280) with the smallest pores had the highest adsorption capacity at an equilibrium concentration range of 0.001 to  $20 \text{ mg L}^{-1}$ . In the column-scale experiment using a flow rate of  $32.5 \text{ ml min}^{-1}$ , feeding an MTBE concentration of  $50 \mu\text{g L}^{-1}$  and an effluent MTBE concentration of  $5 \mu\text{g L}^{-1}$ , MFI zeolite granules (granular size  $250 - 425 \mu\text{m}$ ) had a later breakthrough than granular activated carbon.

Khalid et al. (2004) demonstrated that pure silica BEA zeolite (no Al content) granules showed a better adsorption efficiency for phenol than other tested zeolites, i.e. MOR, BEA and FAU zeolites, and activated carbons. In the column-scale experiment with an EBCT of 1 min and an influent concentration of  $100 \text{ mg L}^{-1}$ , BEA zeolite exhibited a breakthrough time 4.5 times longer than granular activated carbon.

The adsorption competition of aromatic compounds was studied in column-scale experiments by Koubaissy et al. (2011). The equal molar mixture of 2,4-DCP/2,4-DNP and ONP/ONA in distilled water was fed to a column with an EBCT of 4 – 6.7 min and a flow rate of  $2 \text{ ml min}^{-1}$ . The breakthrough curves showed that ONP decreased ONA adsorption and 2,4-DNP desorbed 2,4-DCP, both of which were determined by functional groups.

## **4.2 Preventing unfavourable adsorption of natural organic matters (NOM) in natural water**

In practice, the OMP adsorption performance of adsorbents is affected by BOM, a mixture of organic molecules that is unique for each water type. NOM may cover the surface of adsorbents or prevent adsorption of OMPs, e.g. NOM was proven to compete strongly with OMPs and considerably impair the adsorption capacity of activated carbon (de Ridder et al., 2012; Hung and Lin 2006; Hung et al., 2005). However, NOM competition in natural water was hardly observed during high-silica zeolite adsorption of OMPs, such as MTBE (Abu-

Lail et al., 2010; Rossner and Knappe 2008), sulfonamide antibiotics (Braschi et al., 2010), nitrosamines and various pharmaceuticals (de Ridder et al., 2012). The micropores of zeolites could prevent the entrance of most NOM components present in water (de Ridder et al., 2012; Ebie et al., 2001; Pelekani and Snoeyink 1999). However, slower adsorption kinetics of OMPs were observed in the presence of NOM since NOM could block the surface openings and hinder the diffusional paths of OMPs (Hung and Lin 2006; Rossner and Knappe 2008).

In some cases, low molecular weight compounds are also present in natural water as a fraction of NOM (Hem 1959). Braschi et al., (2016b) studied the adsorption efficiency of FAU zeolites with a Si/Al ratio of 100 for sulfamethoxazole in the presence of two humic monomers: vanillin and caffeic acid with molecular weights of 152 and 180 mol g<sup>-1</sup>, respectively. Since humic monomers could enter the pores of zeolites, a slightly lower adsorption capacity was observed when sulfamethoxazole was mixed with these humic monomers compared to a single solution. Meanwhile, it was hypothesised that an adduct with sulfamethoxazole and vanillin formed by H-bonding could stabilize the adsorbed OMPs in the pores of high-silica zeolites.

Bottero et al. (1994) investigated atrazine adsorption by FAU and MFI zeolites and observed that atrazine was even better adsorbed in natural water than in pure water. This was attributed to the finding that in natural water, atrazine has a high affinity for NOM compounds, e.g. forming hydroxyaromatics. As a result, the adsorption of atrazine was enhanced because the hydroxyaromatics were well adsorbed by the zeolites.

### **4.3 Possible on-site regeneration and recycling of high-silica zeolites**

Reuse of adsorbents allows for reduction of both treatment costs and waste generation. To regenerate the adsorbents, thermal calcination regeneration, which employs high temperature, is widely used for most adsorbents, including activated carbon and zeolites. In other cases, regeneration using high temperature water is applied to stimulate the desorption of specific strong interactions between zeolites and OMPs (Chica et al., 2004; Chica et al., 2005; García and Lercher 1992; Zhang et al., 2008). However, energy consumption for the current regeneration approaches is high (Lee et al., 2011).

Oxidation is another method for the regeneration of high-silica zeolites since zeolites are resistant to oxidants, e.g. hydroxyl radicals, ozone, etc. A broad range of OMPs, after accumulating in the micropores of zeolites, are found to be oxidised by ozone, Fenton, UV,  $\text{H}_2\text{O}_2$  and other oxidants (Sagehashi et al., 2005; Shahbazi et al., 2014; Wang et al., 2010; Wang et al., 2006). By combining high-silica zeolite adsorption with oxidation of OMPs, on-site regeneration of zeolites could be achieved (Gonzalez-Olmos et al., 2011; Gonzalez-Olmos et al., 2013). Most of these oxidation regeneration processes require a short contact time of less than 30 min, while the thermal approaches might take up to several hours (Fujita et al., 2004; Sun et al., 2010; von Gunten 2003a; Wang et al., 2006; Zhang et al., 2014). Comparably, ozonation of activated carbon will change the properties of activated carbon, e.g. surface area, pore size distribution and surface functional groups which are well-related to the adsorption efficiency (Chiang et al., 2002a; Chiang et al., 2002b; Odivan et al., 2014). Donnet and Ehrburger (1970) conducted experiments on the ozonation of activated carbon and reported that at an ozone dosage of  $13 \text{ mg L}^{-1}$  for 150 h, 66.2% of the activated carbon surface was oxidized to  $\text{CO}_2$ . The long-term oxidation of activated carbon will thus lead to a high carbon loss.

Different forms of oxidant species may exist in the ozone oxidation process. Firstly, zeolites, as catalysts, could promote surface reactions between the adsorbed ozone and OMPs. The catalytic ozonation on zeolites then proceeds via direct reaction of molecular ozone with OMPs (Ikhlaiq et al., 2014). Second, decomposition of ozone molecules may happen at Lewis acid sites to generate reactive oxygen species (Alejandro et al., 2014). Thus, reactive hydroxyl radicals can be generated from ozone decomposition and subsequently react with OMPs from zeolites (Legrini et al., 1993; Leichsenring et al., 1996; Monneyron et al., 2003). Reungoat et al. (2007) studied the adsorption of nitrobenzene and ozone regeneration of zeolites in a sequential process. They found that the initial adsorption capacity of FAU zeolites was completely restored by ozone after the adsorption of nitrobenzene. The effective adsorption of TCP was maintained for at least 8 cycles of adsorption and regeneration. It was also observed that ozonation increased the BET surface area of FAU zeolite by over 60%, which even enhanced the OMP adsorption capacity. The changes in BET surface area might be attributed to the additional defects of zeolites, generated during the oxidation process, which need further investigation.

However, with a further increase in the number of regeneration cycles, the ozone regeneration process could lose efficiency. The decrease of regeneration efficiency was attributed to the oxidation by-products that might accumulate and compete with target OMP adsorption. It has been confirmed that traces of oxidation by-products of toluene, such as acetic acid and acetaldehyde, were formed and remained adsorbed after the regeneration with ozone (Alejandro et al., 2014; Zaitan et al., 2016). Moreover, acid formation during ozonation may have changed the pH of the solution, which hindered the decomposition of ozone and the generation of free radicals (Zhang et al., 2014).

Once hydrogen peroxide is introduced, Fenton or Fenton-like systems are developed as an oxidiser for regeneration of high-silica zeolites (Neyens and Baeyens 2003). Iron, either immobilized on the high-silica zeolites or dissolved into the solution, will catalyse the oxidation process (Gonzalez-Olmos et al., 2013; Shahbazi et al., 2014). Hydroxyl radicals could be generated to decompose the OMPs adsorbed on the zeolites (Gonzalez-Olmos et al., 2013; Wang et al., 2006). Cihanoglu et al. (2015) found that the catalytic activities of MFI zeolites increased with iron loading. In addition, Koryabkina et al. (2007) applied Fe coated FAU zeolites for adsorption of disinfection by-products: chloroform and trichloroacetic acid. Eight regeneration cycles could be achieved, although the adsorption capacity after regeneration decreased because of iron leaching.

However, the regeneration efficiency by both ozone and hydrogen peroxide could be affected by the properties of the zeolites. Braschi et al. (2016a) found that adsorbed sulfonamide antibiotics were only partially oxidised, suspecting that the diffusion of radical oxygenated species, e.g. hydroxyl radicals in the pores of zeolites, was insufficient, although, the number of Brønsted acid sites was found to have a positive relation with the catalytic ability of the tested MFI zeolites (Cihanoglu et al., 2015). Moreover, the ozonation regeneration efficiency was related to the amount of acid sites. As an example, a natural zeolite with a Si/Al ratio of 11, which contains a greater number of Brønsted acid sites than zeolites with higher Si/Al ratios, had a 2.3 times higher activity of hydrogen peroxide decomposition than BEA zeolites with a Si/Al ratio of 400. However, the regeneration efficiency of the BEA zeolites was 2.5 higher than the natural zeolite since more OMPs were adsorbed by BEA zeolites than by the natural zeolite (Shahbazi et al., 2014).

TiO<sub>2</sub> immobilized high-silica zeolites combined with UV light was also studied and found to be an effective photo-catalytic oxidation process to regenerate zeolites (Fukahori and Fujiwara 2014; Mendez-Arriaga and Almanza 2014; Neppolian et al., 2016; Pan et al., 2014; Perisic et al., 2016; Wang et al., 2010). Active free radicals were generated and therefore a fast OMP degradation rate was achieved (Hoffmann et al., 1995). Due to the limited research on the photo-catalytic oxidation process for zeolite regeneration, it is yet unclear what will be the long-term performance with increasing regeneration cycles.

Plasma technology has recently been proposed as a promising advanced oxidation method, since it is able to produce a wide range of reactive species, including electrons, photons, free radicals, ions and reactive molecules, such as ozone and hydrogen peroxide. As such, it can be used to decompose organic matters in a gaseous or liquid phase, as well as for surface treatment of materials. Plasma can be generated by a variety of electrical discharges and several lab-scale designs of electrical discharge reactors appear to be effective for contaminant degradation in water or wastewater (Miklos et al., 2018; Vanraes 2016). Kušić et al. (2005) and Peternel et al. (2006) have reported the application of plasma treatment with high voltage electrical discharge reactors using MFI and FAU zeolites for degradation of OMPs, i.e. phenol and dyes in water. The oxygen, hydrogen and hydroxyl radicals as well as ozone generated from the reactor could promote OMP degradation. The combination of plasma oxidation and high-silica zeolites can potentially be a promising approach for zeolite regeneration. However, to the authors' knowledge, no study has been carried out to demonstrate the system's efficiency of regeneration. The influence of solution chemistry and plasma reactivity inside the zeolite pores on the regeneration efficiency in addition to the scaling up of the electrical discharge reactors are future research topics worth investigation.

## 5. Concluding remarks and prospects

The research on OMP adsorption by high-silica zeolites has been reviewed and the following conclusions can be drawn:

- High-silica zeolites have exhibited a good ability to remove target OMPs from water, e.g. small-sized and polar OMPs that are not effectively removed by other adsorbents.

- A wide range of studies could be found on OMP adsorption efficiencies and mechanisms of high-silica zeolite powders, which were mostly carried out in batch tests. High microporous volume, closely fitted pores and hydrophobicity of high-silica zeolites could promote OMP adsorption.
- NOM in natural water has a minimal effect on the adsorption capacity of OMPs onto high-silica zeolites, which is considered to be an advantage for the application of high-silica zeolites in water treatment. However, small molecules with a similar size relative to OMPs might be present in water and compete with OMP adsorption.
- Oxidants, such as ozone, hydrogen peroxide, Fenton, photo-catalytic oxidation and plasma, have shown to be effective during the regeneration of high-silica zeolites. Structural modification of high-silica zeolites, e.g. the possible generation of additional surface defects by the oxidation, needs further investigation.





## **CHAPTER 3**

# **ADSORPTION OF TRICLOSAN, TRICHLOROPHENOL AND PHENOL BY HIGH-SILICA ZEOLITES: ADSORPTION EFFICIENCIES AND MECHANISMS**

This chapter is based on: Jiang, N., Shang, R., Heijman, S.G., & Rietveld, L.C. (2020). Adsorption of triclosan, trichlorophenol and phenol by high-silica zeolites: Adsorption efficiencies and mechanisms. *Separation and Purification Technology*, 235, 116152.

## Abstract

High-silica zeolites can be used for adsorption of organic micropollutants (OMPs) from water. The adsorption efficacy could vary with the properties of OMPs, as well as the porous and surface features of high-silica zeolites. In this study, the adsorption of triclosan, trichlorophenol (TCP) and phenol by ten high-silica zeolites were investigated. The plateaus of adsorption isotherms were observed in the adsorption of triclosan. The maximum adsorption capacity of triclosan could be related to the surface area and volume of micropores. The adsorption of TCP by FAU zeolites gave an S-shaped isotherm due to the possible lateral interactions of TCP molecules in the specific pore topology of FAU zeolites. The adsorption of phenol by high-silica zeolites had no adsorption plateau. Zeolites with channel structures, e.g. MFI zeolites, possess closely fitted pores for phenol, which slightly promoted its adsorption efficacy. The active adsorption sites of zeolites, i.e. Brønsted acid sites (BAS) and Lewis acid sites (LAS) failed to promote phenol adsorption. Phenol adsorption was favoured by carbon-based adsorbents with aromatic rings and functional groups, e.g. carboxyl and carbonyl, while the lack of active adsorption sites limited the phenol adsorption by high-silica zeolites, especially at the low concentration range.

## 1 Introduction

Zeolites are crystalline aluminosilicates with uniform micropores (pore size of less than 2 nm). The porous structure of zeolites is generated from a three-dimensional framework constructed by  $\text{SiO}_4$  and  $\text{AlO}_4$  tetrahedra (Auerbach et al., 2003; Jacobs et al., 2001). The properties of zeolites vary with the Si and Al content in the framework, typically characterized by the silica to alumina molar ratio (Si/Al ratio). Low-silica zeolites (Si/Al ratio < 2) possess a high ion exchange capacity and therefore have been used for water softening (Behrman 1927). High-silica zeolites (Si/Al ratio up to several thousands) can be synthesized from low-silica zeolites by replacing aluminium with silica (Burton 2018; Burton et al., 2005). High-silica zeolites have been found to be efficient adsorbents for the removal of emerging organic compounds (OMPs), e.g. methyl tert-butyl ether (MTBE) (Gonzalez-Olmos et al., 2013; Knappe and Campos 2005) and N-nitrosamines (de Ridder et al., 2012; He and Cheng 2016), which are hardly adsorbed by activated carbon.

Triclosan, a commonly used antibacterial and antifungal agent, has caused public attention because of its extensive use in personal care products and possible disposal in water (Adolfsson-Erici et al., 2002). Treatment technologies such as biological treatment (Ying and Kookana 2007), oxidation (Suarez et al., 2007; Wu et al., 2012) and adsorption by activated carbon (AC) (Behera et al., 2010; Liu et al., 2014b) and carbon nanotubes (Cho et al., 2011; Zhou et al., 2013) have been used to treat water containing triclosan, while the adsorption of triclosan by high-silica zeolites has not yet been reported in literature.

Phenol and chlorophenol, including 2,4,6-trichlorophenol (TCP) are widely used in the production of industrial commodities and, as a result, have been commonly detected in water bodies (Gao et al., 2008; Schmidt - Bäuml et al., 1999). The adsorption of TCP and phenol in water by some high-silica zeolites has been previously studied. Zhang. et al. (2014) evaluated the adsorption of TCP by FAU type high-silica zeolites. The maximum adsorption capacity could not be determined since an adsorption plateau was not observed. Yang. et al. (2016) studied TCP adsorption by FAU zeolites with different Si/Al ratios. As the isotherm curves with linear shape showed, FAU zeolites with higher Si/Al ratios had better adsorption efficacies than zeolites with lower Si/Al ratios. However, TCP adsorption by high-silica zeolites with other framework types has not been studied before. Phenol adsorption by high-silica zeolites with different frameworks, i.e. FAU, BEA, MOR and MFI types, has been studied by Damjanovic et al. (2010) and Khalid et al. (2004). The maximum adsorption capacity and its relationship to the properties of high-silica zeolites, occurring at several  $\text{g L}^{-1}$ , were well elaborated. However, no attempt has been made to provide insight into the adsorption isotherm of phenol at lower and environmentally relevant concentrations, e.g.  $\mu\text{g L}^{-1}$ .

The adsorption of specific OMPs, e.g. MTBE (Gonzalez-Olmos et al., 2013; Hung and Lin 2006; Knappe and Campos 2005; Rossner and Knappe 2008), and OMP groups, e.g. N-nitrosamines (de Ridder et al., 2012; He and Cheng 2016) and sulfa drugs (Fukahori et al., 2011) in water on high-silica zeolites have been studied in literature. The adsorption efficacy and mechanisms of OMPs on high-silica zeolites were reviewed by Jiang et al (2018). Based on literature, it was concluded that zeolite properties, such as surface hydrophobicity/hydrophilicity, pore size and structure, affect the adsorption of OMPs. The efficacy and mechanism of OMP adsorption can also vary based on the properties of OMPs, e.g. hydrophobicity/hydrophilicity, molecular weight and size. More research is thus

needed to explore the adsorption of representative OMPs by high-silica zeolites, which would indicate the OMP adsorption mechanisms.

In this study, the adsorption of triclosan, TCP and phenol with the same functional groups, i.e. chlorine atoms and hydroxyls attached to aromatic rings, but also different molecular weight, size and hydrophobicity were selected to represent OMPs with diverse properties. The adsorption of three OMPs by high-silica zeolites with different porous and surface properties was investigated. The study examined the relationship between the adsorption efficacy of OMPs and the properties of both high-silica zeolites and OMPs. By comparing the adsorption behaviour of three OMPs on various high-silica zeolites, the dominant adsorption mechanisms, i.e. the size/close-fit or the hydrophobicity interaction, could be concluded. Based on these findings, the adsorption efficacies of high-silica zeolites were compared with commonly used adsorbents, e.g. activated carbon, carbon nanotubes and clays.

## 2 Materials and Methods

### 2.1 High-silica zeolite adsorbents

High-silica zeolite powders of four frameworks, namely FAU, BEA, MOR and MFI, were purchased from commercial companies. The framework types, names, suppliers and Si/Al ratios are listed in Table 1.

**Table 1** Names and supplier information of high-silica zeolites.

Framework type	Zeolite name <sup>a</sup>	Product name	Company	Si/Al ratio <sup>b</sup>
FAU	FAU250	390HUA	Tosoh	250
	FAU50	385HUA	Tosoh	50
	FAU40	CBV901	Zeolyst	40
	FAU30	CBV760	Zeolyst	30
BEA	BEA250	980HOA	Tosoh	250
	BEA150	cp811c-300	Zeolyst	150
	BEA75	CZB 150	Clariant	75
MOR	MOR120	690HOA	Tosoh	120
MFI	MFI750	890HOA	Tosoh	750
	MFI45	CZP90	Clariant	45

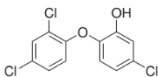
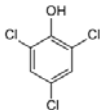
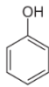
<sup>a</sup> The name of zeolites in this study was composed by framework type and Si/Al ratio provided by suppliers.

<sup>b</sup> Si/Al ratio provided by suppliers

## 2.2 Organic compounds

Triclosan, TCP and phenol (analytical standards) were purchased from Sigma-Aldrich, the Netherlands. Their physicochemical properties are listed in Table 2.

**Table 2** The structures and physicochemical properties of OMPs

Name	Formula	MW (g mol <sup>-1</sup> )	Solubility in water <sup>a</sup> (mg L <sup>-1</sup> )	LogD at pH 6 <sup>b</sup>	pka <sup>b</sup>	Molecular size <sup>c</sup> (Å*Å*Å) X*Y*Z	Structure
Triclosan	C <sub>12</sub> H <sub>7</sub> Cl <sub>3</sub> O <sub>2</sub>	289.54	10	5.21	8.8	5.82*3.40*8.68	
2,4,6-trichloro phenol	C <sub>6</sub> H <sub>3</sub> Cl <sub>3</sub> O	197.45	800	3.58	6.2	5.43*0.32*6.28	
Phenol	C <sub>6</sub> H <sub>6</sub> O	94.11	8.28*10 <sup>4</sup>	1.41	10.0	4.34*0.87*5.55	

<sup>a</sup> Estimated by EPIWEB 4.1

<sup>b</sup> Estimated by ACD/LABs PhysChem Module (Algorithm Version: 5.0.0.184)

<sup>c</sup> Estimated by Hyperchem 7.0 after geometric optimization

## 2.3 Characterization of high-silica zeolites

Multiple methods were used to characterize the material properties of the high-silica zeolites. BET surface area and pore volume of high-silica zeolites were determined by N<sub>2</sub> gas adsorption at 77K (Gemini VII 2390p analyzer, Micromeritics). The surface area and volume of micropores (pore size less than 2nm) were estimated by the t-plot method which separates the micropores from multilayer adsorption of N<sub>2</sub> gas (Lippens and de Boer 1965; Scherdel et al., 2010). XRF analyses were performed with a Panalytical Axios Max WD-XRF spectrometer to characterize the Si/Al ratio of high-silica zeolites. The data evaluation was conducted using SuperQ5.0i/Omnian software.

Two types of acid sites, i.e. Brønsted acid sites (BAS) and Lewis acid sites (LAS), exist in high-silica zeolites. The BAS are weakly bound protons of a bridging hydroxyl group,

typically between silica and aluminium ( $-\text{Si}-\text{OH}^+-\text{Al}-$ ). LAS are formed at the extra framework aluminium species and framework defects of hydrogen-type high-silica zeolites (Weitkamp and Hunger 2007). The number of BAS and LAS were determined by transmission Fourier-transform infrared spectroscopy (FTIR, Nicolet 6700 spectrometer equipped with MCT/B detector) using pyridine as a probe molecule. Zeolite samples were pressed into disks with a radius of 0.8 cm and a weight of 50 mg. The disk was activated in vacuum at 400 °C for 16h to remove the adsorbed species. After activation, the disk was saturated with pyridine vapour and evacuated at 160 °C for 2h. The number of BAS and LAS was derived from the bands at 1545 and 1456  $\text{cm}^{-1}$  of FTIR spectra. The integrated molar extinction coefficients of BAS and LAS were 1.67 and 2.22, respectively (Emeis 1993). By assuming that one pyridine molecule is adsorbed on one acid site, the number of BAS and LAS ( $C_{\text{BAS}}$  and  $C_{\text{LAS}}$ ), was calculated by the following equations:

$$C_{\text{BAS}} = 1.88 \times IA(B) \times R^2 / W \quad \text{Equation 1}$$

$$C_{\text{LAS}} = 1.42 \times IA(L) \times R^2 / W \quad \text{Equation 2}$$

where  $IA(B)$  and  $IA(L)$  are the integrated absorbance of BAS and LAS band ( $\text{cm}^{-1}$ ), respectively,  $R$  is the radius of zeolite disk (cm) and  $W$  is the mass of zeolite sample (mg).

## 2.4 Adsorption isotherm models

The adsorption isotherms were interpreted using different models. The isotherm constants were determined to estimate the maximum adsorption capacity of OMPs and to compare the adsorption efficacy of high-silica zeolites.

The Langmuir model (Langmuir 1916) has been widely used to describe monolayer adsorption. The model assumes that each adsorption site can hold only one adsorbate molecule. There is no interaction between molecules adsorbed on neighbouring sites. The equation can be expressed as:

$$q_e = \frac{q_m K_L C_e}{1 + K_L C_e}$$

where  $q_e$  is the amount of solute adsorbed per unit weight of adsorbent at equilibrium ( $\mu\text{mol g}^{-1}$ ),  $C_e$  is the equilibrium concentration of the solute in the aqueous solution ( $\mu\text{mol}$

$L^{-1}$ ),  $q_m$  is the maximum adsorption capacity ( $\mu\text{mol g}^{-1}$ ), and  $K_L$  is the constant related to the free energy of adsorption ( $L \mu\text{mol}^{-1}$ ).

The Freundlich model (Freundlich 1906) is an empirical model assuming that as the adsorbate concentration increases, the concentration of adsorbate on the adsorbent surface also increases. The Freundlich model can be applied to the adsorption heterogeneous surfaces and for multi-layer adsorption. The equation can be written as:

$$q_e = K_F C_e^n$$

where  $K_F$  is a constant indicative of the relative adsorption capacity of the adsorbent ( $(\mu\text{mol g}^{-1})(L \mu\text{mol}^{-1})^n$ ) and  $n$  is a constant indicative of the intensity of the adsorption. In this study, Freundlich model was interpreted when the adsorption isotherm did not reach a plateau. The adsorption efficiencies of OMPs without adsorption plateau can be compared by simply referring to two constants.

The Langmuir-Freundlich isotherm (Sips 1948) is a combined form of the Langmuir and Freundlich isotherms. At low equilibrium concentrations, the adsorption represents the characteristics of the Freundlich isotherm, while it predicts a monolayer adsorption capacity by the Langmuir isotherm at high concentrations. The equation can be expressed as:

$$q_e = \frac{q_m K_{LF} C_e^n}{1 + K_{LF} C_e^n}$$

where  $q_m$  is the maximum adsorption capacity ( $\mu\text{mol g}^{-1}$ );  $K_{LF}$  is the constant related to the free energy of adsorption ( $L \mu\text{mol}^{-1}$ );  $n$  is a constant indicative of the intensity of the adsorption. In this study, Langmuir-Freundlich model was used to estimate the maximum adsorption capacity where the adsorption plateau appeared.

## 2.5 Adsorption experiments

Batch adsorption experiments were conducted in demineralised water. High-silica zeolites (3 mg) were dosed into 100 ml aqueous solution with the varied concentration of 1 to 60  $\mu\text{mol L}^{-1}$  of a single OMP solute. After the equilibrium time of 24h at room temperature ( $25 \pm 1$  °C) (Damjanovic et al., 2010), high-silica zeolites were separated from the solution by membrane filtration (0.2  $\mu\text{m}$  syringe filter, Whatman SPARTAN™).



## 2.6 HPLC analysis

The concentrations of triclosan, TCP and phenol were determined by HPLC (Shimadzu, Japan) with a C18 column (Phenomenex® KINETEX, 4.6mm) at 30 °C. HPLC-grade acetonitrile (Sigma-Aldrich, The Netherlands) and ultra-pure water (ELGA, Ultra AN MK2 ultrapure water system) were mixed as the mobile phase. The acetonitrile and water ratios (V:V) were 75:25, 65:35 and 25:75 for triclosan, TCP and phenol, respectively. The flow rate of the mobile phase was 1.0 ml min<sup>-1</sup>. The wavelength of the UV detector was set at 280 nm.

## 3 Results

### 3.1 Characterization of high-silica zeolites

The pores of the high-silica zeolites were characterized by surface area and pore volume and are shown in Table 3. As shown in Table 3, zeolites with a higher surface area had a higher micropore volume. The surface area and pore volume of pores per gram of zeolites of various types followed the order of FAU > BEA > MOR > MFI.

**Table 3** The structural and chemical characteristics of high-silica zeolites

Zeolite name	Pore opening size (Å*Å)	Surface area (m <sup>2</sup> g <sup>-1</sup> )	Micropore surface area (m <sup>2</sup> g <sup>-1</sup> )	Pore volume (cm <sup>3</sup> g <sup>-1</sup> )	Micropore volume (cm <sup>3</sup> g <sup>-1</sup> )	Si/Al ratio from XRF	BAS <sup>a</sup> (μmol g <sup>-1</sup> )	LAS <sup>b</sup> (μmol g <sup>-1</sup> )
FAU250	7.4*7.4	727	591	0.5136	0.2623	409	N.D.	N.D.
FAU50		698	571	0.5160	0.2545	43	19	12
FAU40		606	447	0.4819	0.1966	32	13	17
FAU30		789	548	0.5233	0.2445	31	133	45
BEA250	6.6*7.7 5.6*5.6	516	351	0.3022	0.1557	286	16	7
BEA150		524	364	0.3243	0.1623	107	54	8
BEA75		563	396	0.3720	0.1761	78	85	16
MOR120	6.5*7.0 2.6*5.7	431	360	0.2687	0.1606	113	52	8
MFI750	5.1*5.5	334	282	0.1702	0.1260	891	N.D.	N.D.
MFI45	5.3*5.6	359	199	0.5341	0.0891	42	142	40

The proportion of micropores accounting for the total pores of high-silica zeolites is shown in Figure 1. Micropores, which were characterized by micropore surface area and micropore volume, accounted for a large proportion of the zeolite pores. Except for zeolite MFI45, more than 60% of the surface area and 40% of the pore volume were composed by micropores. The surface area and volume of micropores in the FAU zeolites was the highest, while the BEA, MOR and MFI zeolites had a similar but lower surface area and volume of micropores.

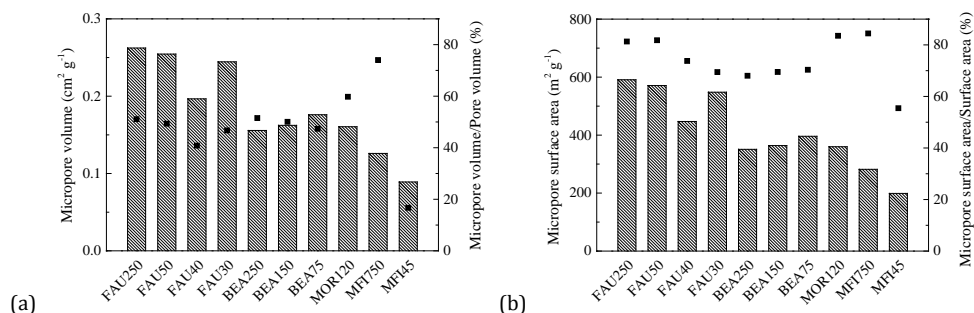


**Figure 1** The proportion of micropores accounting for the total pores of high-silica zeolites. Micropores are represented by micropore volume (the bars in Figure 1a) and micropore surface area (the bars in Figure 1b). ■ represent the percentage proportion of micropores accounting for the total pores.

The properties relating to the surface chemistry of zeolites can be characterized by Si/Al ratios and acid sites. The results are shown in Table 3. Si/Al ratios of zeolites were both provided by suppliers and determined by XRF, shown in Figure 2. Except for zeolite FAU250 with a variation of 64%, variations of -28 % to 18 % were found between the supplier-provided and the XRF-determined Si/Al ratios.

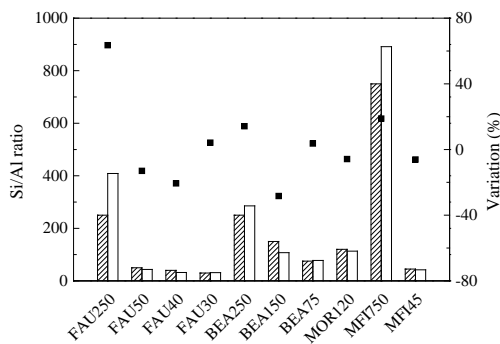


**Figure 2** Comparison of Si/Al ratios given by suppliers (bar with diagonal lines) and measured by XRF analysis (solid bars). ■- is the variation percentage of the XRF-determined Si/Al ratio with the supplier-provided Si/Al ratio.

The number of BAS and LAS in the zeolites are shown in Table 3. The variation of BAS and LAS with Al content of zeolites are plotted in Figure 3. Al content was represented by Al% and expressed by the following equation:

$$Al\% = \frac{Si}{Si+Al} \% = \frac{1}{1+Si/Al \text{ ratio}} \% \quad \text{Equation 3}$$

As shown in Figure 3, zeolites had more BAS than LAS. The number of LAS and BAS in FAU and BEA zeolites increased with Al% of zeolites and thus, decreased with Si/Al ratio of zeolites. For example, the number of BAS and LAS in BEA zeolites followed the order of BEA250 > BEA150 > BEA75. No acid sites could be detected from zeolites FAU250 and MFI750 since their Al content was negligible. One exception was the number of BAS in FAU30, which was lower than LAS and also lower than BAS in FAU40. The number of acid sites varied with the framework of zeolites. As shown in Figure 3, the number of acid sites from BEA, MOR and MFI zeolites was higher than FAU-type zeolites with similar Al content. The effect of Si/Al ratios and acid sites on the OMP adsorption efficacy by high-silica zeolites will be further discussed in Section 4.3.

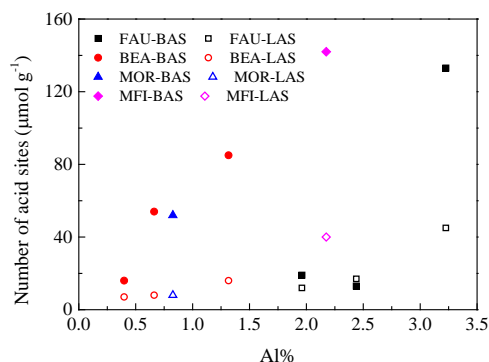
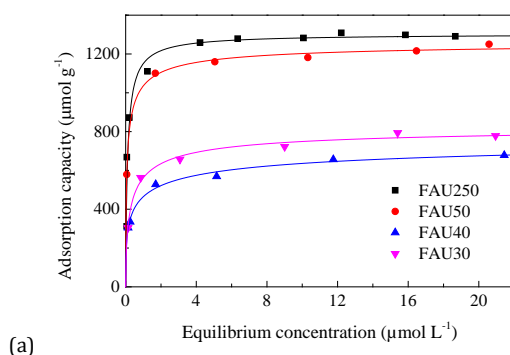


**Figure 3** The variation of BAS (solid symbols) and LAS (open symbols) with Al% of zeolites.

### 3.2 Adsorption of triclosan by high-silica zeolites

The adsorption isotherms of triclosan by high-silica zeolites were compared in Figure 4. The maximum adsorption capacity of zeolites were estimated by the isotherm constants of  $Q_{LF}$  from Langmuir-Freundlich model (Table 4). The isotherms were not interpreted by Freundlich model since Freundlich model could not estimate adsorption capacity. The adsorption capacity of triclosan varied by the framework type of zeolites. FAU zeolites had a higher adsorption capacity than BEA and MOR zeolites (refer to  $Q_{LF}$  in Table 4). The adsorption capacity of MFI zeolites was minimal and therefore excluded from the graph. The adsorption efficacy of triclosan also varied with the properties of high-silica zeolites, e.g. porous properties and Si/Al ratio of zeolites, which will be discussed in Sections 4.2 and 4.5.



(a)

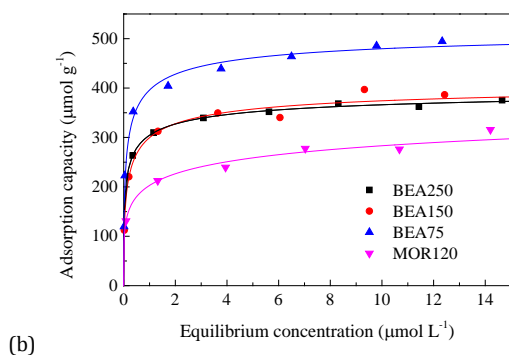


**Figure 4** The adsorption isotherms of triclosan by (a) FAU-type, (b) BEA-type and MOR-type zeolites and the Langmuir-Freundlich model fitting curves (solid lines).

**Table 4** Langmuir-Freundlich isotherm constants for triclosan adsorption onto different zeolites.

	FAU250	FAU50	FAU40	FAU30	BEA250	BEA150	BEA75	MOR120
$Q_{LF}$ ( $\mu\text{mol g}^{-1}$ )	1304	1271	825	837	414	420	530	529
$K_{LF}$ ( $\text{L } \mu\text{mol}^{-1}$ )	7.4891	4.3922	1.2865	2.0359	2.7849	2.4775	2.9514	0.6211
$n$	0.9006	0.5980	0.4157	0.6170	0.4408	0.5142	0.5079	0.2676
$R^2$	0.9373	0.9929	0.9823	0.9873	0.9864	0.9767	0.9836	0.9647

### 3.3 Adsorption of 2,4,6-trichlorophenol (TCP) by high-silica zeolites

As shown in Figure 4, zeolites with same framework type had the same isotherm shape for triclosan adsorption, although the adsorption capacity of triclosan varied with the framework of zeolites. High-silica zeolites with highest Si/Al ratio of each framework type, namely FAU250, BEA250, MOR120 and MFI750, were thus chosen to study the effect of framework type on TCP adsorption. The adsorption isotherms of TCP by FAU250, BEA250 and MOR120 are displayed in Figure 5. FAU250 was the most efficient adsorbent for TCP in the studied concentration range ( $0 - 25 \mu\text{mol L}^{-1}$ ), while the adsorption capacities of BEA250 and MOR120 zeolites were much less than that of FAU250. MFI750 had minimal adsorption of TCP and was therefore not included in the graph.

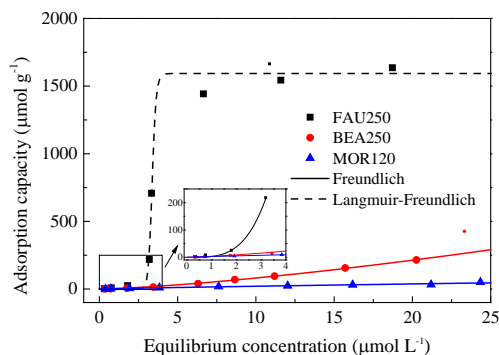


**Figure 5** The adsorption isotherms of TCP by (a) FAU250 and (b) BEA250 and MOR120 and the fitting curves (Solid lines: Freundlich model fitting; Dashed lines: Langmuir-Freundlich model fitting).

FAU250 zeolites showed an S-shaped adsorption isotherm with good fitting to the Langmuir-Freundlich model at the concentration range of 0 - 25  $\mu\text{mol L}^{-1}$  ( $R^2 = 0.9804$ , Figure 5 and Table 5) At the equilibrium concentration range 0 – 4  $\mu\text{mol L}^{-1}$ , the adsorption capacity reached  $\sim 200 \mu\text{mol g}^{-1}$ , which were well fitted with the Freundlich model (isotherm constants, Table 6). The steep slope of the isotherm curve occurred at the equilibrium concentration of about 3.2  $\mu\text{mol L}^{-1}$ . The S-shaped curve reached the plateau with estimated adsorption capacity of 1593  $\mu\text{mol g}^{-1}$  by Langmuir-Freundlich models (Table 5). TCP adsorption by BEA250 and MOR120 zeolites without adsorption plateaus were well fitted with the Freundlich isotherms (Figure 5). The isotherm constants are given in Table 6.

**Table 5** Langmuir-Freundlich isotherm constants for TCP adsorption by FAU250 zeolite fitting at the equilibrium concentration range of 0 - 25  $\mu\text{mol L}^{-1}$ .

$Q_{LF} (\mu\text{mol g}^{-1})$	$K_{LF} (\text{L } \mu\text{mol}^{-1})$	$n$	$R^2$
1593	$3.92 \times 10^{-15}$	27.26	0.9804

**Table 6** Freundlich isotherm constants for TCP adsorption by FAU250 fitting at the equilibrium concentration of 0 - 4  $\mu\text{mol L}^{-1}$ , BEA250 and MOR120 fitting at the equilibrium concentration of 0 - 25  $\mu\text{mol L}^{-1}$ .

	FAU250	BEA250	MOR120
$K_F (\mu\text{mol g}^{-1})(\text{L } \mu\text{mol}^{-1})^n$	2.8621	3.3002	2.7582
$n$	3.7352	1.3911	0.8720
$R^2$	0.9970	0.9867	0.9555

### 3.4 Adsorption of phenol by high-silica zeolites

The adsorption isotherms of phenol by high-silica zeolites with different frameworks are shown in Figure 6. Compared with triclosan and TCP, phenol was adsorbed to a much lesser extent by high-silica zeolites at the same equilibrium concentration range (0 - 20  $\mu\text{mol L}^{-1}$ ). The low adsorption efficacy of phenol was revealed from the low adsorption capacity and the isotherms without adsorption plateaus.

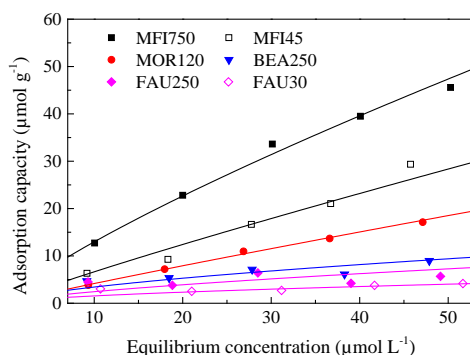


**Figure 6** The adsorption isotherm of phenol by different high-silica zeolites and the Freundlich fitting curves (solid lines).

Phenol adsorption by high-silica zeolites was well fitted with the Freundlich isotherm. The isotherm constants are given in Table 7. MFI zeolites exhibited the best phenol adsorption capacity of the tested zeolites. The adsorption efficacy of zeolites followed the order of  $\text{MFI750} > \text{MFI45} > \text{MOR120} > \text{BEA250} > \text{FAU250} > \text{FAU30}$ , which was in the opposite

order of the maximum adsorption capacity of triclosan and TCP (FAU > BEA > MOR, Figure 4 and Figure 5).

**Table 7** *Freundlich isotherm constants for phenol adsorption by MFI750, MFI45, MOR120 BEA250, FAU250 and FAU30 zeolites.*

	MFI750	MFI45	MOR120	BEA250	FAU250	FAU30
$K_F (\mu\text{mol g}^{-1})(\text{L } \mu\text{mol}^{-1})^n$	2.0350	0.8354	0.4936	0.8097	0.5140	0.3947
$n$	0.8045	0.9009	0.9265	0.6265	0.6771	0.5939
$R^2$	0.9937	0.9672	0.9974	0.9233	0.7342	0.9036

## 4 Discussion

### 4.1 The properties of OMPs and their relationship with the adsorption efficacy

The maximum adsorption capacity of an OMP was related to the OMP size. For example, FAU250 provided a higher adsorption capacity for TCP ( $1593 \mu\text{mol g}^{-1}$ , Table 5) than for triclosan ( $1304 \mu\text{mol g}^{-1}$ , Table 4), while triclosan is more hydrophobic than TCP. Considering that the pore opening size of FAU zeolites is supposed to be larger than the molecular size of both triclosan and TCP, the adsorption of OMPs would happen in the same type of cages with a pore opening size  $7.4 \text{ \AA} \times 7.4 \text{ \AA}$ . Since the molecular size of TCP is smaller than the size of triclosan, more TCP molecules could be trapped in one cage, explaining the preferred adsorption in the case of more TCP-molecules in one cage.

Previous studies have shown that the decreased interactions between OMP and water will enhance the OMP-zeolite interactions, and a strong correlation between the adsorption capacity and hydrophobicity of OMPs has been observed (Fukahori et al., 2011; Koubaissy et al., 2008). In this study, the theory was confirmed by the higher adsorption efficacies of triclosan and TCP than phenol.



## 4.2 The characterization of high-silica zeolites and their effect on the adsorption capacity of triclosan

The maximum adsorption capacity of triclosan by FAU, BEA and MOR zeolites are observed from the isotherms. The effect of volume and surface area of micropores, pore volume, surface area and Al content on the maximum adsorption capacity of triclosan is shown in Figure 7 (The effect of Si/Al ratio and Al content, Section 4.5). The maximum adsorption capacity of zeolites (from Langmuir-Freundlich model, Table 3) was more closely correlated to the volume and surface area of micropores than the pore volume and surface area, which indicate that micropores of zeolites dominated the adsorption of triclosan. Compared with the mesopores (pore diameter of 2-50 nm) and macropores (pore diameter of > 50 nm), the size of the micropores (pore diameter of < 2 nm) is closer to the size of the triclosan. Thus, triclosan would experience stronger adsorption forces originating from the “walls” of the micropores.

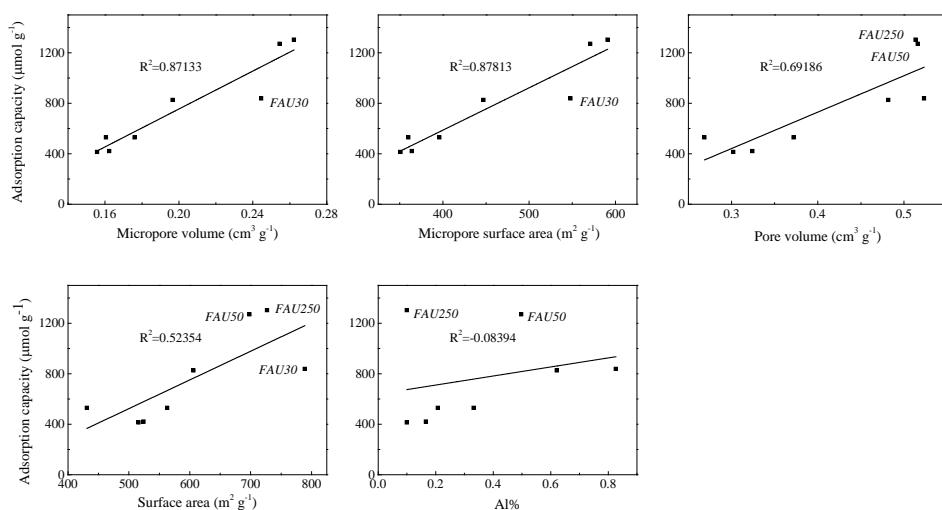


**Figure 7** The correlation between the maximum adsorption capacity of triclosan (estimated from Langmuir-Freundlich isotherms, refer to Table 4) and the properties of high-silica zeolites.

The micropores of zeolites varied in a range due to their different synthetic processes (Yu 2007), while zeolites synthesized in the same way could possess similar micropore volume and surface area. In this case, other properties of zeolites, e.g. Al%, could dominate the

adsorption efficacy (Yonli et al., 2012). Moreover, the effect of micropore volume and surface area has not been determined in some studies since the micropores of zeolites were not measured (Damjanovic et al., 2010; Gonzalez-Olmos et al., 2013).

### 4.3 The occurrence of the S-shaped isotherm curve

Notably, an S-shaped curve was observed for TCP adsorption by FAU250 zeolite. When the OMP intermolecular attraction effects are large, an isotherm with S-shaped is observed (Ruthven 1984). The affinity of TCP for the surface of FAU250 zeolites was low at the starting concentration range of 0 – 3.2  $\mu\text{mol L}^{-1}$  (Figure 5). The pores of high-silica zeolites were then partly filled by TCP molecules. More TCP molecules by experiencing intermolecular attractions could be easily adsorbed, which greatly enhances the adsorption capacity and leads to adsorption saturation (Hinz 2001; Karimi-Lotfabad et al., 1996). The intermolecular attraction might be generated from  $\pi$  -  $\pi$  interactions of TCP benzene rings (Janiak 2000; Waters 2002).

The occurrence of the S-shaped adsorption isotherm might be attributed to the specific pore topology of FAU zeolites. FAU zeolites possess wide  $\alpha$ -cages with an opening size of 7.4 Å\*7.4 Å (Table 3) and an enlarged inner pore diameter 13.7 Å (Baerlocher et al., 2007), which apparently was able to provide accommodation for more than one TCP molecule. As a comparison, BEA and MOR zeolites possess channel systems. The possible locations of adsorbed OMPs in the channels of zeolites are channel intersections with one molecule per intersection (Guvenc and Ahunbay 2012). The distance between channel intersections could inhibit the interaction between TCP molecules.

A high Si/Al ratio could also be an essential condition of the S-shaped curve and interaction of TCP. Zeolites with a lower Si/Al ratio might promote water adsorption and weaken the interaction between TCP molecules, as observed by Zhang et al. (2014) and Yang et al. (2016). Zhang et al. (2014) studied TCP adsorption by FAU zeolites with a lower Si/Al ratio ( $\geq 15$ ). At the TCP concentration range 0 – 150  $\mu\text{mol L}^{-1}$ , which was much higher than the equilibrium concentration in their study, the adsorption isotherm did not show either an S-shaped trend or the adsorption plateau. Yang et al. (2016) also applied FAU zeolites with a Si/Al ratio of 40 for TCP adsorption and the adsorption plateau was observed.

#### 4.4 Phenol adsorption and close-fit theory

At the studied concentration range, phenol adsorption by MFI zeolites, which have smaller pore sizes than other types of zeolites, was higher than on FAU zeolites, which have larger pore opening sizes and a higher volume and surface area of micropores. The favourable adsorption on MFI zeolites could be attributed to the pore size effect. The pores of MFI zeolites originate from a channel system with opening sizes of  $5.1 \text{ \AA} \times 5.5 \text{ \AA}$  and  $5.3 \text{ \AA} \times 5.6 \text{ \AA}$  (Table 3), which closely fit phenol molecules with a molecular size of  $4.34 \text{ \AA} \times 0.87 \text{ \AA} \times 5.55 \text{ \AA}$  (Table 2). Closely fitted pores will promote the adsorption efficacy of OMPs by generating stronger adsorption forces between OMPs and the “wall” of micropores (Su et al., 2005). Damjanovic et al. (2010) found that the heat evolved by phenol adsorption on BEA zeolites was lower than in the case of MFI zeolites with better fitted pores for phenol, thus indicating a weaker interaction. The so-called “close-fit” phenomenon has previously been noted from, e.g. the adsorption of multi-solutes by MOR zeolites, as well as the adsorption of MTBE by MFI zeolites (Erdem-Senatalar et al., 2004). Giaya and Thompson (Giaya and Thompson 2002a; b) proposed that closely fitted pores would reduce the number of water clusters and that the interaction between OMPs and the framework of zeolites would be stronger.

The occurrence of “close-fit” is also influenced by the pore structure. In the channel-based pores, the inner size of pores is the similar to the pore opening size of zeolites. OMPs, e.g. phenol, with a fitted size for the pore opening could then enter and well fit the channel, such as those found in MFI and MOR zeolites. However, “close fit” is unlikely to happen in the cage-based pores, e.g. cages of FAU zeolites, since OMPs with fitted sizes for the pore opening ( $7.4 \text{ \AA}$ ) will be somewhat smaller than the size of internal pores ( $13.7 \text{ \AA}$ ) (Baerlocher et al., 2007), resulting in an unfavoured adsorption of phenol by FAU zeolites (Figure 6).

#### 4.5 Surface hydrophobicity and active adsorption sites of high-silica zeolites

High-silica zeolites feature a high silica content and, thus, a relatively hydrophobic surface. The water affinity for high-silica zeolites was characterized by either Si/Al ratio or the number of acid sites (Table 3).

The effect of Si/Al ratio (Al content) on the adsorption efficacy of high-silica zeolites has been frequently observed. Owing to the highly hydrophobic surface, zeolites with a higher Si/Al ratio (Al content) have shown a higher adsorption capacity of OMPs, e.g. nitrobenzene and  $\alpha$ -endosulfan (Reungoat et al., 2007; Yonli et al., 2012). The surface hydrophobicity of zeolites, however, had a less pronounced effect on the maximum adsorption capacity of triclosan than the micropore volume and surface area in this study (Figure 7). Since triclosan is hydrophobic and weakly interacts with water, triclosan adsorption in the pores of zeolites might trigger the water desorption and pore filling by triclosan (Damjanovic et al., 2010). Thus, water adsorption that was enhanced by the Al content of zeolites would not affect the maximum adsorption capacity of triclosan.

High-silica zeolites possess a certain number of acid sites (number of LAS and BAS, Table 3) and associated base sites, which might act as active adsorption sites for OMPs (Beutel et al., 2001; Beutel and Su 2005). From Table 3, it can be observed that MFI45 and FAU30 possess over 100  $\mu\text{mol L}^{-1}$  more active adsorption sites than MFI750 and FAU250. However, MFI750 and FAU250, with fewer adsorption sites, showed an enhanced adsorption efficacy over MFI45 and FAU30 of phenol (Figure 6 and Table 7). Since the active adsorption sites originated from the Al content of zeolites where water clusters preferably gathered, phenol adsorption could experience even stronger water competition at the active adsorption sites than at other adsorption sites (Bolis et al., 2006). Therefore, phenol adsorption could be inhibited.

A number of silanol groups (Si-OH) exist in the framework of zeolites and are able to adsorb water molecules and polar OMPs, such as methanol, by forming H-bonding (Batonneau-Gener et al., 2008; Meininghaus and Prins 2000). In addition, Bal'zhinimaev et al. (2019) found that the Si-OH groups in FAU250 exist as silanol nests in the cages of the zeolite, while silanol nests in MOR240 are located in the channel entrances. Probably, water molecules interacted with the silanol nests by H-bonding and then formed a strong complex. Since phenol is more hydrophilic and polar than triclosan and TCP, phenol is therefore more likely to be adsorbed on the Si-OH groups by replacing water molecules.

#### 4.6 Comparison with other adsorbents

The adsorption efficacies of triclosan, TCP and phenol by high-silica zeolites and other commonly used adsorbents, e.g. carbonaceous materials and clays, are compared in Table

S1, S2 and S3. When the adsorption plateau was observed, the maximum monolayer adsorption capacity could be estimated by Langmuir and Langmuir-Freundlich isotherms. At the adsorption stage without a plateau, adsorption efficacy was characterized by the  $K_F$  value from Freundlich isotherm and the obtained maximum adsorption loading, either given in the literature or recalculated by given experimental data.

In comparison with other adsorbents, high-silica zeolites featured a high monolayer adsorption capacity for triclosan (378 mg g<sup>-1</sup> in Table S1, translated from the  $Q_{LF}$  of FAU250 zeolite in Table 4). The monolayer adsorption capacity of triclosan increased with the pore surface area. Clay adsorbents with a small surface area of pores, e.g. kaolinite and montmorillonite, proved to be less efficient for triclosan adsorption (Wang et al., 2017). Benefitting from the hydrophobic surface, high-silica zeolites had the highest  $K_F$  value among the reported results (1163 (mg g<sup>-1</sup>)(L mg<sup>-1</sup>)<sup>n</sup>, in Table S1), indicating their high adsorption efficacy at low concentration.

At the low concentration range without the adsorption plateau, carbon nanotubes and graphene showed a high adsorption efficacy too. For instance, carbon nanotubes could achieve an adsorption loading of about 367 mg g<sup>-1</sup> at the concentration range 0 – 1 mg L<sup>-1</sup>. It might be attributed to the surface functional groups of carbonaceous materials, which would provide strong adsorption forces for triclosan (Cho et al., 2011; Wang et al., 2017).

FAU250, activated carbon fibers and carbon nanotubes were able to achieve the maximum monolayer adsorption capacity of TCP, which was promoted by surface area (Table S2). The finding was consistent with the results of triclosan adsorption. Due to the large number of surface functional groups and the possible condensation of TCP molecules in the pores, carbon nanotubes showed great adsorption efficacy at the low concentration range. Other adsorbents, including AC, failed to reach the adsorption plateau, which indicated their low affinity for TCP adsorption.

With the exception of FAU250 zeolites in this study, S-shaped isotherm curves of TCP adsorption by solid adsorbents were not observed. Regarding the pore topology, TCP interactions are more likely to occur in the uniform micropores of zeolites than in the pores of adsorbents with widely distributed sizes, e.g. AC (Radhika and Palanivelu 2006), or in adsorbents with sizes much larger than TCP, e.g. carbon nanotubes with mesopores (Chen et al., 2009). For example, Qin et al. (2012) studied the adsorption of TCP by SBA-15,

a silica based material with mesopores (average pore size 5nm). The adsorbed TCP molecules were more likely to locate separately in the mesopores, which would not support the intermolecular attraction of TCP.

Compared with high-silica zeolites, phenol adsorption was favoured by carbon-based adsorbents, e.g. activated carbon and AC fibres, as indicated by their high adsorption capacity (Dobbs and Cohen 1980; Liu et al., 2010). Roostaei and Tezel (2004) compared phenol adsorption by different solid adsorbents. At the equilibrium concentration of  $\sim 120 \text{ mg L}^{-1}$ , the adsorption loading of activated carbon and FAU zeolites were  $\sim 268 \text{ mg g}^{-1}$  and  $\sim 17 \text{ mg g}^{-1}$ , respectively.

It is well-known that the carbon-based solid adsorbents possess a large number of functional groups as the adsorption sites for phenol, e.g. carboxyl and carbonyl, which would interact with acidic OMPs, e.g. phenol (Chen et al., 2009; Hamdaoui and Naffrechoux 2007; Liu et al., 2010). The aromatic ring of OMPs also experience  $\pi$ - $\pi$  interactions with the carbon surface. Both interactions promote the adsorption efficacy of OMPs, especially at a low concentration range (Dabrowski et al., 2005; Su et al., 2005). The effect of active adsorption sites of high-silica zeolites was less pronounced than the carbon based adsorbents due to lack of organic functional groups in high-silica zeolites and the possible inhibition for phenol adsorption as discussed in Section 4.3.

## 5 Conclusions

The adsorption efficacy of triclosan, TCP and phenol by high-silica zeolites was studied. The adsorption behaviour and mechanisms were illustrated by various shapes of adsorption isotherms. The adsorption efficacy of OMPs by high-silica zeolites was related to the properties of OMPs, the porous and surface chemistry features of high-silica zeolites. The conclusions are summarized as below:

- Triclosan and TCP were more favourably adsorbed by FAU-type high-silica zeolites than BEA-, MOR- and MFI-type zeolites. The maximum adsorption capacity of triclosan was related to the micropore volume or micropore surface area of zeolites, rather than the hydrophobicity of the zeolites. The maximum adsorption capacity of FAU250 zeolites for OMPs with smaller molecular sizes, e.g. TCP, was higher.

- S-shaped adsorption isotherms indicated the inefficient removal of TCP at low concentrations. The occurrence of an S-shaped isotherm in the TCP adsorption by FAU250 zeolites could relate to the large sized cages of FAU zeolites which allowed the intermolecular attractions between multi TCP molecules. A high Si/Al ratio could also be an essential condition of the S-shaped curve and interaction of TCP.
- Closely fitted pores of high-silica zeolites promoted the adsorption efficacy of phenol, which typically has a low affinity for high-silica zeolites. The occurrence of “close-fit” was more observed with channel-based zeolites, e.g. MFI-type zeolites, compared to cage-based zeolites, e.g. FAU-type zeolites.
- The adsorption of OMPs by high-silica zeolites benefitted from the rich amount and closely fitted arrangement of the pores for OMPs. Compared with carbon-based materials, the lack of effective active adsorption sites limited the adsorption of phenol by high-silica zeolites, especially at the low concentration range where no maximum adsorption capacity was observed.

## Supporting information

**Table S1** Comparison of various adsorbents for the adsorption of triclosan.

Adsorbent	Surface area  $\text{m}^2 \text{g}^{-1}$	$C_e$  $\text{mg L}^{-1}$	Adsorption plateau observed in the experiment ?	Estimated Maximum monolayer adsorption capacity  $\text{mg g}^{-1}$	Freundlich isotherm constants  $K_F (\text{mg g}^{-1})(\text{L mg}^{-1})^n/n$	Maximum adsorption loading  $\text{mg g}^{-1}$	Ref.
FAU250	789	0 – 4	Yes	378	1163/2.7 <sup>a</sup>		This work
AC	1334	0 – 20	Yes	714	254/0.83 <sup>b</sup>		(Liu et al., 2014b)
Magnetic activated carbon	674	0 – 35	Yes	303	150/0.21		(Liu et al., 2014b)
Carbon nanotube	1020	0 – 0.1	No		1754/0.68	~367	(Cho et al., 2011)
Graphene	212	0 – 0.02	No		1.0*e5/2.24	~10	(Wang et al., 2017)
Kaolinite	2.3	0 – 55	No		0.04/1.25	~9	(Behera et al., 2010)
Montmorillonite	34	0 – 45	No		0.005/2.0	~18	(Behera et al., 2010)

<sup>a</sup> Recalculated by the experimental data at the fitting concentration range of 0 – 0.04  $\text{mg L}^{-1}$ .

<sup>b</sup> Recalculated by the isotherm data given in the literature at the fitting concentration range of 0 – 1  $\text{mg L}^{-1}$



**Table S2** Comparison of various adsorbents for the adsorption of TCP.

Adsorbent	Surface area  m <sup>2</sup> g <sup>-1</sup>	C <sub>e</sub>  mg L <sup>-1</sup>	Adsorption plateau observed in the experiment ?	Estimated maximum monolayer adsorption capacity  mg g <sup>-1</sup>	Freundlich isotherm constants  K <sub>F</sub> (mg g <sup>-1</sup> )(L mg <sup>-1</sup> ) <sup>n</sup> /n	Maximum adsorption loading  mg g <sup>-1</sup>	Ref.
FAU250	789	0 – 4	Yes	314	143/1.90 <sup>a</sup>		This work
Activated carbon fibers	920	0 - 90	Yes	481	240/ 0.39 <sup>b</sup>		(Liu et al., 2010)
Carbon nanotubes	559	0 - 20	Yes	182	986.9/ 2.10 <sup>c</sup>		(Chen et al., 2009)
BEA250	516	0 – 3.5	No		6.26/ 1.39	31	This work
SBA-15	744	0 - 28	No		0.716/ 0.53	~4	(Qin et al., 2012)
Ash	410	0 - 200	No		8.43/ 0.48	~200	(Chen et al., 2014)
Coconut shell-based AC treated by base	935	0 - 500	No		2.045/ 0.68	~120	(Radhika and Palanivelu 2006)
Coconut shell-based Commercial activated carbon	838	0 - 500	No		0.944/ 0.60	~110	(Radhika and Palanivelu 2006)
Activated clay	13	0 - 150	No		4.42/ 0.69	~70	(Hameed 2007)

<sup>a</sup> Recalculated by the experimental data at the fitting concentration range of 0 – 0.63 mg L<sup>-1</sup>.

<sup>b</sup> Recalculated by the isotherm data given in the literature at the fitting concentration range of 0 – 6.3 mg L<sup>-1</sup>.

<sup>c</sup> Recalculated by the isotherm data given in the literature at the fitting concentration range of 0.1 – 0.26 mg L<sup>-1</sup>.

**Table S3** Comparison of various adsorbents for the adsorption of phenol.

Adsorbent	Surface area m <sup>2</sup> g <sup>-1</sup>	C <sub>e</sub> mg L <sup>-1</sup>	Adsorption plateau observed in the experiment ?	Estimated Maximum monolayer adsorption capacity mg g <sup>-1</sup>	Freundlich isotherm constants K <sub>F</sub> (mg g <sup>-1</sup> )(L mg <sup>-1</sup> ) <sup>n</sup> /n	Maximum adsorption loading mg g <sup>-1</sup>	Ref.
Activated carbon fibers	920	0 - 50	Yes	102	29.32/0.94 <sup>d</sup>		(Liu et al., 2010)
AC	858	0 - 150	Yes	309	15.74/0.99		(Roostaei and Tezel 2004)
MF1140	400	0 - 1400	Yes	48	0.18/0.99		(Damjanovic et al., 2010)
BEA43	650	0 - 2400	Yes	68	0.14/0.99		(Damjanovic et al., 2010)
MF1750	334	0 - 5	No		1.28/0.80	~5	This work
FAU zeolite <sup>a</sup>	355	0 - 210	No		0.047/1.25	~40	(Roostaei and Tezel 2004)
AC	1600	0 - 2600	No		6.25/0.45	~200	(Damjanovic et al., 2010)
Granular activated carbon <sup>b</sup>	1018 <sup>c</sup>	0 - 10	No		21/0.54	74	(Dobbs and Cohen 1980)

<sup>a</sup> Si/Al ratio < 20<sup>b</sup> Filtrasorb 300, commercial granular activated carbon<sup>c</sup> (Newcombe et al., 1993)<sup>d</sup> Recalculated by the experimental data at the fitting concentration range of 0 – 2 mg L<sup>-1</sup>



## **CHAPTER 4**

# **THE ADSORPTION MECHANISMS OF ORGANIC MICROPOLLUTANTS ON HIGH-SILICA ZEOLITES CAUSING S-SHAPED ADSORPTION ISOTHERMS**

This chapter is based on: Jiang N.\*, Erdős M., Moulton O.A.\*, Shang R., Vlugt T.J.H., Heijman, S.G., & Rietveld, L.C. The adsorption mechanisms of organic micropollutants on high-silica zeolites causing S-shaped adsorption isotherms, submitted to *Chemical Engineering Journal*.

## Abstract

High-silica zeolites have been proven to be efficient adsorbents for the removal of organic micropollutants (OMPs) from water. OMP adsorption on high-silica zeolites is characterized by adsorption isotherms with various shapes. The occurrence of an S-shaped adsorption isotherm indicates the lack of adsorption affinity for OMPs at low, environmentally relevant equilibrium concentrations. In this study, S-shaped isotherms were observed during batch experiments with 2,4,6-trichlorophenol (TCP) and FAU zeolites. Monte Carlo (MC) simulations in the grand-canonical ensemble were used to obtain a better understanding of the mechanism of the S-shaped adsorption isotherms. From the MC simulation results, it was observed that multiple TCP molecules were adsorbed in the supercages of the FAU zeolites. It was found that the  $\pi$ - $\pi$  interactions between TCP molecules give rise to the adsorption of multiple TCP molecules per supercage, and thus causing an S-shaped adsorption isotherm. Simulations also revealed that water molecules were preferentially adsorbed in the supercages and sodalite cages of the FAU zeolites. FAU zeolites with a higher Al content adsorbed a higher amount of water molecules and a lower amount of TCP, and showed less pronounced S-shaped isotherms.

## 1 Introduction

Zeolites are crystalline, microporous aluminosilicates with a well-defined 3-dimensional structure, composed of tetrahedral  $\text{SiO}_4$  and  $\text{AlO}_4$  clusters connected to each other by shared oxygen atoms. To compensate the charge imbalance caused by the Al content of the framework, exchangeable cations (usually alkali and alkaline earth cations) are located in the cavities of the structure. Due to these intrinsic characteristics, e.g. exchangeable cations and a well-defined pore structure, zeolites are widely used as catalysts, molecular sieves, and adsorbents for air-pollution remediation, removal of volatile organic compounds, gas separation, and catalytic conversion of biomass. (Alonso et al., 2017; Ennaert et al., 2016; Li et al., 2017; Perego et al., 2017; Shi et al., 2017; Sun and Wang 2014; Wajima 2012; Zhang et al., 2016).

An important characteristic of zeolites is the ratio of the Si and Al atoms contained. This ratio determines the level of hydrophobicity in the framework. Based on the Si to Al molar ratio, three types of zeolites can be identified, the low-silica (i.e.,  $\text{Si}/\text{Al} < 2$ ), the medium-

silica (i.e.,  $\text{Si/Al} = 2 - 5$ ) and the high-silica (i.e.,  $\text{Si/Al} > 5$ ) (Burton 2018; Jacobs et al., 2001). Low- and medium-silica zeolites exhibit a high ion exchange capability and are widely applied as water hardness control ingredients in detergents (Maesen and Marcus 2001). High-silica zeolites are particularly useful for removal of organic micropollutants (OMPs) from water, since their hydrophobic nature promotes the adsorption of OMPs instead of water (Lobo 1997; Maesen 2007; Tsitsishvili 1973). As the framework type of the zeolite defines its unique structural features, including pore opening sizes, and cage and channel structures, it highly affects the adsorption efficiency of OMPs (Baerlocher and McCusker 2017; Jiang et al., 2018). Various families of commercially available high-silica zeolites, including the Faujasite (FAU), Mordenite (MOR), Beta (BEA) and ZSM-5 (MFI) types, have been shown to be effective adsorbents for OMP removal from water (Bottero et al., 1994; Braschi et al., 2010; Damjanovic et al., 2010; de Ridder et al., 2012; Rakic et al., 2010; Rossner et al., 2009).

In the process of OMP adsorption from water on solid adsorbents, the adsorption isotherm describes the relation between the equilibrium concentration of OMPs in water and the adsorption loading of OMPs on the solid adsorbents. Giles et al. (1974) have divided the types of adsorption isotherms into the four groups shown in Figure 1. The C-shaped adsorption isotherm (Figure 1a) describes a linear increase of OMP adsorption loading with the equilibrium concentration of OMPs in water, which is often used for a narrow range of OMP concentrations or for very low OMP concentrations, i.e., from a few  $\text{ng L}^{-1}$  to several  $\mu\text{g L}^{-1}$  (Limousin et al., 2007). When the adsorbent has a limited number of adsorption sites, a plateau in the adsorption isotherm appears after a specific equilibrium concentration of OMPs and above, suggesting the saturation of the adsorbent. This results in the L-shaped (Figure 1b) and H-shaped (Figure 1c) isotherms. The steeper increase of OMP adsorption loading in the H-shaped isotherms compared to the L-shaped ones indicates that the zeolites exhibiting H-shaped isotherms have a higher affinity for OMPs.

In some adsorption processes, the isotherms exhibit a characteristic S-shape (Figure 1d) (Inglezakis et al., 2018). This shape can be attributed to the higher attraction between OMPs at the surface of the adsorbent or to a complexation reaction of the metallic species of OMPs with ligands in water (Hinz 2001; Limousin et al., 2007). In general, the occurrence of S-shaped isotherms indicates the unfavorable OMP adsorption at low equilibrium concentrations.

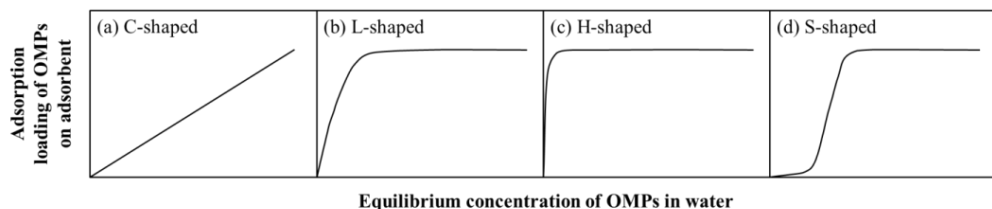


**Figure 1** The four characteristic types of adsorption isotherms as classified by Giles et al., (1974): (a) C-shaped, (b) L-shaped, (c) H-shaped, and (d) S-shaped.

Traditionally, the adsorption of OMPs on adsorbents are mostly obtained from batch experiments. It has been observed in several experimental studies that the adsorption of various OMPs from aqueous solutions on high-silica zeolites result in different types of adsorption isotherms. The adsorption of hydroxycinnamic acids, i.e., p-coumaric acid and ferulic acid, on high-silica zeolites were studied by Simon et al. (2015). At the equilibrium concentration range of 0 – 1 g L<sup>-1</sup>, BEA zeolites showed H-shaped isotherms, while FAU zeolites gave L-shaped isotherms, indicating that BEA zeolites, having smaller pore sizes, have a higher affinity for the hydroxycinnamic acids than FAU zeolites. The plateaus in both isotherms have been attributed to the saturation of the micropores of the zeolites with hydroxycinnamic acids. Zhang et al. (2014) studied 2,4,6 trichlorophenol (TCP) adsorption on FAU zeolites. At an equilibrium concentration of 0 – 30 mg L<sup>-1</sup>, a C-shaped adsorption isotherm was obtained.

Although the adsorption experiments can be used to design or optimize zeolite-based adsorbents for the removal of OMPs from water, they do not provide any information on the exact adsorption mechanisms (Sparks 2003). To that end, molecular simulation provides the necessary atomistic resolution needed to promote the deeper understanding of the governing physical-chemical mechanisms in adsorption equilibrium, and to further guide adsorption experiments. During the last three decades molecular simulations are actively performed in order to support experiments in various industrial and environmental processes (Mackie et al., 1997; Martí-Renom et al., 2000; Wilmer et al., 2012). In particular, Monte Carlo (MC) simulations with classical force fields have been used to study adsorption processes in porous media including metal-organic frameworks (Düren et al., 2009; Erdős et al., 2018; Getman et al., 2011), zeolites (Fuchs and Cheetham 2001; Smit and Krishna 2003), and activated carbon (Matranga et al., 1992; Müller et al.,

1996). Due to the high interest in zeolite structures for adsorption-based applications in energy storage (Dalebrook et al., 2013; Jänchen et al., 2004; Lin et al., 2012), gas separation (Bowen et al., 2004; Tomita et al., 2004), and wastewater treatment (Babel and Kurniawan 2003; Metes et al., 2004; Shevade and Ford 2004), numerous MC simulation studies have been carried out to explain the adsorption mechanisms of various compounds and mixtures (Brunchi et al., 2012; Calero and Gómez-Álvarez 2015; Du et al., 1998; Maginn et al., 1995; Smit and Siepmann 1994).

2,4,6 trichlorophenol (TCP) is an organic compound widely used for the production of industrial products, e.g., fungicide and herbicide. As a result, TCP has been repeatedly reported to occur in water bodies (Gao et al., 2008; Halappa Gowda et al., 1985; Najm et al., 1993; Verschueren 2001) as an important OMP, among others. In the present work, the adsorption of TCP from water on high-silica FAU zeolites was studied by means of both adsorption experiments and MC simulation. FAU zeolites were chosen due to their large pore size and amount of micropores, which is shown to have a high adsorption loading for various OMPs (Fukahori et al., 2011; He and Cheng 2016; Koubaissy et al., 2011; Yonli et al., 2012). The schematic representation of the framework of FAU is shown in Figure 2.

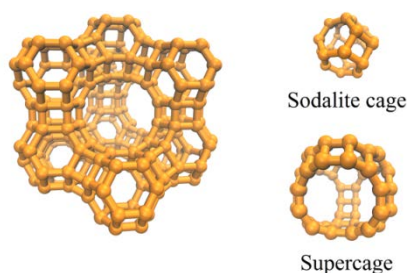


**Figure 2.** The pores in FAU zeolites are made of supercages and sodalite cages with pore opening diameters  $7.4 \text{ \AA}$  and  $2.3 \text{ \AA}$ , respectively (Baerlocher et al., 2007; Faux et al., 1997).

In batch experiments of TCP adsorption on high-silica FAU zeolites, an S-shaped adsorption isotherm was obtained. To the best of our knowledge, this is the first time that an S-shaped isotherm has been reported for the adsorption of OMPs on high-silica zeolites. In this context, MC simulations were carried out to investigate the adsorption mechanisms of the occurring S-shaped isotherm. Moreover, this is also one of the very few MC



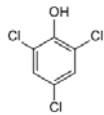
simulation studies reporting the adsorption of organics from water on high-silica zeolites (DeJaco et al., 2016; Narasimhan et al., 2013; Yazaydin 2007). To understand the adsorption mechanism, causing the S-shaped adsorption isotherm, the experimentally measured and the computed adsorption isotherms were compared qualitatively. The relation between the amount of Al content in FAU zeolites and the occurrence of S-shaped isotherms was also discussed.

## 2 Materials and methods

### 2.1 Materials

TCP standards for chromatography analyses were purchased from Sigma-Aldrich, the Netherlands. The basic physicochemical properties of TCP are listed in Table 1.

**Table 1** The physicochemical characteristics of TCP

IUPAC name	Chemical formula	Molecular weight (g mol <sup>-1</sup> )	Solubility in water (mg L <sup>-1</sup> ) <sup>a</sup>	Log D at pH 6 <sup>b</sup>	pka <sup>b</sup>	Molecular size (Å*Å*Å) <sup>c</sup>	Chemical structure
2,4,6-trichlorophenol	C <sub>6</sub> H <sub>3</sub> Cl <sub>3</sub> O	197.45	800	3.58	6.2±0.4	5.43*0.32*6.28	

<sup>a</sup> Estimated by EPIWEB 4.1

<sup>b</sup> Estimated by ACD/LABs PhysChem Module (Algorithm Version: 5.0.0.184)

<sup>c</sup> Estimated by Hyperchem 7.0 after geometric optimization

**Table 2** Information of the high-silica zeolites studied.

Zeolite name <sup>a</sup>	Product name	Supplier	Si/Al ratio <sup>b</sup>
FAU250	390HUA	Tosoh	250
FAU50	385HUA	Tosoh	50
FAU40	CBV901	Zeolyst	40
FAU30	CBV760	Zeolyst	30

<sup>a</sup> The names of the zeolites in this study were based on the framework type and the Si/Al ratio.

<sup>b</sup> Si/Al ratio provided by the suppliers.

High-silica zeolite powders of FAU framework were provided by suppliers. The names, suppliers and Si/Al ratios of zeolites are listed in Table 2.

## 2.2 Adsorption experiments

Batch adsorption experiments were conducted in demineralized water. The FAU zeolites ( $30 \text{ mg L}^{-1}$ ) were dosed in the 100 ml TCP aqueous solution with the TCP concentrations ranging from 0 to  $50 \text{ } \mu\text{mol L}^{-1}$ . After the equilibrium time of 24h at room temperature ( $25 \pm 1 \text{ } ^\circ\text{C}$ ), the zeolites were separated from the TCP solution by membrane filtration ( $0.2 \text{ } \mu\text{m}$  syringe filter, Whatman SPARTAN™).

## 2.3 High performance liquid chromatography (HPLC) analyses

The concentration of filtrated TCP solution was determined by HPLC (Shimadzu, Japan) with a C18 column (Phenomenex® KINETEX, 4.6mm) at  $30 \text{ } ^\circ\text{C}$ . HPLC-grade acetonitrile (Sigma-Aldrich, the Netherlands) and ultra-pure water (Milli-Q ultra-pure water system) were mixed as the mobile phase with a ratio of 65:35 (v:v). The flow rate of the mobile phase was  $1.0 \text{ ml min}^{-1}$ . The wavelength of the UV detector was set at 280 nm.

## 2.4 Monte Carlo simulation

### 2.4.1 Force fields

The force field parameters for TCP, water and zeolites were taken from the Generalized Amber Force Field (GAFF) (Wang et al., 2004), Extended Single Point Charge (SPC/E) (Berendsen et al., 1987) and Clay Force Field (ClayFF) (Cygan et al., 2004) models, respectively. The choice of these force fields is based on the study by Narasimhan et al. (2009) in which it was shown that a similar force field combination was able to reproduce experimental results of the adsorption of paracresol and water onto MFI zeolites reasonably well. As discussed earlier, the adsorption isotherms computed from MC simulations were used only to obtain physical insight into the adsorption mechanisms. To this end, no modifications in the force fields or cross interactions parameters between the different species were applied to achieve better agreement with the experimental measurements. Moreover, exhaustive simulations using various other force field combinations was also not the scope of this study. All the force field parameters used in this study are listed in Table S1 in the Supporting Information.

### 2.4.2 Simulation details

All MC simulations were carried out using the Cassandra open source software package V1.2 (Shah et al., 2017). In the Cassandra software package the chemical potential, which is imposed in the GCMC simulations is shifted with a value containing the partition functions of the molecules which are inserted in the simulation box. To be able to convert this shifted chemical potential to equilibrium concentration additional simulations are performed. The details of the applied method is shown in Section S2 in the Supporting Information.

Short-range van der Waals interactions were considered by the (12–6) Lennard-Jones potential (see Equation S1 in the Supporting Information). For the mixed pair potentials the Lorentz-Berthelot mixing rules (Allen and Tildesley 2017) were used (see Equation S2 in the Supporting Information). Long-range electrostatic interactions were considered by the Ewald summation method (Frenkel and Smit 2001) with a relative precision of  $10^{-5}$ . For the LJ and electrostatic interactions a cutoff radius of 14 Å with analytic tail correction was applied. In all simulations, 8 unit cells per simulation box (a 2x2x2 supercell) were used and periodic boundary conditions were imposed in all direction. The zeolite framework was considered rigid in all simulations. This approach is often being applied in simulations of nanoporous materials to prevent the necessity of excessive computational efforts (Vlugt and Schenk 2002). Zeolite frameworks with specified Si/Al ratios were created based on the structures reported by Hriljac et al. (1993). The desired Si/Al ratios were achieved by randomly exchanging silicon atoms with aluminum atoms while obeying Löwstein's rule which states that the Al – O – Al bonds are prohibited in zeolites (Hriljac et al., 1993). The number of sodium atoms were adjusted in accordance to the number of aluminum atoms to ensure the electro-neutrality of the framework. The sodium atoms were fixed at their crystallographic position in order to simplify the simulation scheme. It is important to note that the choice of fixing the sodium or allowing it to move in the zeolite framework may vastly affect the computed adsorption isotherms as shown by Calero et al. (2004) in alkane adsorption onto FAU zeolites. The effect of fixing the sodium ion to the framework has not yet been studied in MC simulations of adsorption from the liquid phase. Thus, further investigation is needed to show the exact magnitude of this effect on the computed adsorption isotherms.

To obtain the adsorption isotherms, Configurational-Bias Monte Carlo (CBMC) simulations in the grand-canonical ( $\mu VT$ ) ensemble (GCMC) were performed (Frenkel and Smit 2001).

The following types of trial moves were used: translations (~12%), rotations (~12%), partial regrowth (~10%) and molecule exchanges with the reservoir (~66%). In all MC runs an equilibration period of 5,000,000 MC steps was performed. After the equilibration, production runs of 15,000,000 MC steps were carried out, from which ensemble averages were calculated.

The MC simulations were performed for the FAU250, FAU50, FAU40 and FAU30 frameworks. The Si/Al ratios and the number of Al atoms in the framework are listed in Table 3. The simulated zeolite frameworks cover a wider Si/Al range compared to the batch experiments. The Si/Al in simulations was in the range 5 – 250, while in experiments was in the range 30 – 250.

**Table 3** *The list of the FAU zeolite frameworks used in the MC simulations.*

Zeolite name	Si/Al ratio in simulated box	Numbers of Al atom in the framework	Number of Supercages/Sodalite cages in the framework
FAU250	255	6	
FAU50	50	30	
FAU40	41	37	64/64
FAU30	30	50	
FAU5	9	156	

## 3 Results and discussion

### 3.1 TCP adsorption on FAU zeolites: Experimental and simulation results

The experimental results of TCP adsorption isotherms on FAU zeolites with varying Al content are shown in Figure 3. The adsorption isotherms of TCP on FAU250, FAU50 and FAU40 had an S shape, while FAU30 exhibited a C-shaped isotherm. As observed from the adsorption plateaus of S-shaped isotherms, the maximum adsorption loading of TCP on FAU250, FAU50 and FAU40 followed the order FAU250 > FAU50 > FAU40. This indicates that TCP adsorption on FAU zeolites, including the TCP loading and the shape of the adsorption isotherms, was driven by the Si/Al ratio of the zeolite. In the studied

equilibrium concentration range of 0 – 20  $\mu\text{mol L}^{-1}$ , the highest TCP adsorption loading on FAU30 was less than 400  $\mu\text{mol g}^{-1}$ .

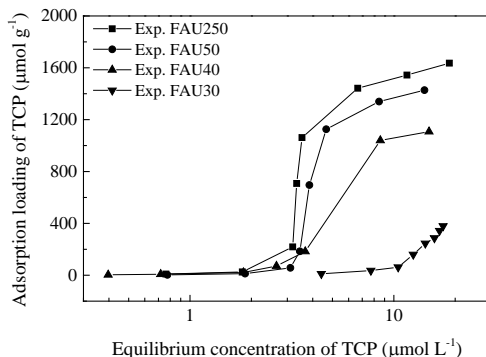


**Figure 3** The adsorption isotherm of TCP on FAU zeolites from batch experiments represented by solid symbols.

In Figure 4, the simulated adsorption isotherms of TCP on FAU zeolites with varying Al contents are shown. As shown in Figure 4, the simulated adsorption isotherms of all five FAU zeolites, including FAU5 (which was not tested in batch experiments), were S-shaped. The adsorption loadings of TCP on FAU zeolites followed the same order as in the experiments: FAU250 > FAU50 > FAU40 > FAU30 > FAU5. As can be seen in Figure 4, the adsorption isotherms for FAU250 and FAU50 computed from MC simulations exhibited almost identical maximum loading to the respective experimentally measured isotherms. By incorporating more Al atoms in the framework, the S-shape of the adsorption isotherms became less pronounced. This is also in line with the experimental measurements shown in Figure 3, indicating that MC simulations captures the effect of Si/Al ratio on the shape of the adsorption isotherm.

The adsorption loading of TCP on FAU40 was underestimated in the simulation, showing a deviation of  $\sim 300 \text{ mg g}^{-1}$  from experimental results. The simulated adsorption isotherms of FAU30 zeolites was S-shaped with a maximum TCP loading of  $\sim 1200 \text{ mg g}^{-1}$  (Figure 4), while the adsorption loading of FAU30 obtained from experiments was  $\sim 400 \text{ mg g}^{-1}$ , which is observed from an C-shaped isotherm without adsorption plateau (Figure 3). The equilibrium concentration at which the adsorption step occurs in the isotherms computed

from MC simulations is not as pronounced as in the experimentally measured ones, and moreover, it seems to deviate quite significantly.

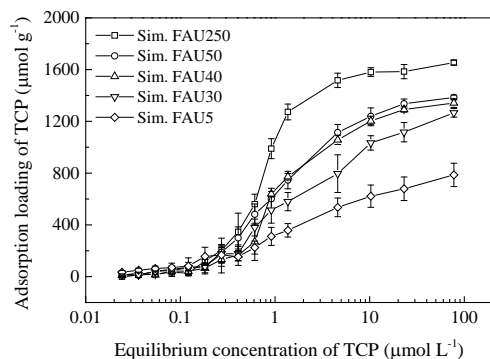


**Figure 4** The adsorption isotherm of TCP on FAU zeolites from MC simulation represented by open symbols.

The possible reason for the discrepancies between experiments and MC simulations is the force fields representing the adsorbent and adsorbates, as well as the fact that sodium ions are fixed in the FAU crystal. Since there were no prior MC simulations of the co-adsorption of water and TCP onto zeolites, the force fields representing water, TCP and zeolites were chosen based on the study by Narasimhan et al. (2009), where the adsorption of water and paracresol onto MFI zeolites was studied. As stated earlier, no modification or refitting of the individual force fields was performed in the current study. However, such modifications in order to improve the accuracy of the simulations, can be realized in several ways: e.g., by optimizing the Lennard-Jones parameters or atomic charges, by explicitly including polarization effects, and by modifying the intermolecular interactions between Al atoms and the adsorbates. Although such modifications may give a better agreement between the simulation and experimental results, their implementation requires significant computational effort which is out of the scope of this study.

### 3.2 The adsorption mechanisms behind the S-shaped adsorption isotherms

Since the adsorption isotherms for FAU250 computed from MC simulations exhibited almost identical maximum loading to the experimentally measured adsorption isotherms,

the MC simulation results of FAU250 were further used to understand the adsorption mechanisms of S-shaped adsorption isotherm.

In Figure 5, the average number of adsorbed TCP molecules in the supercages of FAU250 are plotted as a function of the equilibrium concentration of TCP. The number of adsorbed TCP molecules increased with the increase of TCP equilibrium concentration and the S-shaped curves is observed from Figure 5. The S-shaped curves were qualitatively characterized by a division of three stages. At the low coverage range (equilibrium concentration  $< 0.15 \mu\text{mol L}^{-1}$ ), a minimal amount of TCP molecules (close to 0) were adsorbed on the FAU250 zeolites. There was 0 to 1 TCP molecule adsorbed in the supercages. The average number of adsorbed TCPs increased considerably at the transition stage (equilibrium concentration of  $0.15$  to  $10 \mu\text{mol L}^{-1}$ ). At the stage of high coverage (equilibrium concentration  $> 10 \mu\text{mol L}^{-1}$ ), the maximum number of adsorbed TCP is observed from the plateau.

As shown in Figure 5, the S-shaped curves are observed for both supercages without Al and supercages with Al, while the maximum number of adsorbed TCP in two types of supercages varied. A supercage provided accommodation to approximately 2 TCP molecules in Al containing cages and 2.5 TCP molecules in the none-Al containing cage, respectively. In the supercages with no Al atom, a maximum of 3 TCP molecules could be adsorbed.

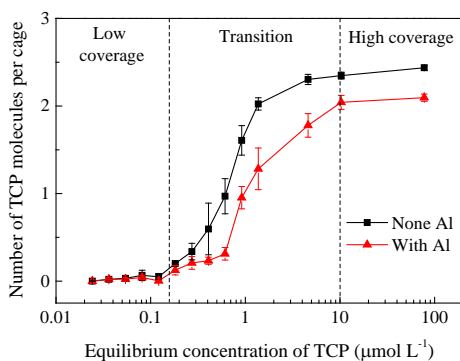


**Figure 5** The number of adsorbed TCP molecules in the supercages of FAU250 zeolite computed from the MC simulations.

The simulated arrangement of the adsorbed TCP molecules with water molecules in the supercages without Al are shown in Figure 6. When 1 TCP molecule was adsorbed in the supercage, TCP preferably excluded the water molecules in between and was arranged close to the wall of the cage (Figure 6a). In the supercages with 2 or 3 adsorbed TCP molecules, less water molecules were adsorbed and the TCP molecules obtained a parallel configuration, with benzene rings facing each other (Figure 6b and 6c).

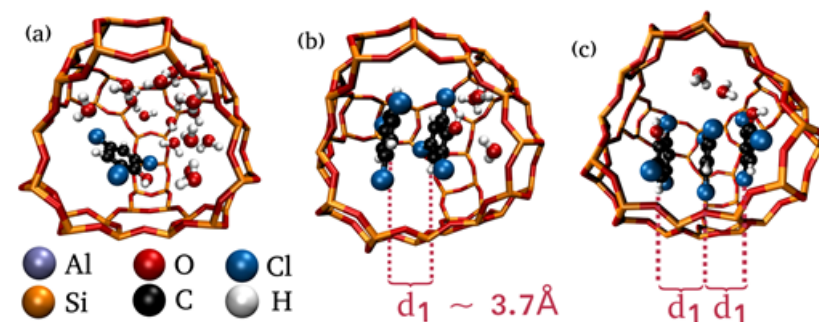


**Figure 6** The arrangements of TCP and water molecules in the none-Al containing supercages of FAU250 zeolites: (a) 1 TCP, (b) 2 TCP, (c) 3 TCP molecule(s) per cage at TCP equilibrium concentration equal to (a) 4.6, (b) 77.6 and (c) 77.6  $\mu\text{mol L}^{-1}$ . The characteristic distance between the center of mass of the benzene rings in the TCP molecules is shown as  $d_1$ .

To obtain further information about the structure of adsorbed molecules in the framework, the radial distribution function (RDF) was calculated (Allen and Tildesley 2017). The RDF, usually represented as  $g(r)$ , defines the probability of finding a particle at distance  $r$  from another tagged particle. In Figure , the RDF between the center of mass of benzene rings on the FAU250 framework at TCP equilibrium concentration of 77.6  $\mu\text{mol L}^{-1}$  is shown. From Figure , it is observed that the characteristic distance between two TCP molecules was  $\sim 3.7 \text{ \AA}$ , which is a typical packing distance between  $\pi$  -  $\pi$  stacked aromatic groups (3.4  $\text{\AA}$  - 3.8  $\text{\AA}$ ). This is in line with literature (Janiak 2000; Martinez and Iverson 2012) as TCP molecules in aqueous solutions could experience  $\pi$  -  $\pi$  interactions, as a form of lateral interactions in the supercages. The lateral interaction considerably promoted TCP adsorption at the transition stage (Figure 5), and led to the S-shaped adsorption isotherm.



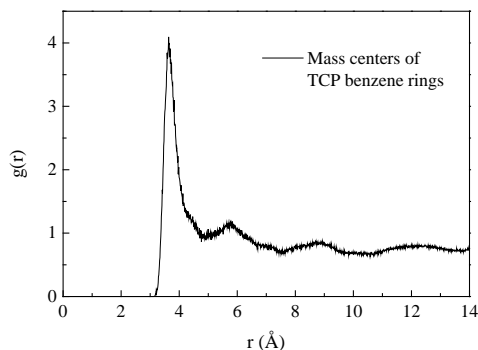


**Figure 7** Radial distribution function (RDF) of mass center of benzene rings in TCP molecules adsorbed on FAU250 at a TCP equilibrium concentration equal to  $77.6 \mu\text{mol L}^{-1}$ . The characteristic distance between two benzene rings is indicated by the first peak of the RDF around  $r = 3.7 \text{ \AA}$ .

The  $\pi$  -  $\pi$  interaction could occur between two TCP molecules with C - C  $\pi$  electrons, originating from benzene rings of TCP molecules. The C - C  $\pi$  electrons of TCP molecules could shift from the center of the benzene ring due to electron donating of hydroxyl groups and electron withdrawing of chlorine atoms to the conjugated  $\pi$  electron. Thus, two TCP molecules could form a  $\pi$  -  $\pi$  interaction with an offset stacked conformation other than a perfect face-to-face alignment, as clearly shown from the simulation snapshots in Figure 6. In this conformation, most of the surface of TCP molecules were covered by each other and the  $\pi$  -  $\pi$  interaction between TCP molecules is expected to be strong (Waters 2002).

### 3.3 The effect of water adsorption on the occurrence of S-shaped adsorption isotherms and TCP adsorption

In Figure 8, the number of adsorbed water molecules in supercages of FAU250 is plotted as a function of the equilibrium concentration of TCP. Figure 8 shows that the number of water molecules in the supercages of FAU250 decreased with equilibrium concentration of TCP. Al-containing cages had a higher number of adsorbed water molecules than the cages without Al. At the higher equilibrium concentration ( $> 77 \mu\text{mol L}^{-1}$ ), about 8 water molecules per cage were adsorbed in the supercages with Al atom, while approximately 5 molecules per cage were adsorbed in the supercages without Al atom. Compared to water adsorption in sodalite cages (0 - 3 water molecules per cage, Figure 10), more water

molecules were adsorbed in supercages (8 – 25 water molecules per cage, Figure 8). This can be attributed to the much less space inside sodalite cages than supercages (Baerlocher et al., 2007).

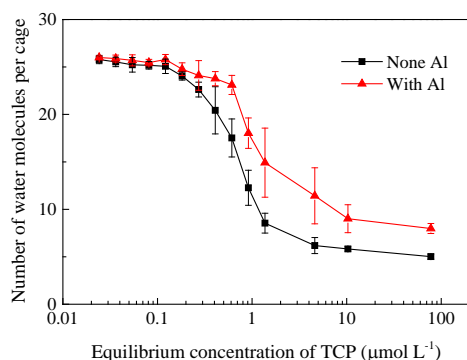


**Figure 8** Number of adsorbed water molecules in the supercages of FAU250 zeolite.

The arrangement of the adsorbed water and TCP molecules in the Al-containing supercages are shown in Figure 9. The distance between hydrogen atoms from water and the oxygen atoms of zeolites, which are connected to Al atom, was computed to be 1.7 Å. In the Al-containing supercages with one TCP molecule adsorbed, a total number of 19 water molecules were adsorbed (Figure 9a), while 10 water molecules were adsorbed in the supercages with 2 adsorbed TCP molecules (Figure 9b). In the non Al-containing supercages, however, 14 water molecules were co-adsorbed along with one TCP molecule, and 3 water molecules were co-adsorbed along with two TCP molecules (Figure 6). This is in line with the results presented in Figure 9, where it is shown that more water molecules were adsorbed in the supercages with Al. The Al-containing supercages with 3 adsorbed TCP molecules were not found in the simulation box, since water molecules hinder the TCP adsorption due to the limited space in the supercages.

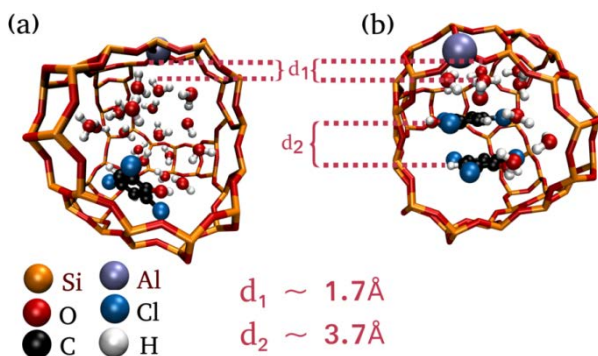


**Figure 9** The arrangements of TCP and water molecules in the supercages of FAU250 zeolite with Al atom: (a) 1 TCP molecule per cage at the equilibrium concentration equal to  $4.6 \mu\text{mol L}^{-1}$  (b) 2 TCP molecules per cage at the equilibrium concentration equal to  $77.6 \mu\text{mol L}^{-1}$ .

The number of adsorbed TCP molecules in sodalite cages of FAU250 zeolites is plotted as a function of the equilibrium concentration of TCP in Figure 10. As shown in Figure 10, water adsorption in sodalite cages was not affected by the equilibrium concentration of TCP. The sodalite cages with Al atom had an average number of approximately 1.5 water molecules per cage with a variation from 1 to 2 water molecules per cage, while the sodalite cages without Al atom exhibited almost no ability for water adsorption.

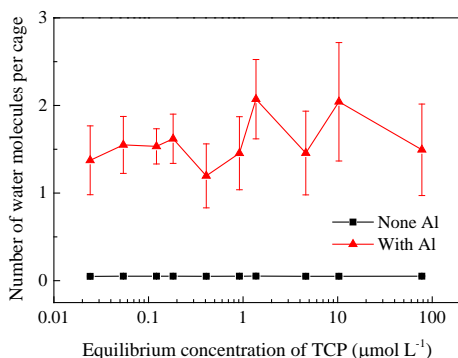
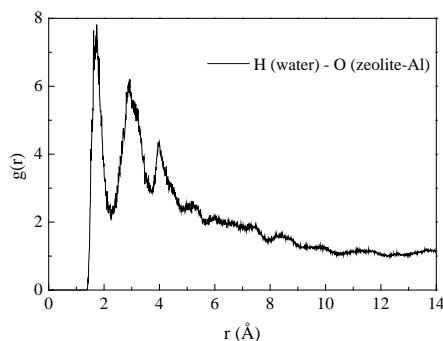


**Figure 10** Number of adsorbed water molecules in the sodalite cages of FAU250 zeolite.

The RDF between the hydrogen atom from water and the oxygen atom connected to Al atom of FAU250 zeolites was calculated to determine the structures of adsorbed water

molecules on FAU250 zeolite. As shown in Figure 11a, one peak is observed at the distance of 1.7 Å, which is the typical H-bond length (Wallwork 1962). Thus, we can safely conclude that water molecules were being adsorbed on FAU zeolites by forming H-bonds with the framework. Narasimhan et al. (2013) indicated that the existence of water clusters could weaken the interaction of water molecules with zeolites, as well as the interaction of OMPs with zeolites, which, however, would strengthen the interactions between OMPs and water. The two wide peaks at distances of 2.9 Å and 4.0 Å shown in Figure 11a, indicate that water molecules which do not form H-bonds with the FAU framework formed water clusters.

As shown in Figure 11b, the RDF between the O atom of adsorbed water molecules and Al atom of zeolite framework has a strong peak at distance of approximately 3.4 Å. Bolis et al. (2006) suggested that water molecules were adsorbed on zeolites by interacting with the –Si-O-Si– groups of zeolites. The distance of 3.4 Å between Al atom of zeolites and water molecules, shown in Figure 11b, clearly indicate that there was an additional driving force for water adsorption on the supercages (Figure 8) and sodalite cages (Figure 10) of the FAU zeolite. The additional driving forces from Al atoms might cause an extra number of water molecules to be adsorbed in the supercages (Figure 8) and sodalite cages (Figure 10). Due to the additional water adsorption on Al atom, FAU zeolite with higher Al content (lower Si/Al ratio) had a lower TCP adsorption loading and less pronounced S-shaped adsorption isotherms (Figure 3 and 4). Zhang et al. (2014) studied TCP adsorption on FAU zeolites with Si/Al ratio 30 and observed a C-shaped adsorption isotherm, which confirms the finding in the present study. The occurrence of C-shaped isotherm instead of S-shaped isotherm was attributed to the low Si/Al ratio of FAU zeolites.



(a)

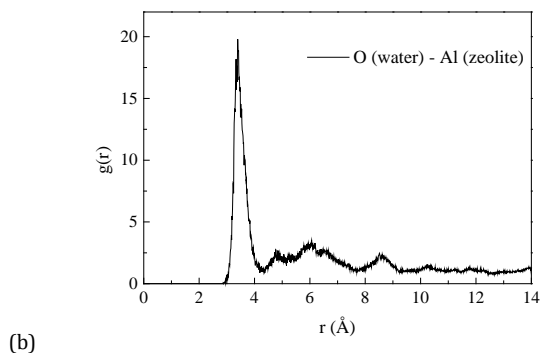


**Figure 11** Radial distribution function (RDF) of (a) H atom from water molecules and O atom connected to Al atom of FAU250 framework; (b) O atom from water molecules and Al atom from FAU250 framework at the TCP equilibrium concentration equal to  $77.6 \mu\text{mol L}^{-1}$

The supercages of FAU zeolite with large pore opening and inner sizes provided the basic conditions for the accommodation of multiple TCP molecules and their lateral interaction in the presence of water molecules, which was crucial for the occurrence of the S-shaped adsorption isotherms. In the zeolite frameworks with channels, the adsorbed OMPs preferred to be located in the channels and channel intersections, whereas water molecules preferably adsorbed in the vicinity of the OMP molecules (Boulet et al., 2009; DeJaco et al., 2016; Guvenc and Ahunbay 2012). Due to the hindering of water molecules, the lateral interaction of adsorbed OMP molecules would be negligible. Therefore, the S-shaped adsorption isotherm was not observed in previous literature, which studied OMP adsorption on zeolites frameworks with channels, e.g. BEA and MFI type zeolites (Damjanovic et al., 2010; Gonzalez-Olmos et al., 2013; Reungoat et al., 2007).

## 4 Conclusions

In this study, MC simulations were used to explain the mechanism of S-shaped adsorption isotherms of TCP adsorption on high-silica FAU zeolites. This study shows that the occurrence of S-shaped adsorption isotherms was attributed to the lateral interaction of TCP, e.g., the  $\pi$ - $\pi$  interaction. The supercages of FAU zeolites provided a possible accommodation for multiple TCP molecules as a potential condition of lateral interactions of TCP. Water molecules were adsorbed in the sodalite cages and supercages of FAU

zeolites by forming H-bonds with the framework of zeolites. Compared to the none-Al containing supercages, more water molecules were stably adsorbed as water clusters in the supercages of FAU zeolites with Al content. An additional amount of adsorbed water molecules in Al-containing supercages could inhibit TCP adsorption and could prevent the occurrence of an S-shaped adsorption isotherm. FAU zeolites with higher Si/Al ratio, therefore, had evident S-shaped adsorption isotherms, and, meanwhile, achieved higher TCP adsorption loadings compared to FAU zeolites with lower Si/Al ratios. MC simulation has thus been proven to be a powerful tool to study the adsorption of OMPs in water to support experimental results. Performing MC simulation will further allow investigating the adsorption mechanisms of OMP adsorption from the view of molecular interaction between OMPs, OMP and adsorbents as well as water and adsorbents.

The unfavourable adsorption of OMPs have been widely observed from OMP adsorption on solid adsorbents. The low adsorption capacity would be followed by a steep increase of OMP adsorption capacity at a certain equilibrium concentration, showing the typical feature of S-shaped isotherms. This study suggests that the increase of OMP adsorption capacity was caused by the interaction between OMPs. Except for the  $\pi$ - $\pi$  interaction between TCP molecules in this study, various types of OMP interactions might exist as driving forces for OMP adsorption, since the physicochemical properties of OMPs also vary.

## Supporting information

### S1 Simulation details

In force field based Monte Carlo simulations the total interaction energy,  $E_{tot}$ , between atoms and molecules is computed from:

$$E_{interaction} = E_{nonbonded} + E_{bonded} \quad \text{Equation S1}$$

#### S1.1 Nonbonded interactions

To calculate the nonbonded interactions between two atoms, the short range van der Waals interactions are taken into account by the (12-6) Lennard-Jones potential ( $E_{LJ}$ ) and the electrostatic interactions are calculated using the Coulomb's law ( $E_{electrostatic}$ ).

$$E_{nonbonded} = E_{LJ}(r_{ij}) + E_{electrostatic}(r_{ij}) = 4\varepsilon_{ij} \left( \left( \frac{\sigma_{ij}}{r_{ij}} \right)^{12} - \left( \frac{\sigma_{ij}}{r_{ij}} \right)^6 \right) + \frac{q_i q_j}{4\pi\epsilon_0 r_{ij}}$$

$$\text{Equation S2}$$

where  $\varepsilon_{ij}$  and  $\sigma_{ij}$  are the LJ parameters, and  $r_{ij}$  is the distance between particle  $i$  and  $j$ ,  $q_i$  is the atomic charge of atom  $i$ ,  $\epsilon_0$  is the permittivity of vacuum. The LJ parameters for the interaction between different types of particles is calculated according to the Lorentz-Berthelot mixing rules:

$$\varepsilon_{ij} = \sqrt{\varepsilon_{ii}\varepsilon_{jj}} \quad \text{Equation S3}$$

$$\sigma_{ij} = \frac{\sigma_{ii} + \sigma_{jj}}{2} \quad \text{Equation S4}$$

The LJ parameters and atomic charges used in this study are listed in Table S1.

#### S1.2 Bonded interactions

To calculate the total energy of the system, two types of bonded interactions, the bond-angle bending and dihedral angle torsion are taken into account:

$$E_{bonded} = E_{angle} + E_{dihedral} \quad \text{Equation S5}$$

where,

$$E_{angle} = \sum_{angles} K_{\theta} (\theta - \theta_0)^2 \quad \text{Equation S6}$$

and

$$E_{dihedral} = \sum_{dihedrals} a_0 (1 + \cos(a_1 \phi - \delta)) \quad \text{Equation S7}$$

where,  $K_{\theta}$  is the force constant for bond-angle bending,  $\theta$  is the bond angle,  $\theta_0$  is the equilibrium bond angle,  $\phi$  is the dihedral angle and  $a_0, a_1, \delta$  are coefficients of the dihedral angle potential. The bond lengths are fixed in all simulations. The parameters used to calculate the bonded interactions in this study are listed in Table S2 and Table S3.

**Table S1** Lennard-Jones parameters and atomic charges used in the simulations. Atom names are shown in Figure S1 for TCP.

Molecule	Atom name	Atom type	$\varepsilon_{ij}/k_B$ / (K)	$\sigma_{ij}$ / (Å)	$q_i$ (e)
2,4,6-trichlorophenol	C1	CA	43.277	3.400	0.543841
	C2	CA	43.277	3.400	-0.246516
	C3	CA	43.277	3.400	-0.246516
	C4	CA	43.277	3.400	0.073606
	C5	CA	43.277	3.400	0.073606
	C6	CA	43.277	3.400	-0.143285
	O	O	105.877	3.066	-0.524338
	Cl1	CL	85.547	3.475	-0.051323
	Cl2	CL	85.547	3.475	-0.051323
	Cl3	CL	85.547	3.475	-0.083382
	H1	HA	7.550	2.600	0.141479
	H2	HA	7.550	2.600	0.141479
	H3	HO	0.000	0.000	0.372672
Water	O	OW	78.208	3.166	-0.8476
	H	HOW	0.000	0.000	0.4238
Zeolite	Si	SI	0.0	3.302	2.1
	Al	AL	0.0	3.302	1.575
	O <sub>Si</sub>	OSI	78.2	3.166	-1.05
	O <sub>Al</sub>	OAL	78.2	3.166	-1.16875
	Na	NA	65.5	2.35	1



**Table S26** Bond angle bending parameters for all angle types used in this study. The atomtypes are shown for each in Table S1.

Molecule	Bond	$K_\theta$ / [K rad <sup>-2</sup> ]	$\theta_0$ / [degrees]
2,4,6-trichlorophenol	CA-CA-CA	33806.3	120.00
	CA-O-CA	35149.9	120.00
	CA-CA-CL	31662.6	120.00
	CA-CA-HA	24386.0	120.00
	CA-O-HO	24582.3	109.47
Water	HW-OW-HW	fixed	109.47

**Table S3** Dihedral angle torsion parameters for all dihedral type used in this study. The atomtypes are shown for each in Table S1.

Molecule	Dihedral angle	$a_0$ / [kJ mol <sup>-1</sup> ]	$a_1$ / [-]	$\delta$ / [degrees]
2,4,6-trichlorophenol	CA-CA-CA-CA	15.166	2	180
	CA-CA-O-HO	3.765	2	180
	CA-CA-CA-CL	4.6	2	180
	CA-CA-O-CA	4.6	2	180
	CA-CA-CA-HA	4.6	2	180

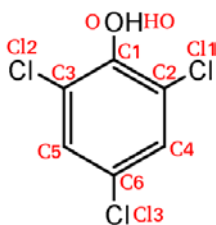


**Figure S1** Representation of the TCP molecule with atom names shown in red color.

## S2 Chemical potential conversion to concentration

### S2.1 Obtaining chemical potential from the shifted chemical potential

In the Cassandra software package the chemical potential is defined as:

$$\mu' = \mu + k_B T \ln \left( Q_{\text{rot+int}} \frac{Z_{\text{frag}} \Omega_{\text{dih}}}{Z_{\text{int}}} \right) \quad \text{Equation S8}$$

where  $\mu'$  is the shifted chemical potential,  $\mu$  is the chemical potential,  $Q_{\text{rot+int}}$  is the rotational and internal degrees of freedom partition function,  $Z_{\text{int}}$  is the internal degrees of freedom configurational partition function,  $\Omega_{\text{dih}}$  is equal to  $(2\pi)^{N_{\text{frag}}-1}$ ,  $Z_{\text{frag}}$  is the configurational partition function of the fragments of the molecule. To obtain the chemical potential based on Equation S8, the following steps were followed in this work:

1. Monte Carlo (MC) simulations are carried out in the grand canonical (GC) ensemble for a range of shifted chemical potentials at temperature  $T$  inserting TCP as an ideal gas.
2. Based on the results obtained in the GCMC simulations (the number of inserted molecules, and the pressure) the chemical potential of an ideal gas is calculated.
3. The shift in the chemical potential is calculated as the difference between the imposed shifted chemical potential and corresponding ideal gas chemical potential.

## S2.2 Converting chemical potential

The conversion of the chemical potential to equilibrium concentration is based on the work of Xiong et. al. (2011). To obtain the equilibrium concentration, the following steps were carried out:

1. The excess chemical potential of TCP in water is calculated by using the Continuous Fractional Component Monte Carlo (CFCMC) method ( $\mu_A^\infty$  in the work of Xiong et. al. (2011)).
2. The chemical potential is calculated using the shift value (see Section S2.1) from the shifted chemical potential. The obtained chemical potential is converted into fugacity using the following equation:

$$\mu = \mu_{\text{ideal}} + \frac{\ln(k_B T f_A)}{k_B T} \quad \text{Equation 9}$$

where  $\mu_{\text{ideal}}$  is the ideal gas chemical potential of TCP,  $f_A$  is the fugacity of TCP.

3. Based on the calculated fugacity, the mole fraction of TCP is calculated using the following equation:

$$f_A = \rho k_B T \exp\left(\frac{\mu_A^\infty}{k_B T}\right) x_A \quad \text{Equation 10}$$

where  $\rho$  is the number density of TCP in the bulk phase,  $k_B$  is the Boltzmann constant,  $T$  is the temperature,  $x_A$  is the mol fraction of TCP in the bulk phase.

## **CHAPTER 5**

# **ADSORPTION OF PHARMACEUTICALS ON HIGH-SILICA ZEOLITES AFFECTED BY NATURAL ORGANIC MATTERS**

This Chapter is based on: Jiang N., Shang R., Heijman S.G.J., Rietveld L.C., Adsorption of pharmaceuticals on high-silica zeolites affected by natural organic matters, in preparation.

## Abstract

High-silica zeolites are promising adsorbents for the removal of organic micropollutants (OMPs). In this study, four high silica zeolites with different frameworks were used for the removal of 23 pharmaceuticals (PHAMs) in the presence of and without NOM. The influence of NOM on adsorption efficacies of PHAMs on high-silica zeolites were related to the properties of PHAMs and zeolites. The mechanisms of NOM affecting the adsorption of PHAMs with a broad range of properties on high-silica zeolites were discussed. In the presence of NOM, positively charged PHAMs were better removed by high-silica zeolites than neutral and negatively charged PHAMs, since positively charged PHAMs experienced electrostatic attraction with the negative sites of the zeolites. Moreover, there was possibly a low concentration of positively charged, competing NOM fractions present in the water. The effect of molecular sizes on the adsorption efficacies were more obvious for neutral and negatively charged PHAMs than for positively charged PHAMs. Neutral and negatively charged PHAMs with similar molecular sizes as the pore opening sizes of zeolites were preferably adsorbed, while PHAMs with larger sizes than the pore size were excluded. Due to the adsorption of NOM on zeolites, the adsorption efficacies of neutral and negatively charged PHAMs were much lower than in ultrapure water. A small fraction of NOM with low molecular weight would enter the micropores of zeolites and compete for the adsorption sites in the micropores. NOM competition in the micropores were likely to happen in multi-solute water, since a broad range of PHAMs were unable to closely fit uniform micropores of zeolites. In addition, NOM fractions were probably adsorbed on the zeolites, blocking the micropores and, meanwhile, competing with PHAM adsorption on the external surface of zeolites. In comparison with the charge and molecular sizes of PHAMs, hydrophobicity/hydrophilicity of PHAMs had less effect on the adsorption efficacies of PHAMs.

## 1 Introduction

Zeolites are crystalline aluminosilicate materials with uniformed micropores (Auerbach et al., 2003; Li and Yu 2014). The surface hydrophobicity/hydrophilicity of zeolites varies with the content of silica and aluminum, typically defined by the molar ratio of silica to aluminum (Si/Al ratio). High-silica zeolites with Si/Al ratios from 10 up to a few thousand

are hydrophobic and effective for the removal of organic micropollutants (OMPs) in water (Maesen 2007; Rakic et al., 2010; Tsitsishvili 1973). The porous structure of zeolites have exclusively been defined by their framework types (McCusker and Baerlocher 2001). OMPs that are closely fitted into the pores of zeolites are preferably adsorbed (de Ridder et al., 2012; Rossner et al., 2009). High-silica zeolites with the framework types of FAU, MOR, BEA and MFI are commercially available and commonly used for studies on OMP adsorption.

Most of the research on the adsorption of OMPs on high-silica zeolites has been conducted by performing batch experiments in water without background compounds (Jiang et al., 2018). However, in all fresh waters, natural organic matter (NOM) is ubiquitously present as background compounds (Bhatnagar and Sillanpää 2017). NOM consists of a complex matrix of organic compounds, such as humic substances, amino sugars, proteins, small hydrophilic acids, with molecular weights ranging from a few hundred to 100,000 Dalton (Leenheer and Croué 2003; Sillanpää 2014; Thurman 2012). The effect of NOM on OMP adsorption on activate carbon, which is one of the most commonly used adsorbent, has been well studied. It has been concluded that NOM competes with OMP for adsorption surface and meanwhile leads to pore blockage and pre-loading of activated carbon (Bjelopavlic et al., 1999; Newcombe 1999; Newcombe et al., 2002). The presence of NOM therefore reduces the adsorption efficacy of targeted OMPs and increases the regeneration frequencies of activated carbon (Narbaitz and Cen 1997; Pelekani and Snoeyink 1999; Zietzschmann et al., 2014b).

The effect of NOM on OMP adsorption on high-silica zeolites has been studied before. The adsorption capacity of e.g. methyl tertiary-butyl ether (MTBE) on MOR and MFI zeolites have not been affected by NOM in natural water, although a decrease of adsorption kinetics was observed in the presence of NOM, probably due to the pore blockage by NOM (Abu-Lail et al., 2010; Hung and Lin 2006; Rossner and Knappe 2008). In addition, de Ridder et al. (2012) studied the adsorption of N-nitrosamines (NDMA) in surface water on MFI zeolites and concluded that the adsorption isotherms in demineralised water and surface water were similar, indicating that NOM did not affect NDMA adsorption. Due to the size exclusion by the micropores, the majority of the NOM could not enter the zeolites and, consequently, did not compete with OMP during adsorption on high-silica zeolites.

However, the micropores of zeolites could allow the entrance of small sized NOM as found by Braschi et al. (2016), who studied the adsorption of sulfamethoxazole on FAU zeolites in the presence of two humic monomers: vanillin and caffeic acid (152 and 180 mol g<sup>-1</sup>, respectively). During their study, the humic monomers were adsorbed on FAU zeolites and consequently the adsorption capacity of sulfamethoxazole decreased. On the contrary, Bottero et al. (1994) found that atrazine, because of the high affinity for some background organic compounds, such as hydroxyaromatics, was better adsorbed on MFI zeolites in river water than in demineralised water. Due to the variation of NOM composition in different water types, it is still hard to predict how NOM in natural water affects OMP adsorption on high-silica zeolites.

Numerous OMP species exist in natural water, including pharmaceuticals (PHAMs), personal care products, endocrine disrupting chemicals, and pesticides. As one of the most concerned OMP species, PHAMs mainly originate from discharges of treated municipal wastewater and have been detected in natural water at trace levels, e.g. several ng L<sup>-1</sup> to a few µg L<sup>-1</sup> (Fick et al., 2009; Heberer 2002; Mompelat et al., 2009). The presence of PHAMs are harmful to the aquatic environment and public health (Alan et al., 2008; Pal et al., 2010). The adsorption of a variety of PHAMs in water on high-silica zeolites has been studied before. Rossner et al. (2009) studied the removal of 28 OMP species, including 16 PHAMs, from lake water on FAU and MOR zeolites. At a zeolite dosage of 100 mg L<sup>-1</sup>, MOR completely or partially removed 15 out of 28 OMPs, while FAU only removed three OMPs. The difference in pore size and shape of zeolites were found to affect the OMP adsorption efficacies on zeolites. In comparison with activated carbon, zeolites were more selective for OMP adsorption in surface water. De Ridder et al. (2012) studied the removal of 16 PHAMs in demineralised water on MOR and MFI zeolites. The MFI zeolite with a Si/Al ratio of 80 partially removed nine PHAMs and the MOR zeolite with a Si/Al ratio of 200 removed 13 PHAMs out of 16 PHAMs. Only two PHAMs, i.e. metoprolol and atenolol, were completely removed by both the MFI and MOR zeolites. In addition, a relationship between the Stokes' diameter of PHAMs and the adsorption efficacies of PHAMs was observed. However, the adsorption efficacies of PHAMs on high-silica zeolites in the presence of and without NOM were not well studied, and thus, the mechanisms of NOM, affecting adsorption of a variety of PHAMs on high-silica zeolites remained unknown.

Therefore, in this study, the adsorption efficacies of 23 PHAMs in water with and without NOM on the high-silica zeolites were investigated. The influence of NOM on adsorption efficacies of PHAMs were related to the properties of the PHAMs, such as hydrophobicity/hydrophilicity, charge and molecular sizes. In addition, the adsorption efficacies of the PHAMs on various framework types of zeolites, i.e. FAU, MOR, BEA and MFI, were compared to understand the effect of porous structures of zeolites on adsorption efficacies of PHAMs in the presence of NOM. Finally, the mechanisms of NOM affecting the adsorption of PHAMs with a broad range of properties on zeolites were discussed.

## 2 Materials and Methods

### 2.1 Materials

High-silica zeolite powders of four frameworks, i.e. FAU, BEA, MOR and MFI zeolites, were purchased from Tosoh Corporation. The pore opening sizes and Si/Al ratios are listed in Table 1. The zeolites were dried at 105 °C for one day and stored in a desiccator before use.

**Table 1** The names and characterizations of high-silica zeolites.

Zeolite framework	Product name	Pore opening size (Å*Å) <sup>a</sup>	Si/Al ratio <sup>b</sup>	BET surface area (m <sup>2</sup> g <sup>-1</sup> )	Micropore surface area (m <sup>2</sup> g <sup>-1</sup> )	External surface area (m <sup>2</sup> g <sup>-1</sup> )
FAU	390HUA	7.4*7.4	250	727	591	136
MOR	690HOA	6.5*7.0 2.6*5.7	120	431	360	71
BEA	980HOA	6.6*7.7 5.6*5.6	250	516	351	165
MFI	890HOA	5.1*5.5 5.3*5.6	750	334	282	52

<sup>a</sup> (Baerlocher and McCusker 2017)

<sup>b</sup> Si/Al ratio provided by suppliers

BET surface area, micropore surface area and external surface area of high-silica zeolites were determined by N<sub>2</sub> gas adsorption at 77K (Gemini VII 2390p analyzer, Micromeritics)



and shown in Table 1. The micropore surface area and external surface area were estimated by the t-plot method which separates the micropores from multilayer adsorption of N<sub>2</sub> gas (Lippens and de Boer 1965).

**Table 2** *The structures and physicochemical properties of pharmaceuticals.*

Name	CAS #	Molecular weight	logD at pH8 <sup>a</sup>	Charge at pH8 <sup>a</sup>	pKa <sup>a</sup>	Molecular Size <sup>b</sup>		
						X (Å)	Y (Å)	Z (Å)
Metformin	1115-70-4	129	-5.37	+	n.a.	3.731	3.894	7.28
Paracetamol	103-90-2	151	0.89	+	9.46	4.739	1.798	8.986
Lignocaine	138-58-6	234	2.65	+/ <sup>0</sup> <sup>c</sup>	13.78	6.469	3.5	11.325
Trimethoprim	738-70-5	290	1.23	+/ <sup>0</sup>	n.a.	6.849	3.849	9.908
Sotalol	959-24-0	309	-1.56	+/ <sup>0</sup>	10.07	6.073	4.053	14.281
Lincomycine(HCl)	7179-49-9	461	0.48	+/ <sup>0</sup>	12.37	8.331	4.893	14.191
Metoprolol	56392-17-7	685	0.09	+/ <sup>0</sup>	14.09	6.082	4.651	15.013
Clarithromycin	81103-11-9	747	2.2	+/ <sup>0</sup>	12.46	11.41	8.735	14.315
Caffeine	58-08-2	194	-0.55	0	n.a.	6.007	1.803	7.168
Primidone	125-33-7	218	1.12	0	11.5	5.757	5.632	8.4
Carbamazepine	298-46-4	236	2.77	0	15.96	7.498	0	10.087
Cyclophosphamide	50-18-0	261	0.1	0	13.48	5.14	3.751	8.542
Hydrochlorthiazide	58-93-5	298	-0.61	0	9.09	5.754	2.912	9.453
Iopromide	73334-07-3	791	-0.45	0	11.09	16.367	7.572	6.304
Theophylline	58-55-9	180	-1.11	-/ <sup>0</sup> <sup>d</sup>	7.82	6.041	1.804	7.625
Phenazon	60-80-0	188	1.22	-	0.49	5.116	1.806	9.452
Clofibric acid	882-09-7	214	-0.6	-	3.37	5.233	3.963	7.376
Sulfamethoxazole	723-46-6	253	-0.11	-	6.16	5.593	2.531	12.691
Ketoprofen	22071-15-4	254	0.18	-	3.88	5.935	1.794	12.601
Fenofibric acid	42017-89-0	319	0.85	-	3.1	6.387	4.35	12.053
Furosemide	54-31-9	331	-1.58	-	4.25	6.553	2.514	12.684
Enalapril	75847-73-3	376	-1.22	-	3.67	7.659	5.197	14.702
Pravastatin	81131-70-6	447	-1.69	-	4.21	8.001	6.982	12.663

<sup>a</sup> Estimated by ChemAxon, Chemicalize Platform.

<sup>b</sup> Estimated by Hyperchem 7.0 after geometric optimization.

<sup>c</sup> +/<sup>0</sup>, positively charged and neutral formed PHAM molecules simultaneously existed at pH 8.

<sup>d</sup> -/<sup>0</sup>, negatively charged and neutral formed PHAM molecules simultaneously existed at pH 8.

Batch adsorption experiments were conducted in ultrapure (UP) water and in the water from a drinking water treatment plant (DWTP). UP water was obtained from ELGA, Ultra AN MK2 ultrapure water system with pH value of 7.8. DWTP water was collected from the DWTP at Kamerik, operated by Oasen, the Netherlands. The extracted groundwater is submitted to aeration, rapid sand filtration, softening, activated carbon filtration and UV disinfection before the treated water is pumped into the distribution system. DWTP water samples were collected from the influent of the activated carbon filtration step. The pH value of the DWTP water was 7.8 – 8.1. The dissolved organic carbon (DOC) concentration of DWTP water was 6.7 -7.3 mg L<sup>-1</sup>.

Adsorption experiments were conducted with a mixture of 23 PHAMs with varying characteristics (size, charge and hydrophobicity/hydrophilicity) that were purchased from Sigma-Aldrich. The physicochemical properties of the selected PHAMs are listed in Table 2.

## 2.2 Adsorption experiments

The PHAMs were dissolved in UP water to obtain a stock solution with PHAM concentrations of approximately 2 mg L<sup>-1</sup> each. The stock solution was diluted 1000 times either in UP water or in the DWTP water to prepare solutions with mixed PHAMs. The measured initial concentration of each PHAM in UP water and DWTP water after spiking were in the range of 0.864 - 2.199 µg L<sup>-1</sup> and 0.986 - 2.499 µg L<sup>-1</sup>, respectively.

High-silica zeolites were dosed into the 1000 ml solutions with mixed PHAMs. The dosages of zeolites were 0, 1, 5, 10, 50, 100, 250, 500 and 1000 mg L<sup>-1</sup>. A mixing time of 24h at room temperature (25±1 °C) was used to reach the adsorption equilibrium (Damjanovic et al., 2010). The solutions without zeolite dosage were used as blanks to test the stability of the PHAMs over the 24h contact time. Prior to analysis, the solutions were filtrated over 0.7 µm glass microfiber filters (Whatman, Grade GF/F).

## 2.3 Analytical methods for water samples

PHAM analyses were done at Het Waterlaboratorium in Haarlem, the Netherlands. Filtrated samples were concentrated by solid phase extraction. The quantification of PHAMs were accomplished by liquid chromatography - tandem mass spectrometry (LC-MSMS). DOC concentration of water samples were analyzed by total organic carbon analyzer (TOC-V<sub>CPH</sub>, Shimadzu).

## 2.4 Adsorption isotherm model

The PHAM adsorption isotherms on four zeolites were fitted to Freundlich model shown in Equation 1:

$$q = Kc^n \quad \text{Equation 1}$$

Where  $q$  is the adsorption capacity of PHAMs in the unit of  $\mu\text{g g}^{-1}$ ;  $c$  is the equilibrium concentration of PHAMs in the unit of  $\mu\text{g L}^{-1}$ ;  $K$  is the fitting constant in the unit of  $(\mu\text{g g}^{-1})(\mu\text{g L}^{-1})^{-n}$ ;  $n$  is the fitting constant without unit.

## 2.5 Correlation

The removal efficacies of PHAMs by zeolites were represented by D80, which is the theoretical zeolite dosage for 80% removal of each PHAM (Zietzschmann et al., 2014a). According to Equation 2, D80 was calculated based on the Freundlich fitting constants  $K$  and  $n$  at PHAM equilibrium concentration equal to 20% of the initial concentration:

$$D80 = \frac{c_0 - c_e}{q} = \frac{c_0 - 20\%c_0}{K * (20\%c_0)^n} \quad \text{Equation 2}$$

Where  $c_0$  is the initial concentration of PHAMs in the unit of  $\mu\text{g L}^{-1}$ ;  $c_e$  is the equilibrium concentration of PHAMs in the unit of  $\mu\text{g L}^{-1}$ . The Freundlich fitting constants, initial concentrations and D80 results of PHAMs are listed in Table S1. D80 was then correlated with the characteristics of PHAMs, i.e. hydrophobicity/hydrophilicity, charge and molecular size,, as well as the pore size of zeolites.

# 3 Results and discussion

## 3.1 PHAM removal in UP water

The removal percentages of PHAMs in UP water on different zeolite frameworks, i.e. FAU, MOR, BEA and MFI zeolites, are summerized in Figure 1a, b, c and d, respectively. PHAMs are grouped by their charge in the solution (pH=8), i.e. positive, neutral and negative. The removal percentage of PHAMs at zeolite dosages of 1, 10, 100, and 1000  $\text{mg L}^{-1}$  are plotted by symbols with different colours and shapes. As shown in Figure 1, the removal percentage of PHAM was higher at higher dosages of zeolites. Figure 1a shows that, at the

zeolite dosage of 1000 mg L<sup>-1</sup>, 16 out of the 23 PHAMs were removed by FAU with removal percentages of > 90%, while paracetamol and clofibric acid with positive and negative charge, respectively, were hardly removed by FAU with a removal percentage of less than 30 %. At the dosage of 10 mg L<sup>-1</sup>, only nine PHAMs, were partially removed by FAU, including six positively charged PHAMs, one neutral PHAM and two negatively charged PHAMs. At the zeolite dosage of 1 mg L<sup>-1</sup>, FAU only removed one positively charged PHAM, i.e. lidocaine.

Figure 1b presents that 16 out of the 23 tested PHAMs were removed by MOR with removal percentages of more than 95% at the zeolite dosage of 1000 mg L<sup>-1</sup>. Only less than 10 % of the iopromide and pravastatin were removed by MOR. MOR completely removed five positively charged PHAMs, i.e. metformin, lignocaine, trimethoprim, sotalol, metoprolol and one negatively charged PHAM, fenazon at a dosage of 10 mg L<sup>-1</sup>. However, furosemide, one negatively charge PHAM, was not removed by MOR at all.

Figure 1c shows that, at the BEA dosage of 1000 mg L<sup>-1</sup>, 13 tested PHAMs were completely removed, while the rest of the 10 PHAMs were partially removed. Neutral PHAMs, i.e. caffeine, primidone and iopromide, were poorly adsorbed by BEA with removal percentages less than 30%. At the dosage of 10 mg L<sup>-1</sup>, six PHAMs with positive charge and one negatively charged PHAM were well adsorbed on BEA with the removal percentage more than 90%.

The results in Figure 1d show that MFI removed all eight PHAMs with positive charge, two neutral PHAMs and three PHAMs with negative charge at a dosage of 1000 mg L<sup>-1</sup>, while 10 PHAMs, which were either neutral or negative, were not adsorbed on the MFI zeolite. The removal percentage of caffeine, a neutral PHAM, and fenazon, with negative charge, by MFI remained less than 20 %. When the zeolite dosage was as low as 10 mg L<sup>-1</sup>, only six PHAMs were adsorbed on MFI, including five PHAMs with positive charge and one negatively charged PHAM.

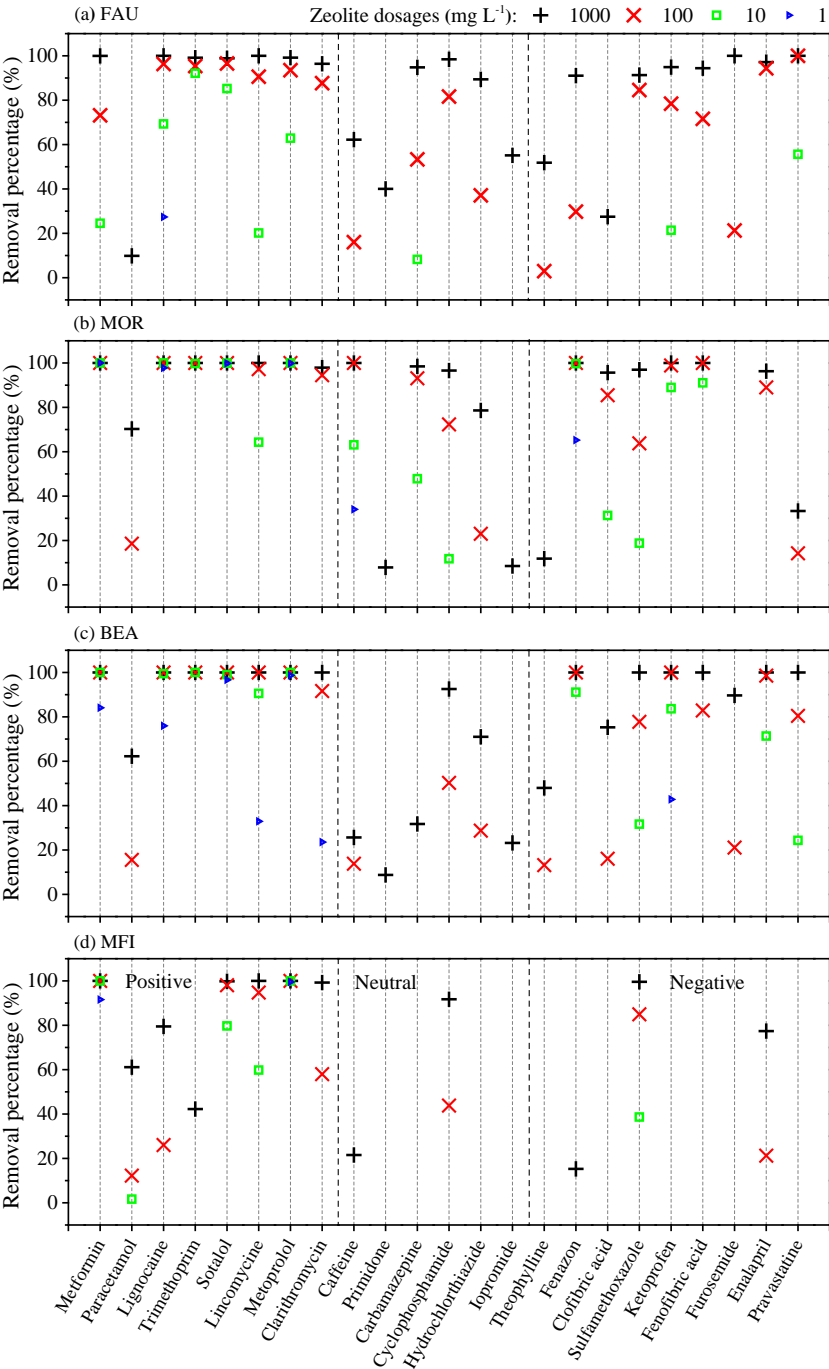


**Figure 1** The removal percentage of PHAMs in UP water on (a) FAU, (b) MOR, (c) BEA and (d) MFI zeolites.

As shown in Figure 1, FAU, MOR, BEA and MFI were selective adsorbents for the removal of PHAMs, which means that one zeolite, with a specific framework, removed only several species of PHAMs with high adsorption efficacies. This finding was confirmed by the research conducted by de Ridder et al. (2012), who studied the adsorption of 16 PHAMs in demineralised water on MOR and MFI. As suggested by Jiang et al. (2018), OMPs are adsorbed in the micropores of zeolites and a specific zeolite framework with uniformed micropore sizes, only provides accommodation for a narrow range of OMPs with molecular sizes comparable to or less than the pore size of zeolites. In comparison to zeolites, adsorbents with a broader range of micropore sizes, e.g. activated carbon, are more effective for the removal of OMPs with various molecular sizes (Kennedy et al., 2015; Li et al., 2002).

## **3.2 The effect of the characteristics of PHAMs and high-silica zeolites on PHAM removal**

### ***3.2.1. Hydrophobicity/hydrophilicity of PHAMs***

The hydrophobicity/hydrophilicity of PHAMs is represented by the logD value (Table 2). The relation between the logD of the PHAMs and the adsorption efficacies of the PHAMs, represented by the D80 value (Table S1), on FAU, MOR, BEA and MFI zeolites are shown in Figure 2a, b, c and d, respectively. Since the zeolite dosages in this study ranged from 1 to 1000 mg L<sup>-1</sup>, the presented results of D80 values equal to 1 and 1000 mg L<sup>-1</sup> means that the calculated D80 could also be lower than 1 mg L<sup>-1</sup> and higher than 1000 mg L<sup>-1</sup>, respectively. When a PHAM was not removed by a zeolite, D80 was not given. As shown in Figure 2, no relation between logD of PHAMs and the D80 value was found for any of the four zeolites.

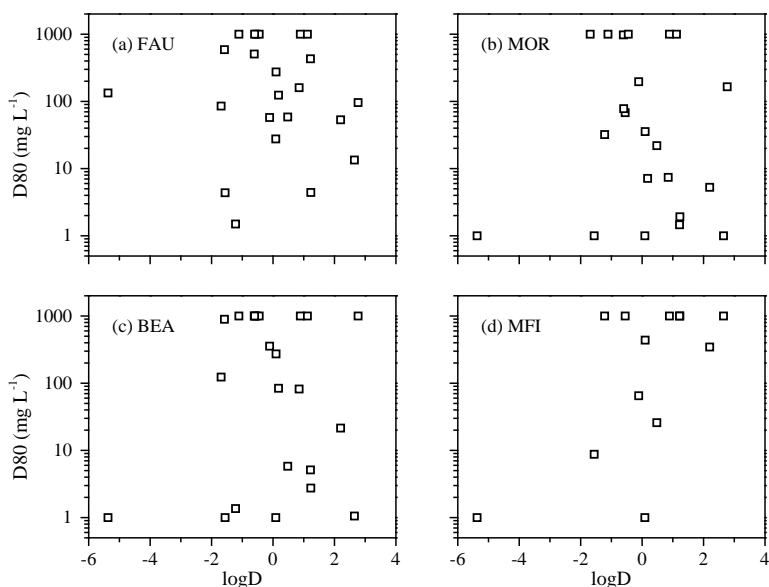


**Figure 2** The effect of  $\log D$  on  $D_{80}$  of PHAMs with (a) FAU, (b) MOR, (c) BEA and (d) MFI.

Previous studies showed that zeolites had lower adsorption efficacies for the more hydrophilic OMPs, e.g. sulfa drugs (Fukahori et al., 2011), nitrophenol compounds (Koubaisy et al., 2008) and N-nitrosamines (de Ridder et al., 2012) with a lower  $\log D$ . However, in our study, some PHAMs with a low  $\log D$  value, e.g. metformin with  $\log D$  -5.37, were well removed by the zeolites. It is speculated that the effect of hydrophobicity/hydrophilicity of PHAMs is obvious for OMPs with similar physicochemical characteristics. However, the adsorption efficacies of the PHAMs, here studied, on zeolites with various properties could have been dominated by other factors, such as the charge and molecular sizes of PHAMs.

### 3.2.2 Charge of PHAMs

The  $D_{80}$  values of the FAU, MOR, BEA and MFI for the 23 PHAMs, with a positive, neutral and negative surface charge, are shown in Figure 3. The  $D_{80}$  values for two out of eight PHAMs with positive charge, i.e. metformin and metoprolol were less than  $1 \text{ mg L}^{-1}$  with MOR, BEA and MFI. The  $D_{80}$  of six out of eight positively charged PHAMs with MOR and BEA were less than  $10 \text{ mg L}^{-1}$ , while the  $D_{80}$  of the positively charged PHAMs with FAU was from 4 to  $200 \text{ mg L}^{-1}$ . As an exception, the  $D_{80}$  for positively charged paracetamol was

higher than 1000 mg L<sup>-1</sup> of all zeolites, which indicates that paracetamol was poorly adsorbed on all zeolites.

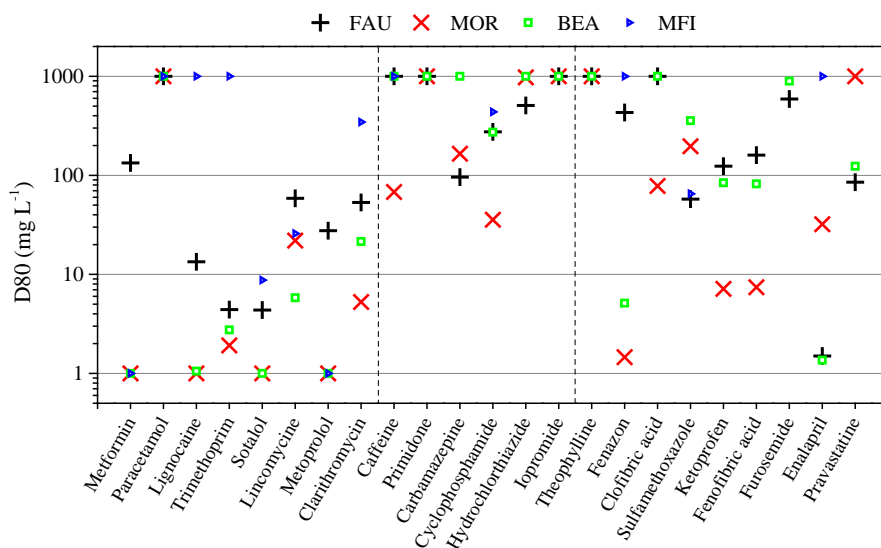


**Figure 3** D80 values of PHAMs with FAU, MOR, BEA and MFI zeolites.

The results in Figure 3 show that the D80 value of neutral and negatively charged PHAMs were higher than these of the positively charged PHAMs. The D80 of neutral PHAMs were above 10 mg L<sup>-1</sup> for all four zeolites, and in most cases, above 100 mg L<sup>-1</sup>. The D80 values of the negatively charged PHAMs were widely distributed in the range of 1 mg L<sup>-1</sup> to 1000 mg L<sup>-1</sup> for all four zeolites, while none of D80 values was < 1 mg L<sup>-1</sup>.

As shown in Figure 3, the charge of PHAMs had a crucial effect on the adsorption efficacies of PHAMs. In fact, most of the framework structures of high-silica zeolites are not charged, while a small number of negatively charged sites exist that are introduced by the Al content in the zeolite (Auerbach et al., 2003). Although, adsorbed PHAMs experience van der Waals forces with the zeolite frameworks, regardless of the charge of PHAMs and zeolites (Israelachvili 2015), apparently, positively charged PHAMs experienced electrostatic attraction with the few negative sites of the zeolites. Neutral PHAMs, however, only experienced van der Waals forces with the zeolite frameworks, which made the neutral PHAMs less adsorbable than the positively charged PHAMs. The hampered adsorption of negatively charged PHAMs could be explained by the electrostatic repulsion



forces between the negatively charged PHAMs and the negative sites of the zeolites, which reduced their adsorption efficacies. The charge effect on OMP adsorption was also observed by Mailler et al. (2015) and de Ridder et al. (2011), both finding that negatively charged activated carbon had better adsorption efficacies for positively charged PHAMs than negative and neutral OMPs. However, two exceptions were observed in Figure 3: the negatively charged fenazon adsorbed well on MOR; and enapril adsorbed well on BEA and FAU. This indicates that the adsorption efficacies of these two PHAMs were apparently affected by other factors than the charge of the PHAMs.

### 3.2.3 Size effect

The effect of molecular sizes of the PHAMs on adsorption efficacies by high-silica zeolites were also studied. In Figure 4a, b, c and d, the molecular sizes of PHAMs are shown in comparison to the pore opening sizes of FAU, MOR, BEA and MFI zeolites, respectively. The molecular sizes of PHAMs were calculated based on the assumption that PHAM molecules are cylindrical shapes with three dimensional sizes as suggested by de Ridder et al. (2012). The results are listed in Table 2. One exception in this study is carbamazepine with a one dimensional size of zero, and was therefore regarded as a two dimensional molecule. In Figure 4, the molecular weight of each PHAM (Table 2) is labelled with the name of the PHAM at X axis. Figure 4 shows that PHAMs with a higher molecular weight generally have larger molecular sizes.

As mentioned in Section 3.2.2, positively charged PHAMs were more favourably adsorbed on MOR, BEA and MFI zeolites than FAU. The porous structures of MOR, BEA and MFI originate from two types of channels each with opening sizes from 2.6 to 7.7 Å and the inner diameter of channels are theoretically comparable to the pore opening sizes. FAU zeolites have cages with an opening size of the pore of 7.4 Å\*7.4 Å and an inner diameter of 13.4 Å. (Baerlocher et al., 2007). In addition to the electrostatic attraction, channels with narrow inner sizes were beneficial for the adsorption of positively charged PHAMs compared with the cages of the zeolites. This was also reflected in Figure 3, showing that the D80 values of positively charged PHAMs with FAU were always higher than D80 with MOR, BEA or MFI.

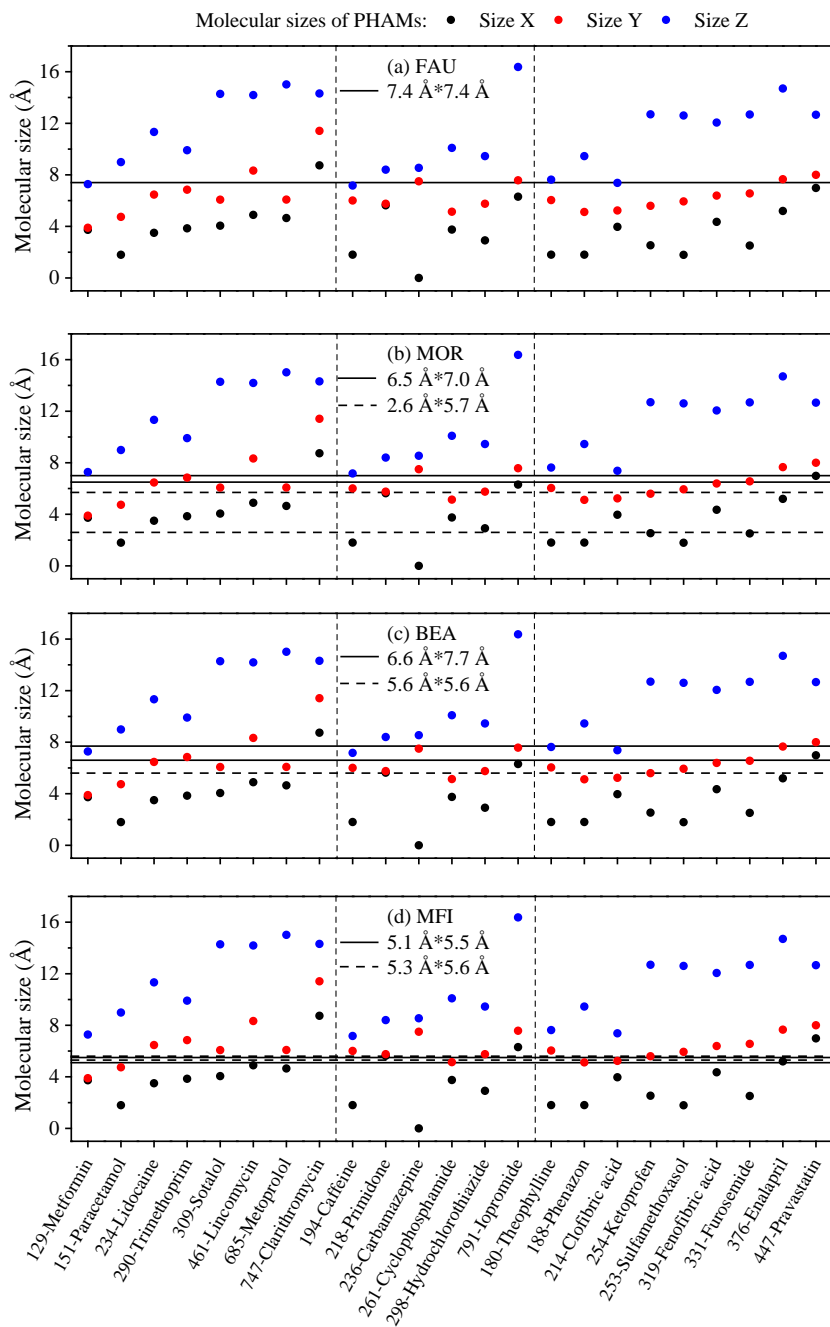


**Figure 4** The comparison between the three dimensional sizes of PHAMs and the pore opening sizes of (a) FAU, (b) MOR, (c) BEA and (d) MFI. X axis label: molecular weight - name of PHAMs.

The adsorption efficacies of neutral and negatively charged PHAMs varied with the framework type of the zeolites (Figure 3). In comparison with other tested zeolites, MOR had better adsorption efficacies for six out of the 15 neutral and negatively charged PHAMs (Figure 3). The removal of PHAMs on MOR might benefit from the wide range of pore sizes, i.e. 2.6 Å – 7.0 Å, from two types of channels with opening sizes of 2.6 Å\*5.7 Å and 6.5 Å\*7.0 Å. Figure 3b shows that one channel type of MOR, with opening sizes of 2.6 Å\*5.7 Å, is smaller than the pore opening sizes of other zeolites, which would specially fit the PHAMs with similar, small sizes, such as caffeine with a size of 1.818 Å \*3.573 Å \*6.505 Å and fenazon with a size of 1.806 Å \*5.116 Å \*9.452 Å. These were therefore effectively adsorbed on MOR (Figure 3). Moreover, two negatively charged PHAMs with relatively large molecular sizes, i.e. enalapril and pravastatine, with molecular sizes of 5.197 Å \*7.659 Å \*14.702 Å and 6.982 Å \*8.001 Å \*12.663 Å, respectively, were more preferably adsorbed on BEA and FAU zeolites with large pore sizes. This phenomenon has previously been explained by de Ridder et al. (2012), Erdem-Senatalar et al. (2014) and Rossner et al. (2009). The closely fitted pores would provide strong interaction between PHAMs and zeolites, and also prevent water adsorption in the framework of zeolites (Giaya and Thompson 2002a; b).

The results in Figure 3 show that a total number of five out of the 15 neutral and negatively charged PHAMs were adsorbed on MFI, being less efficient than the other tested zeolites. Compared with FAU, MOR and BEA, MFI has the smallest pore opening sizes among the four tested zeolites, i.e. 5.1 Å \*5.5 Å, 5.3 Å \*5.6 Å, with two types of channels. As shown in Figure 3d, PHAMs with two dimensional sizes larger than the pore opening size of MFI zeolite, including cabamazepine, iopromide, theophylline, fenofibric acid, furosemide, enalapril and pravastatin, were excluded by MFI. Only two PHAMs i.e. cyclophosphamide and sulfamethoxazol with molecular sizes of 5.14 Å \*3.751 Å \*8.542 Å and 5.593 Å \*2.531 Å \*12.691 Å, respectively, had two dimensional sizes less than or comparable to the pore opening size of MFI zeolite and, thus, were, although poorly, adsorbed on MFI. In most of the cases where PHAMs were adsorbed ( $D_{80} < 1000 \text{ mg L}^{-1}$ , Figure 3), at least two dimensional sizes of molecular sizes of the PHAMs were smaller than or comparable to the pore opening sizes of the zeolites (Figure 3).

As an exception, only clarithromycin with a larger molecular size than the pore opening sizes of the zeolites (Figure 4), was adsorbed on all four tested zeolites, however, with the

least adsorption efficacy of the positively charged PHAMs (Figure 3). Considering that the inner pore size of FAU, i.e. 13.4 Å, is larger than the two dimensional sizes of clarithromycin, FAU potentially allows the adsorption of clarithromycin with sizes of 11.41 Å\*8.735 Å\*14.315 Å inside the pores. Since the pore sizes of MOR, BEA and MFI zeolites are smaller than the three dimensional sizes of clarithromycin, clarithromycin should not be able to enter the pores of zeolites. As shown in Table 1, the external surface area of tested zeolites were in the range of 52 -165 m<sup>2</sup> g<sup>-1</sup>. The external surface area of BEA (165 m<sup>2</sup> g<sup>-1</sup>), e.g., accounted for up to 32 % of the BET surface area (516 m<sup>2</sup> g<sup>-1</sup>). Previous studies showed that local defects, e.g. Si-OH species, were generated at the external surface of zeolites during the synthesis of high-silica zeolites (Burton 2018; Yu 2007). Molecules which are too large to diffuse into the pores, could therefore be adsorbed onto the external surface of zeolites by interacting with -OH groups at the defects (Bevilacqua and Busca 2002; Bolis et al., 2006).

### 3.3 PHAM removal in the presence of NOM

To study the effect of NOM on PHAM adsorption, the removal percentages of PHAMs by FAU, MOR, BEA and MFI in UP water and DWTP water are shown in Figure 5 and Figure 6 with zeolite dosages of 1000 and 10 mg L<sup>-1</sup>, respectively.

At a zeolite dosage of 1000 mg L<sup>-1</sup>, the removal percentages of most PHAMs in DWTP water were comparable to or lower than in UP water (Figure 5). As in UP water, some of the positively charged PHAMs in DWTP water were completely removed by the four zeolites, e.g. lincomycin and metoprolol in the presence of NOM. Positively charged PHAMs were better removed than neutral or negatively charged PHAMs in DWTP water. For example, BEA removed all eight positively charged PHAMs in DWTP water with comparable removal percentages as in UP water, while only two out of the six neutral PHAMs, i.e. cyclophosphamide and hydrochlorothiazide, and four out of the nine negatively charged PHAMs, at the zeolite dosage of 1000 mg L<sup>-1</sup>. In comparison with the adsorption efficacies in UP water, the adsorption efficacies of some negatively charged and neutral PHAMs in DWTP water were less or even absent, such as for primidone, iopromide, sulfamethoxazole, fenofibric acid, furosemide and pravastatine.

As shown in Figure 6, positively charged PHAMs, e.g. metformin, sotalol and metoprolol, were even completely removed by MOR and MFI at a zeolite dosage of 10 mg L<sup>-1</sup> in DWTP

water. However, at the zeolite dosage of  $10 \text{ mg L}^{-1}$ , the removal percentages of neutral and negatively charged PHAMs in DWTP water were much lower than in UP water. Except for carbamazepine, fenazon and enalapril, which were removed by MOR and BEA with removal percentages of less than 15%, the rest of the neutral and negatively charged PHAMs were not removed by any of the tested zeolites. The results in Figure 6 show that, as in UP water, positively charged PHAMs were still more preferably adsorbed on zeolites than neutral and negatively charged PHAMs in DWTP water at a zeolite dosage of  $10 \text{ mg L}^{-1}$ .

As mentioned in the previous section, positively charged PHAMs would experience electrostatic attraction with zeolites framework, while the bonding between zeolites and neutral/negatively charged PHAMs was weaker. Additionally, there was possibly a low concentration of competing positively charged NOM fractions in the tested DWTP water, e.g. aromatic amines, than the neutral and negatively charged fractions, e.g. fulvic acid, hydrocarbons and tannins (Leenheer and Croué 2003). NOM would therefore have more effect on the adsorption of neutral and negatively charged PHAMs than on the positively charged PHAMs.

The results in Figure 6 show that, at the zeolite dosage of  $10 \text{ mg L}^{-1}$  in DWTP water, MOR, BEA and MFI achieved high removal efficacies for positively charged PHAMs, e.g. metformin, sotalol and metoprolol, with removal percentages of more than 80%, while only two positively charged PHAMs, i.e. trimethoprim and metoprolol, were removed by FAU with removal percentages of less than 30%. The finding that zeolites with channel structures, e.g. MOR, BEA and MFI, were more capable of removing positively charged PHAMs than FAU zeolites with cages in the presence of NOM is consistent with the observation in UP water. It is thus assumed that the channel structures with narrow inner sizes would prevent the effect of NOM on PHAM adsorption.

Rosner et al. (2009) found that, at a zeolite dosage of  $100 \text{ mg L}^{-1}$ , iopromide and sulfamethoxazole were not removed by FAU or MOR at all and trimethoprim was partially removed by MOR, which is partially consistent with our finding. We showed that trimethoprim was already removed by FAU at zeolite dosage of  $10 \text{ mg L}^{-1}$ , with a removal percentage of about 20%, while trimethoprim was not removed by FAU. The better removal efficacies might be attributed to the higher spiked concentration of PHAMs in our

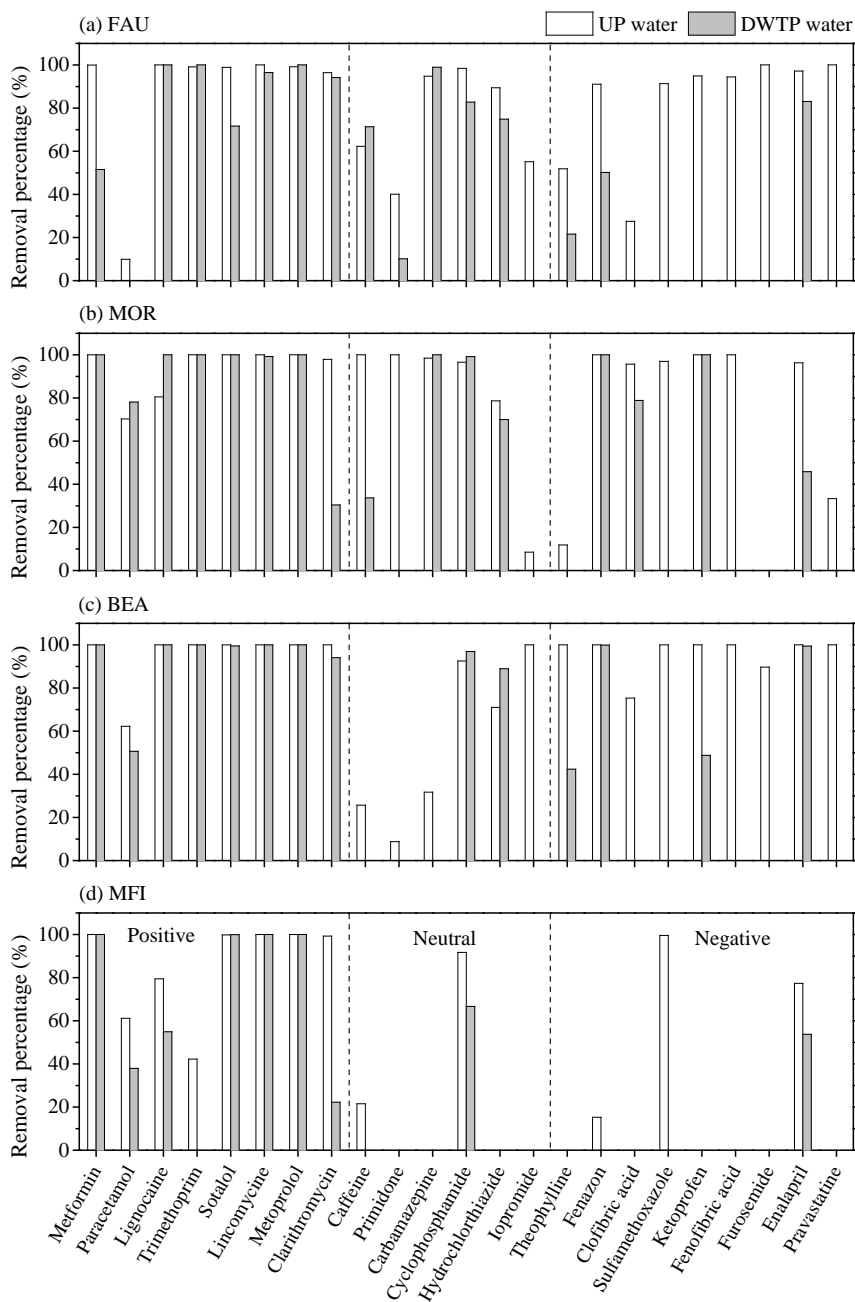


**Figure 5** The removal percentages of PHAMs on (a) FAU, (b) MOR, (c) BEA and (d) MFI at the zeolite dosage of  $1000 \text{ mg L}^{-1}$  in UP water and DWTP water.

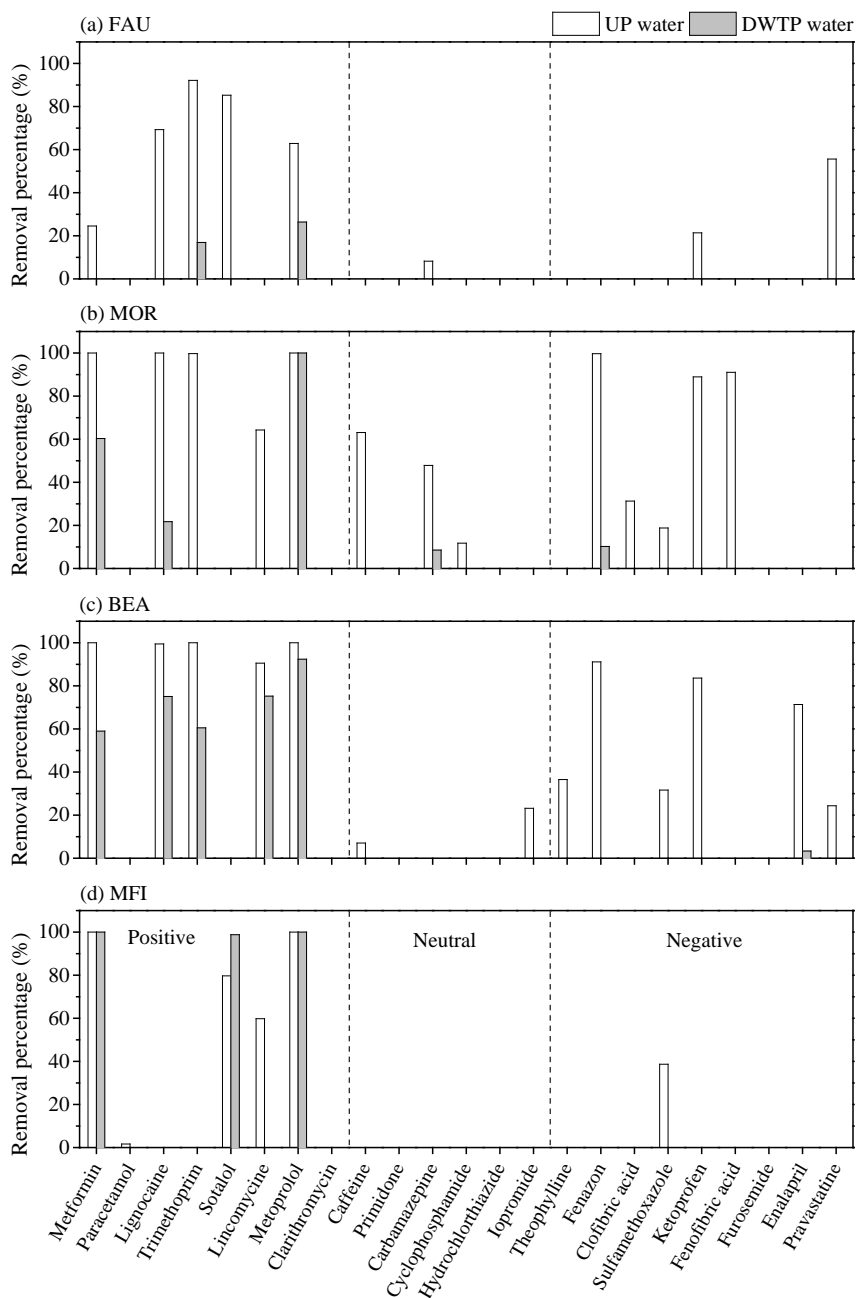


**Figure 6** The removal percentages of PHAMs on (a) FAU, (b) MOR, (c) BEA and (d) MFI at the zeolite dosage of  $10 \text{ mg L}^{-1}$  in UP water and DWTP water.

study ( $0.986 - 2.499 \mu\text{g L}^{-1}$ ) than the initial concentration used by Rossner et al., i.e. 200 to  $900 \text{ ng L}^{-1}$ .

The effect of NOM on PHAM adsorption is also reflected in the Freundlich adsorption isotherms. The adsorption isotherms of enalapril, as an example, in UP water and DWTP water are presented in Figure 7. Due to the effect of NOM, the adsorption capacities of enalapril in DWTP water were about 1 log lower than in UP water. Pelekani and Snoeyink (1999) mentioned that the capacity reductions of activated carbon for OMP adsorption with one or two orders of magnitude are common. When the equilibrium concentration of enalapril reached about  $1 \mu\text{g L}^{-1}$ , the adsorption capacities of enalapril on FAU, MOR and BEA zeolites started to decrease, resulting in curved isotherms. When the equilibrium concentration of enalapril was higher, the dosages of zeolites were lower and the effect of NOM on PHAM adsorption would be stronger.

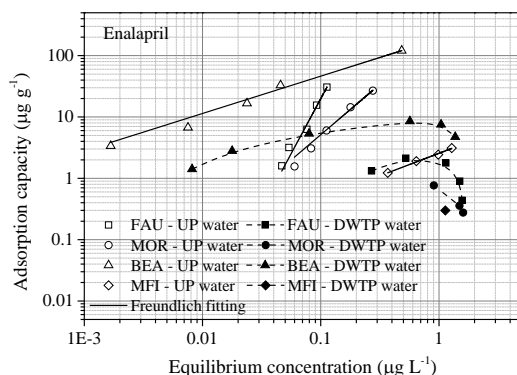


**Figure 7** The adsorption isotherms of enalapril on zeolites in UP water and DWTP water. Solid lines: Freundlich model fitting for the adsorption isotherms of enalapril in UP water; Dash lines: Indicative lines for the adsorption isotherms of enalapril in DWTP water.

The DOC concentrations of DWTP water with different zeolite dosages are shown in Figure 8. When zeolites were not dosed in DWTP water, the DOC concentration was in the range of  $6.7 - 7.3 \text{ mg L}^{-1}$ , which was about 1000 times higher than the concentration of targeted PHAMs (Figure 8). With the increase in zeolite dosage from 1 to  $1000 \text{ mg L}^{-1}$  in DWTP water, hardly any DOC removal was observed for the four tested zeolites. The DOC



concentration in DWTP slightly decreased from 6.8 to 6.4 mg L<sup>-1</sup> with the increase in dosage of FAU from 1 to 1000 mg L<sup>-1</sup>. In addition, in comparison with the zeolite dosage of 0 mg L<sup>-1</sup>, a slight decrease of DOC concentration, e.g. 0.3 mg L<sup>-1</sup>, was found at the MOR dosage of 1000 mg L<sup>-1</sup>. DOC concentrations in DWTP water with the dose of BEA and MFI had no variation with the dosage of zeolites. Therefore, it is assumed that the majority of NOM fractions, e.g. humic acids, were excluded by zeolites. Certain low molecular weight DOC fractions, e.g. humic monomers, with sizes less than the pore sizes of zeolites could however be adsorbed on zeolite frameworks with relatively large pore size, e.g. FAU (Braschi et al., 2016b).

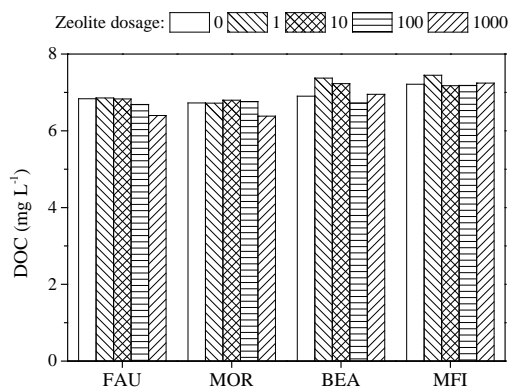


**Figure 8** DOC concentration in DWTP water at the zeolite dosage of 0, 1, 10, 100 and 1000 mg L<sup>-1</sup>.

Previous studies showed that the adsorption of specific neutral OMPs on zeolites, e.g. MTBE on MOR and MFI (Hung and Lin 2006; Knappe and Campos 2005) and N-nitrosamines on MFI (de Ridder et al., 2012), were not affected by NOM in water. It has been assumed that NOM fractions failed to compete with these OMPs for the adsorption sites in the micropores, which closely fitted the adsorbed OMPs. Since zeolites with uniform micropores were unable to fit OMPs with a broad range of characteristics, the competition of NOM in multi-solute water would be more severe than in single-solute water. Pelekani and Snoeyink (1999) suggested that NOM effect on atrazine adsorption on activated carbon fibers was caused by pore blockage. This explanation could also be applicable for zeolites, as the uniform pore size of activated carbon fibers, e.g. 6 – 8 Å, are in the same range as the tested zeolites, e.g. 2 – 8 Å. A small portion of NOM fractions was adsorbed on zeolites (Figure 7) and possibly located at the external surface of zeolites. The

entrance of the cages and channels for PHAM adsorption would thus be blocked and PHAM adsorption could therefore be inhibited. NOM fractions might also compete for adsorption sites with PHAMs at the external surface of zeolites, e.g. clarithromacine, resulting in a decrease of PHAM adsorption efficacies.

## 4 Conclusions

The adsorption efficacies of 23 PHAMs in UP water and DWTP water on high-silica zeolites with four different frameworks were studied. The adsorption efficacies of PHAMs on zeolites were related to the properties of PHAMs, i.e. hydrophobicity/hydrophilicity, charge and molecular size. The mechanisms of NOM affecting PHAM adsorption on four zeolites were discussed. The following conclusions were drawn:

- All tested PHAMs in UP water were completely or partially adsorbed on FAU and BEA zeolites, while MOR removed 21 PHAMs except for theophylline and furosemide. MFI removed all eight PHAMs with positively charge, two neutral PHAMs and three negatively charged PHAMs.
- The effect of hydrophobicity/hydrophilicity of PHAMs on the adsorption efficacies of PHAMs on zeolites was not observed. The adsorption efficacies of PHAMs on zeolites with various properties were dominated by other factors, e.g. charge and molecular size of PHAMs.
- The adsorption efficacies of positively charged PHAMs in UP water were higher than those of neutral and negatively charged PHAMs. The effect of NOM on the adsorption of positively charged PHAMs was less pronounced or even absent compared to the adsorption of neutral and negatively charged PHAMs, since positively charged PHAMs were steadily adsorbed on high-silica zeolites by experiencing electrostatic attraction with the negative sites of the zeolites. Moreover, there was possibly a lower concentration of positively charged competing NOM fractions in DWTP water than neutral and negatively charged NOM fractions.
- Zeolites with channels, i.e. MOR, BEA and MFI, proved to be better adsorbents for positively charged PHAMs than FAU with cages. The channels with a narrow inner

size would prevent the competition of NOM with the adsorption of positively charged PHAMs, while NOM might enter the cages of FAU with large inner sizes.

- The adsorption of neutral and negatively charged PHAMs were affected by the molecular sizes of PHAMs and pore sizes of zeolites. PHAMs with molecular sizes in two dimensions larger than the pore opening sizes of zeolites were not adsorbed. When the molecular sizes of PHAMs were similar to the sizes of zeolites, PHAMs were preferably adsorbed.
- A considerable effect of NOM on the adsorption of neutral and negatively charged PHAMs was observed. The adsorption efficacies in DWTP water were much lower than in UP water, due to weak bonding between neutral/negatively charged PHAMs and zeolites. In the presence of NOM, the adsorption capacity of PHAMs would even decrease with the decrease of zeolite dosing, as indicated by the curved adsorption isotherms in DWTP water.
- A small portion of NOM fractions with low molecular weight would enter the micropores of the zeolites. NOM competition with PHAMs for the adsorption sites in the micropores were likely to happen in multi-solute water, since a broad range of PHAMs were unable to closely fit uniform micropores of zeolites. In addition, NOM fractions would be adsorbed on the external surface of zeolites and caused the blockage of micropores.

Supporting information

Table S1 The initial concentration, Freundlich isotherm constants and D80 values of PHAMs.

FAU					MOR						
c <sub>0</sub>	D80	n	logK	K (μg g <sup>-1</sup> ) (μg L <sup>-1</sup> ) <sup>-n</sup>	R <sup>2</sup>	c <sub>0</sub>	D80	n	logK	K (μg g <sup>-1</sup> ) (μg L <sup>-1</sup> ) <sup>-n</sup>	R <sup>2</sup>
μg L <sup>-1</sup>	mg g <sup>-1</sup>	n				μg L <sup>-1</sup>	mg g <sup>-1</sup>	n			
Metformin	134	1.0005	1.4768	29.97782	0.9914	0.85	1	Complete removal			
Paracetamol	1000	2 data, limited removal				1.63	1000	1.0184	0.3776	2.385613	0.9745
Lignocaine	13	1.0991	2.5148	327.19	0.9739	1.73	1	1 data, good removal			
Trimethoprim	4	1.8556	3.3935	2474.571	0.8877	1.47	2	0.3076	2.9519	895.1586	0.9742
Sotalol	4	1.8118	3.2965	1979.247	0.9683	1.84	1	2 data, good removal			0.9784
Lincomycine	59	0.6906	1.6896	48.93279	0.947	2.65	22	0.6624	2.1676	147.0957	0.9805
Metoprolol	28	1.1981	2.2735	187.7154	0.9464	1.42	1	1 data, good removal			
Clarithromycin	53	1.6974	2.3312	214.3878	0.9193	1.86	5	2.001	3.3106	2044.561	0.9764
Caffeine	1000	2 data, limited removal				2.11	68	2.0134	2.1503	141.3514	0.71
Primidone	1000	0.5582	-0.1441	0.717629	0.7888	1.78	1000	1 data, limited removal			
Carbamazepine	96	0.8419	1.5515	35.6041	0.9833	1.78	165	0.7684	1.2804	19.07217	0.9603
Cyclophosphamide	275	0.7399	1.0155	10.36335	0.987	1.31	36	0.7626	1.913	81.84648	0.9971
Hydrochlorthiazide	507	0.813	0.8015	6.331404	0.9832	1.36	977	0.7954	0.4965	3.136895	0.9677
Iopromide	1000	0.6405	0.2964	1.978791	1	2.15	1000	1 data, limited removal			
Theophylline	1000	0.5759	-0.0088	0.979941	0.86	1.72	1000	1 data, limited removal			
Fenazon	431	0.4236	0.7213	5.263808	0.9428	1.93	1	0.3769	3.1804	1514.956	0.9802
Clofibric acid	1000	1 data, limited removal				1.87	78	0.9747	1.6989	49.99194	0.9815
Sulfamethoxazole	58	1.3886	2.0056	101.2978	0.9717	2.10	196	0.8457	1.2507	17.81148	0.961
Ketoprofen	124	0.8832	1.4591	28.78061	0.9935	1.80	7	0.836	2.6756	473.8054	0.9801
Fenofibric acid	160	1.1498	1.4581	28.71442	0.9587	1.76	7	2 data, good removal, linear correlation			
Furosemide	589	0.3741	0.5215	3.322768	0.7514	1.36	-	no removal			
Enalapril	1	3.207	4.4914	31002.73	0.9802	1.62	32	1.8836	2.5284	337.5981	0.9933
Pravastatine	85	1.4099	1.9812	95.7635	0.4795	0.85	1000	5.9492	0.9155	8.231898	0.999

Table S1 The initial concentration, Freundlich isotherm constants and D80 values of PHAMs (Continued).

BEA					MFI							
c <sub>0</sub>	D80	n	logK	K	R <sup>2</sup>	c <sub>0</sub>	D80	n	logK	K	R <sup>2</sup>	
μg L <sup>-1</sup>	mg g <sup>-1</sup>	n		(μg g <sup>-1</sup> ) (μg L <sup>-1</sup> ) <sup>-n</sup>		μg L <sup>-1</sup>	mg g <sup>-1</sup>	n		(μg g <sup>-1</sup> ) (μg L <sup>-1</sup> ) <sup>-n</sup>		
Metformin	1.63	1	2 data, good removal			1.16	1	1 data, good removal				
Paracetamol	1.78	1000	1.2769	0.2351	1.718304	0.9419	1.69	1000	1.0077	0.1906	1.550958	
Lignocaine	2.76	1	0.8139	3.5308	3394.689	0.8404	1.37	1000	0.8859	0.4878	3.074681	
Trimethoprim	1.62	3	0.3246	2.832	679.2036	0.7703	1.62	1000	1.2676	-0.1336	0.735191	
Sotalol	2.28	1	1.1681	4.4553	28529.88	0.9782	1.69	9	1.0534	2.6848	483.9494	
Lincomycine	1.47	6	0.8427	2.7542	567.806	0.9926	1.01	26	0.8996	2.1204	131.9471	
Metoprolol	1.28	1	0.8103	4.5007	31673.79	0.9953	1.28	1	1 data, good removal			
Clarithromycin	0.74	21	1.4371	2.6328	429.3387	0.9972	0.74	345	1.1195	1.1632	14.56129	
Caffeine	1.97	1000	2 data, limited removal			2.25	1000	1 data, limited removal				
Primidone	1.96	1000	1 data, limited removal			1.82	-	no removal				
Carbamazepine	2.00	1000	1.1583	-0.3528	0.443813	0.9970	1.79	-	no removal			
Cyclophosphamide	1.31	273	0.6853	0.9832	9.620552	0.9458	1.43	437	0.8151	0.8604	7.251035	
Hydrochlorothiazide	1.73	1000	1.4882	0.544	3.499452	0.9884	1.55	-	no removal			
Iopromide	1.40	1000	1 data, limited removal			0.7464	0.88	-	no removal			
Theophylline	1.82	1000	1.8654	-0.0112	0.974541	0.9789	1.70	-	no removal			
Fenazon	1.93	5	0.9225	2.8604	725.1035	0.9892	1.74	1000	1 data, limited removal			
Clofibric acid	1.95	1000	0.5432	0.3213	2.09556	0.8781	1.95	-	no removal			
Sulfamethoxazole	1.77	356	0.9905	1.0462	11.12244	0.9446	1.81	65	0.7347	1.6722	47.01106	
Ketoprofen	1.89	84	0.581	1.4999	31.6155	0.8985	1.90	-	no removal			
Fenofibric acid	2.20	82	0.525	1.5189	33.02935	0.9865	1.98	-	no removal			
Furosemide	1.93	894	0.1603	0.3035	2.011407	0.9633	1.50	-	no removal			
Enalapril	1.69	1	0.6542	3.3053	2019.761	0.9877	1.63	1000	0.7292	0.4076	2.55623	
Pravastatine	0.86	123	0.9471	1.4701	29.51889	0.9502	0.92	-	no removal			

## **CHAPTER 6**

### **CONCLUSIONS AND OUTLOOK**

## 1 Conclusions

In this thesis, a study on adsorption efficacies and mechanisms of OMPs on high-silica zeolites was conducted. The adsorption efficacies of OMPs with a variety of characteristics, i.e. molecular weight/sizes, charge and hydrophobicity/hydrophilicity, on high-silica zeolites with different porous structures and surface chemistry were explored. In addition, in order to gain insight in the adsorption of OMPs in real water, the adsorption of multiple OMPs in the presence of natural organic matter (NOM) was studied.

It can be concluded that high-silica zeolites have a good ability to remove several OMPs from water. However, the adsorption efficacies were affected by the characteristics of the OMPs and the high-silica zeolites. A combination of high-silica zeolites with different pore sizes could be a barrier for a broad range of OMPs. However, the adsorption efficacies of certain neutral and negatively charged OMPs were hampered by the presence of NOM, which is not favourable for the application of high-silica zeolites in water treatment as only barrier against OMPs. More insight in the removal mechanisms was obtained by estimating the adsorption efficacy of 2,4,6-trichlorophenol (TCP) by molecular simulation which corresponded well with the results from batch experiments.

The specific conclusions in response to the research questions proposed in Chapter 1 are highlighted.

### **Research question 1: What is the current understanding of OMP adsorption on high-silica zeolites?**

The state-of-the-art knowledge on OMP adsorption on high-silica zeolites was reviewed and reported in Chapter 2. It was concluded that high-silica zeolites have the ability for adsorption of a variety of OMPs, including the small sized and polar OMPs, which are not well adsorbed on other adsorbents. The good adsorption efficacies of high-silica zeolites benefit from the featured properties, i.e. large number of micropores, closely fitted pores for OMPs and high surface hydrophobicity. The effect of NOM in natural water on certain OMP adsorption, i.e. MTBE and N-nitrosamines, was not observed, while the effect of NOMs on a broader range of OMPs is unknown. Further it was found that oxidative regeneration of high-silica zeolites could be an efficient method to restore the adsorption capacities of high-silica zeolites, although, during oxidative regeneration, an increase in BET surface

area and defects of high-silica zeolites was observed. The combination of high-silica zeolite adsorption and on-site oxidative regeneration, therefore, potentially allows for a reduction of investment and operational costs and waste generation compared to conventional activated carbon filtration. Specific OMPs, which are not removed by activated carbon could thus be targeted by high-silica zeolites.

### **Research question 2: What are the OMP adsorption mechanisms on high-silica zeolites?**

In Chapter 3, the adsorption of triclosan, TCP and phenol with the same functional groups, but diverse properties, i.e. molecular weight and water affinity, on ten high-silica zeolites were studied. Triclosan was more favourably adsorbed on FAU zeolites than on BEA, MOR and MFI zeolites. The maximum adsorption capacities of triclosan were more related to the micropore surface area/volume than the hydrophobicity of the zeolites. The adsorption isotherm of TCP on FAU zeolite was S-shaped, which means that TCP adsorption loading was minimal at low equilibrium concentrations and started increasing to a plateau after an inflection. Since phenol is more hydrophilic and thus had a lower affinity for high-silica zeolites, maximum adsorption capacities of phenol were not observed at the same equilibrium concentration range as triclosan and TCP. The adsorption capacities of phenol on high-silica zeolites were lower than of triclosan and TCP. MFI zeolites with more closely fitted pores for phenol had a higher adsorption capacity than FAU, BEA and MOR for phenol adsorption. Compared with carbon based adsorbents, apparently, the lack of efficient active adsorption sites, however, limited the adsorption efficacies of OMPs at the relatively low concentration range.

To further explore the adsorption mechanisms behind the S-shaped isotherm which was observed during the adsorption of TCP on high-silica zeolites, Monte Carlo (MC) simulation was carried out and reported in Chapter 4. FAU zeolites with a high Si/Al ratio showed an obvious S-shaped adsorption isotherm and a high adsorption capacity of TCP. Results from MC simulation corresponded well with the results from batch experiments, regarding the shape of adsorption isotherms, the maximum adsorption capacities of TCP and the effect of Si/Al ratios. It was concluded that the occurrence of S-shaped isotherms originated from the  $\pi$ - $\pi$  interaction between TCP molecules. At low TCP equilibrium concentrations, one TCP was adsorbed in the cage of FAU. With the increase of TCP equilibrium concentration,



the cages of the FAU zeolite allowed the adsorption of multiple TCP molecules, which was a potential condition for enhanced  $\pi$ - $\pi$  interaction of TCP. A higher Al content in the framework of FAU zeolites and thus a lower Si/Al ratio promoted the adsorption of water molecules, which inhibited TCP adsorption and thus prevented the occurrence of an S-shaped isotherm.

From the results of the study it can be further concluded that the adsorption of OMPs on high-silica zeolites is based on monolayer adsorption. The maximum adsorption capacities of OMPs are decided by the micropore surface area/volume of zeolites. The maximum adsorption capacity of neutral OMPs at high equilibrium concentrations by high-silica zeolites are higher compared to same species of charged OMPs, since the surface of high-silica zeolites are almost neutral (Fukahori et al., 2011). However, at low equilibrium concentration, the adsorption efficacies of positively charged OMPs were higher than those of neutral and negatively charged OMPs, since positively charged OMPs were steadily adsorbed on high-silica zeolites by experiencing electrostatic attraction with the negative sites of the zeolites (Chapter 5). The hydrophobicity of high-silica zeolites prevent the water adsorption and the pore blockage by water molecules. More pores of zeolites are thus available for the diffusion and adsorption of OMPs (Damjanovic et al., 2010; de Ridder et al., 2012). The pore opening size of zeolites determines the accessibility of the OMPs during the adsorption process. OMPs with a molecular size larger than the pore opening size of zeolites are excluded by zeolite frameworks due to steric hindrance (Roque-Malherbe et al., 1995; Rungsirisakun et al., 2006). The pores of zeolites closely fitted for OMPs disrupt the structure of water clusters in the micropores of zeolites and provide a strong interaction between OMPs and zeolites (Giaya and Thompson 2002a; b). Therefore, high-silica zeolites are better adsorbents than activated carbon for the removal of small sized, polar and non-aromatic OMPs, which closely fit the pores of zeolites.

### **Research question 3: How do NOMs affect OMP adsorption on high-silica zeolites?**

The effect of NOM on the adsorption of 23 pharmaceuticals (PHAMs) onto high-silica zeolites is presented Chapter 5. FAU, MOR, BEA and MFI zeolites were found to be selective adsorbents for the removal of PHAMs, which means that one zeolite with a specific framework, removed only several species of PHAMs with high adsorption efficacies. In the presence of NOM, positively charged PHAMs were preferably removed by high-silica

zeolites, because of electrostatic attraction with the negative sites of high-silica zeolites. Additionally, the concentration of competing positively charged NOM fractions present in the tested water were probably lower than the neutral and negatively charged fractions. Zeolites with channel structures also prevented the negative effect of NOM on the adsorption of positively charged PHAMs.

The adsorption of neutral and negatively charged PHAMs were affected by their molecular sizes. When the sizes of neutral and negatively charged PHAMs fitted the pore sizes of zeolites, PHAMs were reasonably well adsorbed. Neutral and negatively charged PHAMs with molecular sizes larger than the pore sizes of zeolites were excluded. Compared with the positively charged PHAMs, the bonding between neutral/negatively charged PHAMs and the framework of zeolites were weak. The adsorption efficacies of neutral and negatively charged PHAMs were thus impaired in the presence of NOM. NOM fractions with sizes less than the pore size of zeolites would probably enter the framework of zeolites and compete with the adsorption of weakly bonded PHAMs. NOM competition with PHAMs for the adsorption sites in the micropores were likely to happen in multi-solute water, since a broad range of PHAMs were unable to closely fit uniform micropores of zeolites. In addition, NOM fractions would possibly be adsorbed on the external surface of zeolites and caused the blockage of micropores.

## **2 Outlook**

### **2.1 The potential of high-silica zeolites as adsorbents in water treatment**

High-silica zeolites have a high selectivity for OMP adsorption as can be seen in chapter 2 and 3. Therefore it is expected that high-silica zeolites are suitable for the removal of specific targeted OMPs, e.g. MTBE (Knappe and Campos 2005; Li et al., 2003b), which closely fit the pores of zeolites. For the adsorption of a wider spectrum of OMPs, a combination of high-silica zeolites with different frameworks would thus be preferred. For further application, zeolites granules should be developed by synthesizing zeolite powders with clay binders. Zeolites granules can then be packed in a column and saturated zeolites can be regenerated on-site. In water treatment, the adsorption process is then supposed to be combined with other process, e.g. oxidation and membrane filtration, as multi barriers

for OMPs. Zeolite adsorption can be included in the multi barriers for the removal of specific OMPs or a broader range of OMPs when a combination of zeolites are used.

The resistance of zeolites to chemical reactions allows for oxidative regeneration after adsorption. The oxidative regeneration of high-silica zeolites has been shown as an effective process to restore the OMP saturated high-silica zeolites (Sagehashi et al., 2005; Shahbazi et al., 2014; Wang et al., 2010; Wang et al., 2006). Oxidative regeneration can be carried out on-site (Gonzalez-Olmos et al., 2011; Gonzalez-Olmos et al., 2013), minimizing transportation costs and CO<sub>2</sub> emissions. The combination of high-silica zeolite adsorption and oxidative regeneration will therefore result in cost savings and a lower environmental impact compared to the thermal reactivation of activated carbon. In practice, zeolite granules should be frequently regenerated by oxidative processes. Short empty bed contact time can then be applied and the investment cost will be reduced. It is supposed that only a small fraction of NOM with sizes less than the pore sizes of zeolites can be adsorbed, which potentially results in a low consumption of oxidants by NOM.

## 2.2 Further research

Most of the current research on OMP removal by high-silica zeolites focused on powdered zeolites (Damjanovic et al., 2010; Rakic et al., 2010; Rossner et al., 2009). For the application in water treatment, high-silica zeolites should be engineered into granules and less selective for OMPs, e.g. by combining zeolites with different frameworks. The characteristics of high-silica zeolites' granules, e.g. mechanical strength and porous structures, adsorption kinetics and efficacies of OMPs need further investigation. High-silica zeolites need to be tested in column experiments to validate the models for full scale implementation, regarding breakthrough curve and contact time.

Compared with high-silica zeolites, natural zeolites are much cheaper adsorbents. Natural zeolites might be capable of removing certain NOM fractions (Niri et al., 2014; Wang and Peng 2010), which affect OMP adsorption. Natural zeolites would thus be a promising pre-treatment for high-silica zeolites and activated carbon adsorption process and needs further investigation.

To fulfil the application of high-silica zeolites in water treatment, the on-site oxidative regeneration needs to be further developed. The knowledge on the optimized dosages of

oxidants, the possible defects of zeolites in oxidative conditions, and the optimal configuration of adsorption – oxidative regeneration remains unknown, which also requires further research. Also metal-zeolite catalyst could be synthesized by loading metal oxides, for example, iron and copper oxides, on zeolites, enhancing the rates of oxidation regeneration in a catalytic process (Becker and Förster 1998; Gonzalez-Olmos et al., 2013).



## SUMMARY

A broad range of organic micropollutants (OMPs), including pesticides, pharmaceuticals and personal care products, are present in drinking water sources and effluent of wastewater treatment plants (Kolpin et al., 2002; Stackelberg et al., 2004). The presence of OMPs in water significantly threatens public health and thus calls for effective treatment technologies (Alan et al., 2008; Pal et al., 2010). Zeolites are highly structured minerals with uniform micropores (pore diameters < 2nm) (McCusker and Baerlocher 2001). The pores of zeolites allow for the adsorption of OMPs and potentially avoid the negative influence of natural organic matter (NOM) (de Ridder et al., 2012; Hung and Lin 2006; Knappe and Campos 2005). High-silica zeolites have hydrophobic surfaces, which could prevent water competition with OMP adsorption (Maesen 2007; Rakic et al., 2010; Tsitsishvili 1973). High-silica zeolites are thus expected to be potential alternative adsorbents for activated carbon in water treatment.

Zeolite research has mainly focused on specifically adsorbing OMPs, while the insight in the adsorption mechanisms of a broad range of OMPs is limited. In addition, adsorption mechanisms of multiple OMPs on high-silica zeolites in the presence of NOM have not been studied. Therefore, the objective of this research was to obtain further insight in the adsorption mechanisms of high-silica zeolites for a broad spectrum of OMPs, in order to establish an alternative adsorption technology in current water treatment.

A literature study was conducted to review the available knowledge and experience on the adsorption of OMPs on high-silica zeolites. It was found that high-silica zeolites have the ability for adsorption of a variety of OMPs, including the small sized and polar OMPs, which are not well adsorbed on other adsorbents. The good adsorption efficacies of high-silica zeolites benefit from the featured properties, i.e. large number of micropores, closely fitted pores for OMPs and high surface hydrophobicity. The effect of NOM in natural water on adsorption of certain OMPs, e.g. MTBE and N-nitrosamines, was even not observed, while the effect of NOM on a broader range of OMPs was unknown. Oxidative regeneration of high-silica zeolites was found to be an efficient method to restore the adsorption capacities of high-silica zeolites. The combination of high-silica zeolite adsorption and on-site oxidative regeneration, therefore, potentially allows for a reduction of investment and operational costs and waste generation compared to conventional activated carbon filtration.

To study the adsorption mechanisms of a variety of OMPs on high-silica zeolites, the adsorption of triclosan, 2,4,6-trichlorophenol (TCP) and phenol, with the same functional groups, but diverse properties, i.e. molecular weight and water affinity, on ten high-silica zeolites were studied in the batch experiments. The maximum adsorption capacity of triclosan was more related to the micropore surface area/volume than to the hydrophobicity of the zeolites. The maximum adsorption capacity of TCP was observed from an S-shaped isotherm with a low adsorption efficacy at the low concentrations. At the same equilibrium concentration range as triclosan and TCP, the maximum adsorption capacity of phenol was not observed since phenol is more hydrophilic than triclosan and TCP. MFI with more closely fitted pores for phenol had a higher adsorption capacity than FAU, BEA and MOR for phenol adsorption.

To further explore the origin of the S-shaped adsorption isotherm, Monte Carlo (MC) simulation was carried out to study TCP adsorption on high-silica zeolites. Results from MC simulation corresponded well with the results from batch experiments, regarding the shape of adsorption isotherms, the maximum adsorption capacity of TCP and the effect of Si/Al ratios. The occurrence of S-shaped isotherms was found to originate from  $\pi$ - $\pi$  interactions between TCP molecules. A higher Al content in the framework of FAU zeolites with a lower Si/Al ratio promoted the adsorption of water molecules, which inhibited TCP adsorption and thus prevented the occurrence of an S-shaped isotherm.

The effect of NOM on OMP adsorption was studied by the adsorption of 23 pharmaceuticals (PHAMs) on high-silica zeolites. The results showed that The effect of NOM on the adsorption of positively charged PHAMs was less pronounced or even absent compared to the adsorption of neutral and negatively charged PHAMs. Zeolites with channels, i.e. MOR, BEA and MFI, proved to be better adsorbents for positively charged PHAMs than FAU with cages. The adsorption of neutral and negatively charged PHAMs were affected by the molecular sizes of PHAMs and pore sizes of zeolites. However, the effect of hydrophobicity/hydrophilicity of PHAMs on the adsorption efficacies of PHAMs on zeolites was not observed.

Overall, it can be concluded that high-silica zeolites have a good ability to remove several OMPs from water. The adsorption efficacies were affected by the characteristics of OMPs and high-silica zeolites. A combination of high-silica zeolites with different framework



types could therefore be a barrier for a broad range of OMPs. However, the adsorption efficacies of certain OMPs were hampered by the presence of NOM, which is not favourable for the application of high-silica zeolites in water treatment as only barrier against OMPs.

## **BIBLIOGRAPHY**

Abu-Lail, L., Bergendahl, J.A. and Thompson, R.W., 2010. Adsorption of methyl tertiary butyl ether on granular zeolites: Batch and column studies. *Journal of Hazardous Materials* 178, 363-369.

Achten, C., Kolb, A., Püttmann, W., Seel, P. and Gühr, R., 2002. Methyl tert-butyl ether (MTBE) in river and wastewater in Germany. 1. *Environmental Science & Technology* 36, 3652-3661.

Adolfsson-Erici, M., Pettersson, M., Parkkonen, J. and Sturve, J., 2002. Triclosan, a commonly used bactericide found in human milk and in the aquatic environment in Sweden. *Chemosphere* 46, 1485-1489.

Ahmaruzzaman, M., 2010. A review on the utilization of fly ash. *Progress in Energy and Combustion Science* 36, 327-363.

Alan, M.V., Barber, L.B., Gray, J.L., Lopez, E.M., Woodling, J.D. and Norris, D.O., 2008. Reproductive disruption in fish downstream from an estrogenic wastewater effluent. *Environmental Science and Technology* 42, 3407-3414.

Alejandro, S., Valdes, H., Manero, M.H. and Zaror, C.A., 2014. Oxidative regeneration of toluene-saturated natural zeolite by gaseous ozone: The influence of zeolite chemical surface characteristics. *Journal of Hazardous Materials* 274, 212-220.

Ali, I. and Gupta, V., 2006. Advances in water treatment by adsorption technology. *Nature Protocols* 1, 2661.

Allen, M.P. and Tildesley, D.J., 2017. *Computer simulation of liquids*, Oxford university press.

Alonso, A., Moral-Vico, J., Markeb, A.A., Busquets-Fite, M., Komilis, D., Puentes, V., Sanchez, A. and Font, X., 2017. Critical review of existing nanomaterial adsorbents to capture carbon dioxide and methane. *Science of the Total Environment* 595, 51-62.

Alsbaiee, A., Smith, B.J., Xiao, L.L., Ling, Y.H., Helbling, D.E. and Dichtel, W.R., 2016. Rapid removal of organic micropollutants from water by a porous beta-cyclodextrin polymer. *Nature* 529, 190-U146.

Álvarez-Ayuso, E., García-Sánchez, A. and Querol, X., 2003. Purification of metal electroplating waste waters using zeolites. *Water Research* 37, 4855-4862.

Anderson, M.A., 2000. Removal of MTBE and other organic contaminants from water by sorption to high silica zeolites. *Environmental Science & Technology* 34, 725-727.

Auerbach, S.M., Carrado, K.A. and Dutta, P.K., 2003. *Handbook of zeolite science and technology*, CRC press.

Australian Government National Health and Medical Research Council, 2011. *Australian drinking water guidelines*

Baerlocher, C. and McCusker, L.B., 2017. Database of zeolite structures, <http://www.iza-structure.org/databases/>.

Baerlocher, C., McCusker, L.B. and Olson, D.H., 2007. *Atlas of zeolite framework types*, Elsevier.

- Bal'zhinimaev, B.S., Paukshtis, E.A., Toktarev, A.V., Kovalyov, E.V., Yaranova, M.A., Smirnov, A.E. and Stompel, S., 2019. Effect of water on toluene adsorption over high silica zeolites. *Microporous and Mesoporous Materials* 277, 70-77.
- Bal, A.S. and Dhagat, N.N., 2001. Upflow anaerobic sludge blanket reactor--a review. *Indian Journal of Environmental Health* 43, 1-82.
- Bansal, R.C. and Goyal, M., 2005. Activated carbon adsorption, CRC press.
- Batonneau-Gener, I., Yonli, A., Hazael-Pascal, S., Pedro Marques, J., Madeira Lopes, J., Guisnet, M., Ramôa Ribeiro, F. and Mignard, S., 2008. Influence of steaming and acid-leaching treatments on the hydrophobicity of HBEA zeolite determined under static conditions. *Microporous and Mesoporous Materials* 110, 480-487.
- Batonneau-Gener, I., Yonli, A., Trouvé, A., Mignard, S., Guidotti, M. and Sgobba, M., 2010. Tailoring the hydrophobic character of mesoporous silica by silylation for VOC removal. *Separation Science and Technology* 45, 768-775.
- Bautista-Toledo, I., Ferro-García, M.A., Rivera-Utrilla, J., Moreno-Castilla, C. and Vegas Fernández, F.J., 2005. Bisphenol A removal from water by activated carbon. Effects of carbon characteristics and solution chemistry. *Environmental Science & Technology* 39, 6246-6250.
- Becker, L. and Förster, H., 1998. Oxidative decomposition of benzene and its methyl derivatives catalyzed by copper and palladium ion-exchanged Y-type zeolites. *Applied Catalysis B: Environmental* 17, 43-49.
- Behera, S.K., Oh, S.-Y. and Park, H.-S., 2010. Sorption of triclosan onto activated carbon, kaolinite and montmorillonite: Effects of pH, ionic strength, and humic acid. *Journal of Hazardous Materials* 179, 684-691.
- Behrman, A.S., 1927. Recent developments in zeolite softening. *Industrial & Engineering Chemistry* 19, 445-447.
- Berendsen, H.J.C., Grigera, J.R. and Straatsma, T.P., 1987. The missing term in effective pair potentials. *The Journal of Physical Chemistry* 91, 6269-6271.
- Beutel, T., Peltre, M.J. and Su, B.L., 2001. Interaction of phenol with NaX zeolite as studied by  $^1\text{H}$  MAS NMR,  $^{29}\text{Si}$  MAS NMR and  $^{29}\text{Si}$  CP MAS NMR spectroscopy. *Colloids and Surfaces A: Physicochemical and Engineering Aspects* 187-188, 319-325.
- Beutel, T. and Su, B.L., 2005. Behavior of phenol (phenol- $d_5$ ) on NaX zeolite as studied by  $^1\text{H}$  NMR and FT-IR techniques. *Chemical Physics Letters* 43, 341-359.
- Bevilacqua, M. and Busca, G., 2002. A study of the localization and accessibility of Brønsted and Lewis acid sites of H-mordenite through the FT-IR spectroscopy of adsorbed branched nitriles. *Catalysis Communications* 3, 497-502.
- Bhatnagar, A. and Sillanpää, M., 2017. Removal of natural organic matter (NOM) and its constituents from water by adsorption – A review. *Chemosphere* 166, 497-510.

Bjelopavlic, M., Newcombe, G. and Hayes, R., 1999. Adsorption of NOM onto activated carbon: effect of surface charge, ionic strength, and pore volume distribution. *Journal of Colloid and Interface Science* 210, 271-280.

Blasioli, S., Martucci, A., Paul, G., Gigli, L., Cossi, M., Johnston, C.T., Marchese, L. and Braschi, I., 2014. Removal of sulfamethoxazole sulfonamide antibiotic from water by high silica zeolites: A study of the involved host-guest interactions by a combined structural, spectroscopic, and computational approach. *Journal of Colloid and Interface Science* 419, 148-159.

Bolis, V., Busco, C. and Ugliengo, P., 2006. Thermodynamic study of water adsorption in high-silica zeolites. *The Journal of Physical Chemistry B* 110, 14849-14859.

Bottero, J.Y., Khatib, K., Thomas, F., Jucker, K., Bersillon, J.L. and Mallevialle, J., 1994. Adsorption of atrazine onto zeolites and organoclays, in the presence of background organics. *Water Research* 28, 483-490.

Boulet, P., Narasimhan, L., Berg'e-Lefranc, D., Kuchta, B., Schäf, O. and Denoyel, R., 2009. Adsorption into the MFI zeolite of aromatic molecule of biological relevance. Investigations by Monte Carlo simulations. *Journal of Molecular Modeling* 15, 573-579.

Braschi, I., Blasioli, S., Buscaroli, E., Montecchio, D. and Martucci, A., 2016a. Physicochemical regeneration of high silica zeolite Y used to clean-up water polluted with sulfonamide antibiotics. *Journal of Environmental Sciences* 43, 302-312.

Braschi, I., Blasioli, S., Gigli, L., Gessa, C.E., Alberti, A. and Martucci, A., 2010. Removal of sulfonamide antibiotics from water: Evidence of adsorption into an organophilic zeolite Y by its structural modifications. *Journal of Hazardous Materials* 178, 218-225.

Braschi, I., Martucci, A., Blasioli, S., Mzini, L.L., Ciavatta, C. and Cossi, M., 2016b. Effect of humic monomers on the adsorption of sulfamethoxazole sulfonamide antibiotic into a high silica zeolite Y: An interdisciplinary study. *Chemosphere* 155, 444-452.

Burgess, R.M., Perron, M.M., Cantwell, M.G., Ho, K.T., Serbst, J.R. and Pelletier, M.C., 2004. Use of zeolite for removing ammonia and ammonia-caused toxicity in marine toxicity identification evaluations. *Archives of Environmental Contamination and Toxicology* 47, 440-447.

Burton, A., 2018. Recent trends in the synthesis of high-silica zeolites. *Catalysis Reviews* 60, 132-175.

Burton, A.W., Zones, S.I. and Elomari, S., 2005. The chemistry of phase selectivity in the synthesis of high-silica zeolites. *Current Opinion in Colloid & Interface Science* 10, 211-219.

Calero, S., Dubbeldam, D., Krishna, R., Smit, B., Vlugt, T.J.H., Denayer, J.F.M., Martens, J.A. and Maesen, T.L.M., 2004. Understanding the role of sodium during adsorption: A force field for alkanes in sodium-exchanged faujasites. *Journal of the American Chemical Society* 126, 11377-11386.

Cerjan Stefanović, Š., Zabukovec Logar, N., Margeta, K., Novak Tušar, N., Arčon, I., Maver, K., Kovač, J. and Kaučič, V., 2007. Structural investigation of  $Zn^{2+}$  sorption on clinoptilolite tuff from the Vranjska Banja deposit in Serbia. *Microporous and Mesoporous Materials* 105, 251-259.

Chen, G., Wang, Y. and Pei, Z., 2014. Adsorption and desorption of 2,4,6-trichlorophenol onto and from ash as affected by  $\text{Ag}^+$ ,  $\text{Zn}^{2+}$ , and  $\text{Al}^{3+}$ . *Environmental Science and Pollution Research* 21, 2002-2008.

Chen, G.C., Shan, X.Q., Wang, Y.S., Wen, B., Pei, Z.G., Xie, Y.N., Liu, T. and Pignatello, J.J., 2009. Adsorption of 2,4,6-trichlorophenol by multi-walled carbon nanotubes as affected by  $\text{Cu(II)}$ . *Water Research* 43, 2409-2418.

Chen, N.Y., 1976. Hydrophobic properties of zeolites. *The Journal of Physical Chemistry* 80, 60-64.

Chen, X.Q., Fujiwara, T., Fukahori, S. and Ishigaki, T., 2015. Factors affecting the adsorptive removal of bisphenol A in landfill leachate by high silica Y-type zeolite. *Environmental Science and Pollution Research* 22, 2788-2799.

Chiang, H.-L., Chiang, P.C. and Huang, C.P., 2002a. Ozonation of activated carbon and its effects on the adsorption of VOCs exemplified by methylethylketone and benzene. *Chemosphere* 47, 267-275.

Chiang, H.-L., Huang, C.P. and Chiang, P.C., 2002b. The surface characteristics of activated carbon as affected by ozone and alkaline treatment. *Chemosphere* 47, 257-265.

Chica, A., Strohmaier, K. and Iglesia, E., 2004. Adsorption, desorption, and conversion of thiophene on H-ZSM5. *Langmuir* 20, 10982-10991.

Chica, A., Strohmaier, K.G. and Iglesia, E., 2005. Effects of zeolite structure and aluminum content on thiophene adsorption, desorption, and surface reactions. *Applied Catalysis B: Environmental* 60, 223-232.

Cho, H.-H., Huang, H. and Schwab, K., 2011. Effects of solution chemistry on the adsorption of ibuprofen and triclosan onto carbon nanotubes. *Langmuir* 27, 12960-12967.

Cihanoglu, A., Gunduz, G. and Dukkanci, M., 2015. Degradation of acetic acid by heterogeneous Fenton-like oxidation over iron-containing ZSM-5 zeolites. *Applied Catalysis B: Environmental* 165, 687-699.

Cooney, D.O., Nagerl, A. and Hines, A.L., 1983. Solvent regeneration of activated carbon. *Water Research* 17, 403-410.

Çoruh, S. and Ergun, O.N., 2009.  $\text{Ni}^{2+}$  removal from aqueous solutions using conditioned clinoptilolites: Kinetic and isotherm studies. *Environmental Progress & Sustainable Energy* 28, 162-172.

Cygan, R.T., Liang, J.-J. and Kalinichev, A.G., 2004. Molecular models of hydroxide, oxyhydroxide, and clay phases and the development of a general force field. *The Journal of Physical Chemistry B* 108, 1255-1266.

Dabrowski, A., Podkościelny, P., Hubicki, Z. and Barczak, M., 2005. Adsorption of phenolic compounds by activated carbon - a critical review. *Chemosphere* 58, 1049-1070.

Damjanovic, L., Rakic, V., Rac, V., Stosic, D. and Auroux, A., 2010. The investigation of phenol removal from aqueous solutions by zeolites as solid adsorbents. *Journal of Hazardous Materials* 184, 477-484.

Davis, S.W. and Powers, S.E., 2000. Alternative sorbents for removing MTBE from gasoline-contaminated ground water. *Journal of Environmental Engineering* 126, 354-360.

de Lucas, A., Cañizares, P., García, M.A., Gómez, J. and Rodríguez, J.F., 1998. Recovery of nicotine from aqueous extracts of tobacco wastes by an H<sup>+</sup>-form strong-acid ion exchanger. *Industrial & Engineering Chemistry Research* 37, 4783-4791.

de Ridder, D., Verliefde, A., Heijman, S., Verberk, J., Rietveld, L., van der Aa, L., Amy, G. and van Dijk, J., 2011. Influence of natural organic matter on equilibrium adsorption of neutral and charged pharmaceuticals onto activated carbon. *Water Science and Technology* 63, 416-423.

de Ridder, D.J., Verberk, J.Q.J.C., Heijman, S.G.J., Amy, G.L. and van Dijk, J.C., 2012. Zeolites for nitrosamine and pharmaceutical removal from demineralised and surface water: Mechanisms and efficacy. *Separation and Purification Technology* 89, 71-77.

DeJaco, R.F., Bai, P., Tsapatsis, M. and Siepmann, J.I., 2016. Adsorptive separation of 1-Butanol from aqueous solutions using MFI- and FER-type zeolite frameworks: A Monte Carlo study. *Langmuir* 32, 2093-2101.

Delgado, L.F., Charles, P., Glucina, K. and Morlay, C., 2012. The removal of endocrine disrupting compounds, pharmaceutically activated compounds and cyanobacterial toxins during drinking water preparation using activated carbon-A review. *Science of the Total Environment* 435, 509-525.

Dias, J.M., Alvim-Ferraz, M.C.M., Almeida, M.F., Rivera-Utrilla, J. and Sánchez-Polo, M., 2007. Waste materials for activated carbon preparation and its use in aqueous-phase treatment: A review. *Journal of Environmental Management* 85, 833-846.

Dobbs, R.A. and Cohen, J.M., 1980. Carbon adsorption isotherms for toxic organics, Municipal Environmental Research Laboratory, Office of Research and Development, US Environmental Protection Agency.

Dubinin, M.M., 1967. Adsorption in micropores. *Journal of Colloid and Interface Science* 23, 487-499.

Eberly Jr, P.E., Kimberlin Jr, C.N. and Voorhies Jr, A., 1971. Effect of SiO<sub>2</sub>/Al<sub>2</sub>O<sub>3</sub> ratio on physicochemical properties of mordenite and activity for n-pentane isomerization. *Journal of Catalysis* 22, 419-426.

Ebie, K., Li, F., Azuma, Y., Yuasa, A. and Hagishita, T., 2001. Pore distribution effect of activated carbon in adsorbing organic micropollutants from natural water. *Water Research* 35, 167-179.

Eggen, R.I.L., Hollender, J., Joss, A., Schärer, M. and Stamm, C., 2014. Reducing the discharge of micropollutants in the aquatic environment: The benefits of upgrading wastewater treatment plants. *Environmental Science & Technology* 48, 7683-7689.

- Emeis, C.A., 1993. Determination of integrated molar extinction coefficients for infrared absorption bands of pyridine adsorbed on solid acid catalysts. *Journal of Catalysis* 141, 347-354.
- Ennaert, T., Van Aelst, J., Dijkmans, J., De Clercq, R., Schutyser, W., Dusselier, M., Verboekend, D. and Sels, B.F., 2016. Potential and challenges of zeolite chemistry in the catalytic conversion of biomass. *Chemical Society Reviews* 45, 584-611.
- Erdem-Senatalar, A., Bergendahl, J.A., Giaya, A. and Thompson, R.W., 2004. Adsorption of methyl tertiary butyl ether on hydrophobic molecular sieves. *Environmental Engineering Science* 21, 722-729.
- Esplugas, S., Bila, D.M., Krause, L.G.T. and Dezotti, M., 2007. Ozonation and advanced oxidation technologies to remove endocrine disrupting chemicals (EDCs) and pharmaceuticals and personal care products (PPCPs) in water effluents. *Journal of Hazardous Materials* 149, 631-642.
- Farkas, A., Rozic, M. and Barbaric-Mikocevic, Z., 2005. Ammonium exchange in leakage waters of waste dumps using natural zeolite from the Krapina region, Croatia. *Journal of Hazardous Materials* 117, 25-33.
- Fick, J., Söderström, H., Lindberg, R.H., Phan, C., Tysklind, M. and Larsson, D.J., 2009. Contamination of surface, ground, and drinking water from pharmaceutical production. *Environmental Toxicology and Chemistry* 28, 2522-2527.
- First, E.L., Gounaris, C.E., Wei, J. and Floudas, C.A., 2011. Computational characterization of zeolite porous networks: an automated approach. *Physical Chemistry Chemical Physics* 13, 17339-17358.
- Foster, M.D., Rivin, I., Treacy, M.M.J. and Delgado Friedrichs, O., 2006. A geometric solution to the largest-free-sphere problem in zeolite frameworks. *Microporous and Mesoporous Materials* 90, 32-38.
- Frenkel, D. and Smit, B., 2001. *Understanding molecular simulation: from algorithms to applications*, Elsevier.
- Freundlich, H., 1906. Über die absorption in lösungen. Über Die Adsorption in Lösungen, 385-470.
- Fujita, H., Izumi, J., Sagehashi, M., Fujii, T. and Sakoda, A., 2004. Decomposition of trichloroethene on ozone-adsorbed high silica zeolites. *Water Research* 38, 166-172.
- Fukahori, S. and Fujiwara, T., 2014. Modeling of sulfonamide antibiotic removal by TiO<sub>2</sub>/high-silica zeolite HSZ-385 composite. *Journal of Hazardous Materials* 272, 1-9.
- Fukahori, S., Fujiwara, T., Ito, R. and Funamizu, N., 2011. pH-Dependent adsorption of sulfa drugs on high silica zeolite: Modeling and kinetic study. *Desalination* 275, 237-242.
- Gao, J., Liu, L., Liu, X., Zhou, H., Huang, S. and Wang, Z., 2008. Levels and spatial distribution of chlorophenols – 2, 4-dichlorophenol, 2, 4, 6-trichlorophenol, and pentachlorophenol in surface water of China. *Chemosphere* 71, 1181-1187.



García, C.L. and Lercher, J.A., 1992. Adsorption and surface reactions of thiophene on ZSM5 zeolites. *Journal of Physical Chemistry* 96, 2669-2675.

Gerecke, A.C., Schärer, M., Singer, H.P., Müller, S.R., Schwarzenbach, R.P., Sägesser, M., Ochsenbein, U. and Popow, G., 2002. Sources of pesticides in surface waters in Switzerland: pesticide load through waste water treatment plants—current situation and reduction potential. *Chemosphere* 48, 307-315.

Giaya, A. and Thompson, R.W., 2002a. Observations on an equation of state for water confined in narrow slit-pores. *The Journal of Chemical Physics* 116, 2565-2571.

Giaya, A. and Thompson, R.W., 2002b. Water confined in cylindrical micropores. *The Journal of Chemical Physics* 117, 3464-3475.

Giles, C.H., Smith, D. and Huitson, A., 1974. A general treatment and classification of the solute adsorption isotherm. I. Theoretical. *Journal of Colloid and Interface Science* 47, 755-765.

Gonzalez-Olmos, R., Holzer, F., Kopinke, F.D. and Georgi, A., 2011. Indications of the reactive species in a heterogeneous Fenton-like reaction using Fe-containing zeolites. *Applied Catalysis A: General* 398, 44-53.

Gonzalez-Olmos, R., Kopinke, F.-D., Mackenzie, K. and Georgi, A., 2013. Hydrophobic Fe-Zeolites for Removal of MTBE from Water by Combination of Adsorption and Oxidation. *Environmental Science & Technology* 47, 2353-2360.

Gracia-Lor, E., Sancho, J.V. and Hernández, F., 2011. Multi-class determination of around 50 pharmaceuticals, including 26 antibiotics, in environmental and wastewater samples by ultra-high performance liquid chromatography-tandem mass spectrometry. *Journal of Chromatography A* 1218, 2264-2275.

Grieco, S.A. and Ramarao, B.V., 2013. Removal of TCEP from aqueous solutions by adsorption with zeolites. *Colloids and Surfaces A: Physicochemical and Engineering Aspects* 434, 329-338.

Gschwend, P.M., 2016. *Environmental organic chemistry*, John Wiley & Sons.

Guvenc, E. and Ahunbay, M.G., 2012. Adsorption of methyl tertiary butyl ether and trichloroethylene in MFI-type zeolites. *Journal of Physical Chemistry C* 116, 21836-21843.

Guzzella, L., Feretti, D. and Monarca, S., 2002. Advanced oxidation and adsorption technologies for organic micropollutant removal from lake water used as drinking-water supply. *Water Research* 36, 4307-4318.

Hamdaoui, O. and Naffrechoux, E., 2007. Modeling of adsorption isotherms of phenol and chlorophenols onto granular activated carbon - Part I. Two-parameter models and equations allowing determination of thermodynamic parameters. *Journal of Hazardous Materials* 147, 381-394.

Hameed, B.H., 2007. Equilibrium and kinetics studies of 2,4,6-trichlorophenol adsorption onto activated clay. *Colloids and Surfaces A: Physicochemical and Engineering Aspects* 307, 45-52.

- He, Y.Z. and Cheng, H.F., 2016. Degradation of N-nitrosodimethylamine (NDMA) and its precursor dimethylamine (DMA) in mineral micropores induced by microwave irradiation. *Water Research* 94, 305-314.
- Heberer, T., 2002. Tracking persistent pharmaceutical residues from municipal sewage to drinking water. *Journal of hydrology* 266, 175-189.
- Hem, J.D., 1959. Study and interpretation of the chemical characteristics of natural water, US Government Printing Office.
- Hepplewhite, C., Newcombe, G. and Knappe, D., 2004. NOM and MIB, who wins in the competition for activated carbon adsorption sites? *Water Science and Technology* 49, 257-265.
- Hinz, C., 2001. Description of sorption data with isotherm equations. *Geoderma* 99, 225-243.
- Hoffmann, M.R., Martin, S.T., Choi, W. and Bahnemann, D.W., 1995. Environmental applications of semiconductor photocatalysis. *Chemical Reviews* 95, 69-96.
- Hriljac, J., Eddy, M., Cheetham, A., Donohue, J. and Ray, G., 1993. Powder neutron diffraction and <sup>29</sup>Si MAS NMR studies of siliceous zeolite-Y. *Journal of Solid State Chemistry* 106, 66-72.
- Hughes, S.R., Kay, P. and Brown, L.E., 2013. Global synthesis and critical evaluation of pharmaceutical data sets collected from river systems. *Environmental Science and Technology* 47, 661-677.
- Hung, H.-W. and Lin, T.-F., 2006. Adsorption of MTBE from contaminated water by carbonaceous resins and mordenite zeolite. *Journal of Hazardous Materials* 135, 210-217.
- Hung, H.W., Lin, T.F., Baus, C., Sacher, F. and Brauch, H.J., 2005. Competitive and hindering effects of natural organic matter on the adsorption of MTBE onto activated carbons and zeolites. *Environmental Technology* 26, 1371-1382.
- Hutchins, R., 1973. Economic factors in granular carbon thermal regeneration. *Chemical Engineering Progress* 69, 48-55.
- Ikhlaq, A., Brown, D.R. and Kasprzyk-Hordern, B., 2014. Catalytic ozonation for the removal of organic contaminants in water on ZSM-5 zeolites. *Applied Catalysis B: Environmental* 154-155, 110-122.
- Israelachvili, J.N., 2015. Intermolecular and surface forces, Academic Press.
- Jacobs, P., Flanigen, E.M., Jansen, J. and van Bekkum, H., 2001. Introduction to zeolite science and practice, Elsevier.
- Janiak, C., 2000. A critical account on  $\pi$ - $\pi$  stacking in metal complexes with aromatic nitrogen-containing ligands. *Journal of the Chemical Society, Dalton Transactions*, 3885-3896.
- Janos, P., Buchtova, H. and Ryznarova, M., 2003. Sorption of dyes from aqueous solutions onto fly ash. *Water Research* 37, 4938-4944.
- Jiang, N., Shang, R., Heijman, S.G. and Rietveld, L.C., 2018. High-silica zeolites for adsorption of organic micro-pollutants in water treatment: A review. *Water Research*.

Joss, A., Siegrist, H. and Ternes, T.A., 2008. Are we about to upgrade wastewater treatment for removing organic micropollutants? *Water Science and Technology* 57, 251-255.

Karanfil, T. and Kilduff, J.E., 1999. Role of granular activated carbon surface chemistry on the adsorption of organic compounds. 1. Priority pollutants. *Environmental Science & Technology* 33, 3217-3224.

Karimi-Lotfabad, S., Pickard, M.A. and Gray, M.R., 1996. Reactions of polynuclear aromatic hydrocarbons on soil. *Environmental science & technology* 30, 1145-1151.

Katsou, E., Malamis, S. and Haralambous, K., 2010a. Examination of zinc uptake in a combined system using sludge, minerals and ultrafiltration membranes. *Journal of Hazardous Materials* 182, 27-38.

Katsou, E., Malamis, S., Haralambous, K.J. and Loizidou, M., 2010b. Use of ultrafiltration membranes and aluminosilicate minerals for nickel removal from industrial wastewater. *Journal of Membrane Science* 360, 234-249.

Kennedy, A.M., Reinert, A.M., Knappe, D.R.U., Ferrer, I. and Summers, R.S., 2015. Full- and pilot-scale GAC adsorption of organic micropollutants. *Water Research* 68, 238-248.

Khalid, M., Joly, G., Renaud, A. and Magnoux, P., 2004. Removal of phenol from water by adsorption using zeolites. *Industrial & Engineering Chemistry Research* 43, 5275-5280.

Klavarioti, M., Mantzavinos, D. and Kassinos, D., 2009. Removal of residual pharmaceuticals from aqueous systems by advanced oxidation processes. *Environment International* 35, 402-417.

Knappe, D. and Campos, A.R., 2005. Effectiveness of high-silica zeolites for the adsorption of methyl tertiary-butyl ether from natural water. *Water Science and Technology: Water Supply* 5, 83-91.

Kolpin, D.W., Furlong, E.T., Meyer, M.T., Thurman, E.M., Zaugg, S.D., Barber, L.B. and Buxton, H.T., 2002. Pharmaceuticals, hormones, and other organic wastewater contaminants in U.S. streams, 1999-2000: a national reconnaissance. *Environmental Science & Technology* 36, 1202-1211.

Koryabkina, N., Bergendahl, J.A., Thompson, R.W. and Giaya, A., 2007. Adsorption of disinfection byproducts on hydrophobic zeolites with regeneration by advanced oxidation. *Microporous and Mesoporous Materials* 104, 77-82.

Koubaissy, B., Joly, G., Batonneau-Gener, I. and Magnoux, P., 2011. Adsorptive removal of aromatic compounds present in wastewater by using dealuminated faujasite zeolite. *Industrial & Engineering Chemistry Research* 50, 5705-5713.

Koubaissy, B., Joly, G. and Magnoux, P., 2008. Adsorption and competitive adsorption on zeolites of nitrophenol compounds present in wastewater. *Industrial & Engineering Chemistry Research* 47, 9558-9565.

Koubaissy, B., Toufaily, J., El-Murr, M., Daou, T.J., Hafez, H., Joly, G., Magnoux, P. and Hamieh, T., 2012. Adsorption kinetics and equilibrium of phenol drifts on three zeolites. *Central European Journal of Engineering* 2, 435-444.

Kušić, H., Koprivanac, N. and Locke, B.R., 2005. Decomposition of phenol by hybrid gas/liquid electrical discharge reactors with zeolite catalysts. *Journal of Hazardous Materials* 125, 190-200.

Kwakye-Awuah, B., Labik, L.K., Nkrumah, I. and Williams, C., 2014. Removal of ammonium ions by laboratory-synthesized zeolite linde type A adsorption from water samples affected by mining activities in Ghana. *Journal of Water and Health* 12, 151-160.

Langmuir, I., 1916. The constitution and fundamental properties of solids and liquids. Part I. Solids. *Journal of the American chemical society* 38, 2221-2295.

Lee, D.G., Kim, J.H. and Lee, C.H., 2011. Adsorption and thermal regeneration of acetone and toluene vapors in dealuminated Y-zeolite bed. *Separation and Purification Technology* 77, 312-324.

Leenheer, J.A. and Croué, J.-P., 2003. Peer Reviewed: Characterizing Aquatic Dissolved Organic Matter. *Environmental Science & Technology* 37, 18A-26A.

Lefebvre, O. and Moletta, R., 2006. Treatment of organic pollution in industrial saline wastewater: A literature review. *Water Research* 40, 3671-3682.

Legrini, O., Oliveros, E. and Braun, A.M., 1993. Photochemical processes for water-treatment. *Chemical Reviews* 93, 671-698.

Leichsenring, S., Lenoir, D., May, H.G., Schramm, K.W. and Kettrup, A., 1996. A new regenerative method for adsorption and oxidation of organic trace contaminants from flue gases. *Chemosphere* 32, 1763-1770.

Li, L., Quinlivan, P.A. and Knappe, D.R.U., 2002. Effects of activated carbon surface chemistry and pore structure on the adsorption of organic contaminants from aqueous solution. *Carbon* 40, 2085-2100.

Li, Q., Snoeyink, V.L., Mariñas, B.J. and Campos, C., 2003a. Pore blockage effect of NOM on atrazine adsorption kinetics of PAC: the roles of PAC pore size distribution and NOM molecular weight. *Water Research* 37, 4863-4872.

Li, S., Tuan, V.A., Noble, R.D. and Falconer, J.L., 2003b. MTBE adsorption on all-silica  $\beta$  zeolite. *Environmental Science & Technology* 37, 4007-4010.

Li, Y., Li, L. and Yu, J., 2017. Applications of zeolites in sustainable chemistry. *Chem* 3, 928-949.

Li, Y. and Yu, J., 2014. New stories of zeolite structures: Their descriptions, determinations, predictions, and evaluations. *Chemical Reviews* 114, 7268-7316.

Lippens, B.C. and de Boer, J.H., 1965. Studies on pore systems in catalysts. V. The t method. *Journal of Catalysis* 4, 319-323.

Liu, Q.S., Zheng, T., Wang, P., Jiang, J.P. and Li, N., 2010. Adsorption isotherm, kinetic and mechanism studies of some substituted phenols on activated carbon fibers. *Chemical Engineering Journal* 157, 348-356.

Liu, S., Lim, M. and Amal, R., 2014a. TiO<sub>2</sub>-coated natural zeolite: Rapid humic acid adsorption and effective photocatalytic regeneration. *Chemical Engineering Science* 105, 46-52.

Liu, Y., Zhu, X., Qian, F., Zhang, S. and Chen, J., 2014b. Magnetic activated carbon prepared from rice straw-derived hydrochar for triclosan removal. *RSC Advances* 4, 63620-63626.

Lobo, R.F., 1997. High-silica zeolites: From synthesis to structure. *Abstracts of Papers of the American Chemical Society* 213, 345-COLL.

Luo, Y., Guo, W., Ngo, H.H., Nghiem, L.D., Hai, F.I., Zhang, J., Liang, S. and Wang, X.C., 2014. A review on the occurrence of micropollutants in the aquatic environment and their fate and removal during wastewater treatment. *Science of the total environment* 473, 619-641.

Maesen, T., 2007. Introduction to Zeolite Science and Practice. Cejka, J., Bekkum, H.V., Corma, A. and Schuth, F. (eds), pp. 1-12, Elsevier Science BV, Amsterdam.

Maesen, T. and Marcus, B., 2001. *Studies in Surface Science and Catalysis*, pp. 1-9, Elsevier.

Magdeburg, A., Stalter, D., Schlüsener, M., Ternes, T. and Oehlmann, J., 2014. Evaluating the efficiency of advanced wastewater treatment: target analysis of organic contaminants and (geno-) toxicity assessment tell a different story. *Water Research* 50, 35-47.

Mailler, R., Gasperi, J., Coquet, Y., Deshayes, S., Zedek, S., Cren-Olivé, C., Cartiser, N., Eudes, V., Bressy, A., Caupos, E., Moilleron, R., Chebbo, G. and Rocher, V., 2015. Study of a large scale powdered activated carbon pilot: Removals of a wide range of emerging and priority micropollutants from wastewater treatment plant effluents. *Water Research* 72, 315-330.

Margeta, K., Logar, N.A.Z., Šiljeg, M. and Farkas, A., 2013. *Water treatment*, InTech.

Marsh, H., Heintz, E.A. and Rodríguez-Reinoso, F., 1997. Introduction to carbon technologies, Universidad de Alicante.

Martin, R.J. and Ng, W.J., 1984. Chemical regeneration of exhausted activated carbon - I. *Water Research* 18, 59-73.

Martinez, C.R. and Iverson, B.L., 2012. Rethinking the term "pi-stacking". *Chemical Science* 3, 2191-2201.

Martucci, A., Pasti, L., Marchetti, N., Cavazzini, A., Dondi, F. and Alberti, A., 2012. Adsorption of pharmaceuticals from aqueous solutions on synthetic zeolites. *Microporous and Mesoporous Materials* 148, 174-183.

McCusker, L.B. and Baerlocher, C., 2001. *Studies in Surface Science and Catalysis*. H. van Bekkum, E.M.F.P.A.J. and Jansen, J.C. (eds), pp. 37-67, Elsevier.

Meier, W. and Baerlocher, C., 1999. *Structures and Structure Determination*, pp. 141-161, Springer.

Meininghaus, C.K.W. and Prins, R., 2000. Sorption of volatile organic compounds on hydrophobic zeolites. *Microporous and Mesoporous Materials* 35-6, 349-365.

Melin, G., 1999. Evaluation of the applicability of synthetic resin sorbents for MTBE removal from water, Center for Groundwater Restoration and Protection, National Water Research Institute.

Mendez-Arriaga, F. and Almanza, R., 2014. Water remediation by UV-vis/H<sub>2</sub>O<sub>2</sub> process, photo-Fenton-like oxidation, and zeolite ZSM5. *Desalination and Water Treatment* 52, 5822-5832.

Michael, I., Rizzo, L., McArdeell, C., Manaia, C., Merlin, C., Schwartz, T., Dagot, C. and Fatta-Kassinos, D., 2013. Urban wastewater treatment plants as hotspots for the release of antibiotics in the environment: A review. *Water Research* 47, 957-995.

Miklos, D.B., Remy, C., Jekel, M., Linden, K.G., Drewes, J.E. and Hübner, U., 2018. Evaluation of advanced oxidation processes for water and wastewater treatment – A critical review. *Water Research* 139, 118-131.

Mitch, W.A., Sharp, J.O., Trussell, R.R., Valentine, R.L., Alvarez-Cohen, L. and Sedlak, D.L., 2003. N-nitrosodimethylamine (NDMA) as a drinking water contaminant: A review. *Environmental Engineering Science* 20, 389-404.

Mompelat, S., Le Bot, B. and Thomas, O., 2009. Occurrence and fate of pharmaceutical products and by-products, from resource to drinking water. *Environment International* 35, 803-814.

Monneyron, P., Mathe, S., Manero, M.H. and Foussard, J.N., 2003. Regeneration of high silica zeolites via advanced oxidation processes - A preliminary study about adsorbent reactivity toward ozone. *Chemical Engineering Research & Design* 81, 1193-1198.

Moreno-Castilla, C., 2004. Adsorption of organic molecules from aqueous solutions on carbon materials. *Carbon* 42, 83-94.

Nakamoto, H. and Takahashi, H., 1982. Hydrophobic natures of zeolite ZSM-5. *Zeolites* 2, 67-68.

Nam, S.-W., Choi, D.-J., Kim, S.-K., Her, N. and Zoh, K.-D., 2014. Adsorption characteristics of selected hydrophilic and hydrophobic micropollutants in water using activated carbon. *Journal of Hazardous Materials* 270, 144-152.

Narasimhan, L., Boulet, P., Kuchta, B., Schaef, O., Denoyel, R. and Brunet, P., 2009. Molecular simulations of water and paracresol in MFI zeolite-a Monte Carlo study. *Langmuir* 25, 11598-11607.

Narasimhan, L., Kuchta, B., Schaef, O., Brunet, P. and Boulet, P., 2013. Mechanism of adsorption of p-cresol uremic toxin into faujasite zeolites in presence of water and sodium cations – A Monte Carlo study. *Microporous and Mesoporous Materials* 173, 70-77.

Narbaitz, R.M. and Cen, J., 1997. Alternative methods for determining the percentage regeneration of activated carbon. *Water Research* 31, 2532-2542.

Nelson, P.O. and Yang, M.Y., 1995. Equilibrium adsorption of chlorophenols on granular activated carbon. *Water Environment Research* 67, 892-898.

Neppolian, B., Mine, S., Horiuchi, Y., Bianchi, C.L., Matsuoka, M., Dionysiou, D.D. and Anpo, M., 2016. Efficient photocatalytic degradation of organics present in gas and liquid phases using Pt-TiO<sub>2</sub>/Zeolite (H-ZSM). *Chemosphere* 153, 237-243.

Newcombe, G., 1999. Charge vs. porosity—some influences on the adsorption of natural organic matter (NOM) by activated carbon. *Water Science and Technology* 40, 191-198.

Newcombe, G., Hayes, R. and Drikas, M., 1993. Granular activated carbon: Importance of surface properties in the adsorption of naturally occurring organics. *Colloids and Surfaces A: Physicochemical and Engineering Aspects* 78, 65-71.

Newcombe, G., Morrison, J., Hepplewhite, C. and Knappe, D., 2002. Simultaneous adsorption of MIB and NOM onto activated carbon: II. Competitive effects. *Carbon* 40, 2147-2156.

Neyens, E. and Baeyens, J., 2003. A review of classic Fenton's peroxidation as an advanced oxidation technique. *Journal of Hazardous Materials* 98, 33-50.

Nikolakis, V., 2005. Understanding interactions in zeolite colloidal suspensions: A review. *Current Opinion in Colloid & Interface Science* 10, 203-210.

Niri, M.V., Mahvi, A.H., Alimohammadi, M., Shirmardi, M., Golastanifar, H., Mohammadi, M.J., Naeimabadi, A. and Khishdost, M., 2014. Removal of natural organic matter (NOM) from an aqueous solution by NaCl and surfactant-modified clinoptilolite. *Journal of Water and Health* 13, 394-405.

Odivan, Z., Cristina, T.I. and Amaral, F.L., 2014. Desorption - and decomposition - based techniques for the regeneration of activated carbon. *Chemical Engineering & Technology* 37, 1447-1459.

Olson, D.H., Haag, W.O. and Borghard, W.S., 2000. Use of water as a probe of zeolitic properties: interaction of water with HZSM-5. *Microporous and Mesoporous Materials* 35-36, 435-446.

Olson, D.H., Haag, W.O. and Lago, R.M., 1980. Chemical and physical properties of the ZSM-5 substitutional series. *Journal of Catalysis* 61, 390-396.

Omorogie, M.O., Babalola, J.O. and Unuabonah, E.I., 2016. Regeneration strategies for spent solid matrices used in adsorption of organic pollutants from surface water: A critical review. *Desalination and Water Treatment* 57, 518-544.

Pal, A., Gin, K.Y.-H., Lin, A.Y.-C. and Reinhard, M., 2010. Impacts of emerging organic contaminants on freshwater resources: Review of recent occurrences, sources, fate and effects. *Science of the Total Environment* 408, 6062-6069.

Pan, Z., Stemmler, E.A., Cho, H.J., Fan, W., LeBlanc, L.A., Patterson, H.H. and Amirbahman, A., 2014. Photocatalytic degradation of 17 alpha-ethinylestradiol (EE2) in the presence of TiO<sub>2</sub>-doped zeolite. *Journal of Hazardous Materials* 279, 17-25.

Pelekani, C. and Snoeyink, V., 1999. Competitive adsorption in natural water: Role of activated carbon pore size. *Water Research* 33, 1209-1219.

Perego, C., Bosetti, A., Ricci, M. and Millini, R., 2017. Zeolite materials for biomass conversion to biofuel. *Energy & Fuels* 31, 7721-7733.

Perisic, D.J., Gilja, V., Stankov, M.N., Katancic, Z., Kusic, H., Stangar, U.L., Dionysiou, D.D. and Bozic, A.L., 2016. Removal of diclofenac from water by zeolite-assisted advanced oxidation processes. *Journal of Photochemistry and Photobiology A: Chemistry* 321, 238-247.

Peternel, I., Kusic, H., Koprivanac, N. and Locke, B.R., 2006. The roles of ozone and zeolite on reactive dye degradation in electrical discharge reactors. *Environmental Technology* 27, 545-557.

Petrie, B., Barden, R. and Kasprzyk-Hordern, B., 2015. A review on emerging contaminants in wastewaters and the environment: Current knowledge, understudied areas and recommendations for future monitoring. *Water Research* 72, 3-27.

Phung, T.K. and Busca, G., 2015. On the Lewis acidity of protonic zeolites. *Applied Catalysis A: General* 504, 151-157.

Purna Chandra Rao, G., Satyaveni, S., Ramesh, A., Sessaiah, K., Murthy, K.S.N. and Choudary, N.V., 2006. Sorption of cadmium and zinc from aqueous solutions by zeolite 4A, zeolite 13X and bentonite. *Journal of Environmental Management* 81, 265-272.

Qin, Q., Liu, K., Fu, D. and Gao, H., 2012. Effect of chlorine content of chlorophenols on their adsorption by mesoporous SBA-15. *Journal of Environmental Sciences-China* 24, 1411-1417.

Radhika, M. and Palanivelu, K., 2006. Adsorptive removal of chlorophenols from aqueous solution by low cost adsorbent — Kinetics and isotherm analysis. *Journal of Hazardous Materials* 138, 116-124.

Rakic, V., Damjanovic, L., Rac, V., Stosic, D., Dondur, V. and Auroux, A., 2010. The adsorption of nicotine from aqueous solutions on different zeolite structures. *Water Research* 44, 2047-2057.

Reemtsma, T., Berger, U., Arp, H.P.H., Gallard, H., Knepper, T.P., Neumann, M., Quintana, J.B. and Voogt, P.d., 2016. Mind the gap: Persistent and mobile organic compounds - water contaminants that slip through. *Environmental Science & Technology* 50, 10308-10315.

Reungoat, J., Pic, J.S., Manero, M.H. and Debellefontaine, H., 2007. Adsorption of nitrobenzene from water onto high silica zeolites and regeneration by ozone. *Separation Science and Technology* 42, 1447-1463.

Rhodes, C.J., 2010. Properties and applications of zeolites. *Science Progress* 93, 223-284.

Roostaei, N. and Tezel, F.H., 2004. Removal of phenol from aqueous solutions by adsorption. *Journal of Environmental Management* 70, 157-164.

Roque-Malherbe, R., Wendelbo, R., Mifsud, A. and Corma, A., 1995. Diffusion of aromatic hydrocarbons in H-ZSM-5, H-Beta, and H-MCM-22 zeolites. *The Journal of Physical Chemistry* 99, 14064-14071.

Rossner, A. and Knappe, D.R.U., 2008. MTBE adsorption on alternative adsorbents and packed bed adsorber performance. *Water Research* 42, 2287-2299.



Rossner, A., Snyder, S.A. and Knappe, D.R.U., 2009. Removal of emerging contaminants of concern by alternative adsorbents. *Water Research* 43, 3787-3796.

Rouquerol, J., Rouquerol, F., Llewellyn, P., Maurin, G. and Sing, K.S., 2013. Adsorption by powders and porous solids: principles, methodology and applications, Academic Press.

Rungsirisakun, R., Nanok, T., Probst, M. and Limtrakul, J., 2006. Adsorption and diffusion of benzene in the nanoporous catalysts FAU, ZSM-5 and MCM-22: A molecular dynamics study. *Journal of Molecular Graphics and Modelling* 24, 373-382.

Ruthven, D.M., 1984. Principles of adsorption and adsorption processes, John Wiley & Sons.

Sabio, E., González, E., González, J.F., González-García, C.M., Ramiro, A. and Gañan, J., 2004. Thermal regeneration of activated carbon saturated with p-nitrophenol. *Carbon* 42, 2285-2293.

Sagehashi, M., Shiraishi, K., Fujita, H., Fujii, T. and Sakoda, A., 2005. Ozone decomposition of 2-methylisoborneol (MIB) in adsorption phase on high silica zeolites with preventing bromate formation. *Water Research* 39, 2926-2934.

Santos, L.H.M.L.M., Araújo, A.N., Fachini, A., Pena, A., Delerue-Matos, C. and Montenegro, M.C.B.S.M., 2010. Ecotoxicological aspects related to the presence of pharmaceuticals in the aquatic environment. *Journal of Hazardous Materials* 175, 45-95.

Scherdel, C., Reichenauer, G. and Wiener, M., 2010. Relationship between pore volumes and surface areas derived from the evaluation of N<sub>2</sub>-sorption data by DR-, BET- and t-plot. *Microporous and Mesoporous Materials* 132, 572-575.

Schmidt - Bäumlér, K., Heberer, T. and Stan, H.J., 1999. Occurrence and distribution of organic contaminants in the aquatic system in Berlin. Part II: substituted phenols in Berlin surface water. *Acta Hydrochimica et Hydrobiologica* 27, 143-149.

Schork, J.M. and Fair, J.R., 1988. Parametric analysis of thermal regeneration of adsorption beds. *Industrial & Engineering Chemistry Research* 27, 457-469.

Schwarzenbach, R.P., Escher, B.I., Fenner, K., Hofstetter, T.B., Johnson, C.A., Von Gunten, U. and Wehrli, B., 2006. The challenge of micropollutants in aquatic systems. *Science* 313, 1072-1077.

Shah, J.K., Marin - Rimoldi, E., Mullen, R.G., Keene, B.P., Khan, S., Paluch, A.S., Rai, N., Romanielo, L.L., Rosch, T.W. and Yoo, B., 2017. Cassandra: An open source Monte Carlo package for molecular simulation. *Journal of Computational Chemistry* 38, 1727-1739.

Shahbazi, A., Gonzalez-Olmos, R., Kopinke, F.-D., Zarabadi-Poor, P. and Georgi, A., 2014. Natural and synthetic zeolites in adsorption/oxidation processes to remove surfactant molecules from water. *Separation and Purification Technology* 127, 1-9.

Shi, Y.C., Xing, E.H., Wu, K.J., Wang, J.L., Yang, M.D. and Wu, Y.L., 2017. Recent progress on upgrading of bio-oil to hydrocarbons over metal/zeolite bifunctional catalysts. *Catalysis Science & Technology* 7, 2385-2415.

Shu, H.-T., Li, D., Scala, A.A. and Ma, Y.H., 1997. Adsorption of small organic pollutants from aqueous streams by aluminosilicate-based microporous materials. *Separation and Purification Technology* 11, 27-36.

Siegrist, H. and Joss, A., 2012. Review on the fate of organic micropollutants in wastewater treatment and water reuse with membranes. *Water Science and Technology* 66, 1369-1376.

Sillanpää, M., 2014. *Natural organic matter in water: Characterization and treatment methods*, Butterworth-Heinemann.

Simon, V., Thuret, A., Candy, L., Bassil, S., Duthen, S., Raynaud, C. and Masseron, A., 2015. Recovery of hydroxycinnamic acids from renewable resources by adsorption on zeolites. *Chemical Engineering Journal* 280, 748-754.

Sing, K.S., 1985. Reporting physisorption data for gas/solid systems with special reference to the determination of surface area and porosity (Recommendations 1984). *Pure and Applied Chemistry* 57, 603-619.

Sips, R., 1948. On the structure of a catalyst surface. *The Journal of Chemical Physics* 16, 490-495.

Snyder, S.A., Adham, S., Redding, A.M., Cannon, F.S., DeCarolis, J., Oppenheimer, J., Wert, E.C. and Yoon, Y., 2007. Role of membranes and activated carbon in the removal of endocrine disruptors and pharmaceuticals. *Desalination* 202, 156-181.

Squillace, P.J., Zogorski, J.S., Wilber, W.G. and Price, C.V., 1996. Preliminary assessment of the occurrence and possible sources of MTBE in groundwater in the United States, 1993-1994. *Environmental Science & Technology* 30, 1721-1730.

Stackelberg, P.E., Furlong, E.T., Meyer, M.T., Zaugg, S.D., Henderson, A.K. and Reissman, D.B., 2004. Persistence of pharmaceutical compounds and other organic wastewater contaminants in a conventional drinking-water-treatment plant. *Science of the Total Environment* 329, 99-113.

Stackelberg, P.E., Gibs, J., Furlong, E.T., Meyer, M.T., Zaugg, S.D. and Lippincott, R.L., 2007. Efficiency of conventional drinking-water-treatment processes in removal of pharmaceuticals and other organic compounds. *Science of the Total Environment* 377, 255-272.

Su, F., Lv, L., Hui, T.M. and Zhao, X.S., 2005. Phenol adsorption on zeolite-templated carbons with different structural and surface properties. *Carbon* 43, 1156-1164.

Suarez, S., Dodd, M.C., Omil, F. and von Gunten, U., 2007. Kinetics of triclosan oxidation by aqueous ozone and consequent loss of antibacterial activity: relevance to municipal wastewater ozonation. *Water Research* 41, 2481-2490.

Sun, J. and Wang, Y., 2014. Recent advances in catalytic conversion of ethanol to chemicals. *ACS Catalysis* 4, 1078-1090.

Sun, Z., Li, C. and Wu, D., 2010. Removal of methylene blue from aqueous solution by adsorption onto zeolite synthesized from coal fly ash and its thermal regeneration. *Journal of Chemical Technology and Biotechnology* 85, 845-850.

Suzuki, M., Mistic, D.M., Koyama, O. and Kawazoe, K., 1978. Study of thermal regeneration of spent activated carbons: Thermogravimetric measurement of various single component organics loaded on activated carbons. *Chemical Engineering Science* 33, 271-279.

Swiss Federal Council, 1998. Waters protection ordinance.

Terbouche, A., Ramdane-Terbouche, C.A., Hauchard, D. and Djebbar, S., 2011. Evaluation of adsorption capacities of humic acids extracted from Algerian soil on polyaniline for application to remove pollutants such as Cd(II), Zn(II) and Ni(II) and characterization with cavity microelectrode. *Journal of Environmental Sciences-China* 23, 1095-1103.

Thurman, E.M., 2012. Organic geochemistry of natural waters, Springer Science & Business Media.

Tipnis, P.R. and Harriott, P., 1986. Thermal regeneration of activated carbons. *Chemical Engineering Communications* 46, 11-28.

Tsai, W.T., Hsu, H.C., Su, T.Y., Lin, K.Y. and Lin, C.M., 2006. Adsorption characteristics of bisphenol-A in aqueous solutions onto hydrophobic zeolite. *Journal of Colloid and Interface Science* 299, 513-519.

Tsitsishvili, G.V., 1973. Molecular Sieves, pp. 291-298, American Chemical Society.

United States Environmental Protection Agency, 2009. National primary drinking water regulations.

Ursini, O., Lilla, E. and Montanari, R., 2006. The investigation on cationic exchange capacity of zeolites: The use as selective ion trappers in the electrokinetic soil technique. *Journal of Hazardous Materials* 137, 1079-1088.

Van Vliet, B., 1991. The regeneration of activated carbon. *Journal of the Southern African Institute of Mining and Metallurgy* 91, 159-167.

Vanraes, P., 2016. Electrical discharge as water treatment technology for micropollutant decomposition, Ghent University.

Verliefde, A.R.D., Heijman, S.G.J., Cornelissen, E.R., Amy, G., Van der Bruggen, B. and van Dijk, J.C., 2007. Influence of electrostatic interactions on the rejection with NF and assessment of the removal efficiency during NF/GAC treatment of pharmaceutically active compounds in surface water. *Water Research* 41, 3227-3240.

Vlugt, T.J. and Schenk, M., 2002. Influence of framework flexibility on the adsorption properties of hydrocarbons in the zeolite silicalite. *The Journal of Physical Chemistry B* 106, 12757-12763.

von Gunten, U., 2003a. Ozonation of drinking water: Part I. Oxidation kinetics and product formation. *Water Research* 37, 1443-1467.

von Gunten, U., 2003b. Ozonation of drinking water: Part II. Disinfection and by-product formation in presence of bromide, iodide or chlorine. *Water Research* 37, 1469-1487.

- Wajima, T., 2012. Ion exchange properties of Japanese natural zeolites in seawater. *Analytical Sciences* 29, 139-141.
- Wallwork, S., 1962. Hydrogen-bond radii. *Acta Crystallographica* 15, 758-759.
- Wang, F., Lu, X., Peng, W., Deng, Y., Zhang, T., Hu, Y. and Li, X.-y., 2017. Sorption behavior of bisphenol A and triclosan by graphene: Comparison with activated carbon. *ACS Omega* 2, 5378-5384.
- Wang, H., Yang, B. and Zhang, W.J., 2010. Photocatalytic degradation of methyl orange on Y zeolite supported TiO<sub>2</sub>, pp. 733-737, *Trans Tech Publ.*
- Wang, J., Wolf, R.M., Caldwell, J.W., Kollman, P.A. and Case, D.A., 2004. Development and testing of a general amber force field. *Journal of Computational Chemistry* 25, 1157-1174.
- Wang, S., Li, H., Xie, S., Liu, S. and Xu, L., 2006. Physical and chemical regeneration of zeolitic adsorbents for dye removal in wastewater treatment. *Chemosphere* 65, 82-87.
- Wang, S. and Peng, Y., 2010. Natural zeolites as effective adsorbents in water and wastewater treatment. *Chemical Engineering Journal* 156, 11-24.
- Waters, M.L., 2002. Aromatic interactions in model systems. *Current Opinion in Chemical Biology* 6, 736-741.
- Weitkamp, J. and Hunger, M., 2007. *Studies in Surface Science and Catalysis on Zeolites*, pp. 787-835.
- Wols, B.A. and Hofman-Caris, C.H.M., 2012. Review of photochemical reaction constants of organic micropollutants required for UV advanced oxidation processes in water. *Water Research* 46, 2815-2827.
- Worch, E., 2012. *Adsorption technology in water treatment: fundamentals, processes, and modeling*, Walter de Gruyter.
- World Health Organization, 2011. *Guidelines for drinking-water quality*.
- Wu, Q., Shi, H., Adams, C.D., Timmons, T. and Ma, Y., 2012. Oxidative removal of selected endocrine-disruptors and pharmaceuticals in drinking water treatment systems, and identification of degradation products of triclosan. *Science of The Total Environment* 439, 18-25.
- Wu, Q.H., Shi, H.L., Ma, Y.F., Adams, C., Jiang, H., Wang, J.M., Eichholz, T. and Timmons, T., 2015. Removal of N-nitrosamine precursors in drinking water system using adsorption methods. *Separation and Purification Technology* 156, 972-979.
- Xiong, R., Sandler, S.I. and Vlachos, D.G., 2011. Alcohol adsorption onto silicalite from aqueous solution. *The Journal of Physical Chemistry C* 115, 18659-18669.
- Yang, H., Hu, Y. and Cheng, H., 2016. Sorption of chlorophenols on microporous minerals: mechanism and influence of metal cations, solution pH, and humic acid. *Environmental Science and Pollution Research* 23, 19266-19280.

Ying, G.-G. and Kookana, R.S., 2007. Triclosan in wastewaters and biosolids from Australian wastewater treatment plants. *Environment International* 33, 199-205.

Yonli, A.H., Batonneau-Gener, I. and Koulidiati, J., 2012. Adsorptive removal of alpha-endosulfan from water by hydrophobic zeolites. An isothermal study. *Journal of Hazardous Materials* 203, 357-362.

Yu, J., 2007. Synthesis of zeolites. *Introduction to Zeolite Science and Practice* 168, 39.

Yu, J., Jir, C. and Corma HvBA, F.S., 2007. Synthesis of zeolites. *Introduction to Zeolite Science and Practice* 168, 39.

Zaitan, H., Manero, M.H. and Valdes, H., 2016. Application of high silica zeolite ZSM-5 in a hybrid treatment process based on sequential adsorption and ozonation for VOCs elimination. *Journal of Environmental Sciences* 41, 59-68.

Zhang, L., Peng, Y., Zhang, J., Chen, L., Meng, X. and Xiao, F.-S., 2016. Adsorptive and catalytic properties in the removal of volatile organic compounds over zeolite-based materials. *Chinese Journal of Catalysis* 37, 800-809.

Zhang, Y., Mancke, R.G., Sabelfeld, M. and Geissen, S.-U., 2014. Adsorption of trichlorophenol on zeolite and adsorbent regeneration with ozone. *Journal of Hazardous Materials* 271, 178-184.

Zhang, Z.Y., Shi, T.B., Jia, C.Z., Ji, W.J., Chen, Y. and He, M.Y., 2008. Adsorptive removal of aromatic organosulfur compounds over the modified Na-Y zeolites. *Applied Catalysis B: Environmental* 82, 1-10.

Zhao, Y.Y., Boyd, J.M., Woodbeck, M., Andrews, R.C., Qin, F., Hrudey, S.E. and Li, X.F., 2008. Formation of N-nitrosamines from eleven disinfection treatments of seven different surface waters. *Environmental Science & Technology* 42, 4857-4862.

Zhou, S., Shao, Y., Gao, N., Deng, J. and Tan, C., 2013. Equilibrium, kinetic, and thermodynamic studies on the adsorption of triclosan onto multi-walled carbon nanotubes. *Clean-Soil Air Water* 41, 539-547.

Zhu, J.H., Yan, D., Xai, J.R., Ma, L.L. and Shen, B., 2001. Attempt to adsorb N-nitrosamines in solution by use of zeolites. *Chemosphere* 44, 949-956.

Zietzschmann, F., Altmann, J., Ruhl, A.S., Dünnebier, U., Dommisch, I., Sperlich, A., Meinel, F. and Jekel, M., 2014a. Estimating organic micro-pollutant removal potential of activated carbons using UV absorption and carbon characteristics. *Water Research* 56, 48-55.

Zietzschmann, F., Worch, E., Altmann, J., Ruhl, A.S., Sperlich, A., Meinel, F. and Jekel, M., 2014b. Impact of EfOM size on competition in activated carbon adsorption of organic micro-pollutants from treated wastewater. *Water Research* 65, 297-306.

## ACKNOWLEDGEMENT

致谢

By counting from the date I arrived at Delft, 6<sup>th</sup> November 2014, five years have passed. I did enjoy my five years' stay in the Netherlands, although sometimes had to suffer from my research and own life. Now, I am at the time point to express my thanks to all of you, who have helped and supported me during my PhD life.

I would like to thank my promotor Luuk Rietveld. You always read my paper carefully and explain to me patiently. I can still remember how you comforted me when you worked on our first paper: "You will see a lot of red in your manuscript. Don't be afraid of that. It will make your paper better". But I was indeed scared after I saw corrections and comments everywhere. I have learned a lot from you during the past years. We also know each other much better than before.

I want to thank my promotor Bas Heijman. We used to have weekly meeting. Actually, I went to knock on your door several times a week. You have many good experiences in practice, while you are still open to the unknown and keep learning. I enjoyed a lot working with you.

Boss Shang, "research father" in office 4.44, my supervisor Ran, thank you so much for your support and help. You are always smart, kind and helpful. I learned to be patient from you, which is the most important lesson in my PhD life. I am sorry I could not stick to the schedule you set for me. I wish you enjoy your work and family time with Jenny and Ray in the Netherlands.

My deep gratitude to Mate, Otto and Thijs for bridging their knowledge and enriching this work with molecular simulation. Thanks to David de Ridder for supervising me for the start stage of PhD life. Frederik, thanks for your knowledge share and lessons on LC-MS. I got great inspiration from our talk and your paper. Wish you all the best in Berlin. Thanks to Rafael Gonzalez-Olmos for sharing me your knowledge on zeolites. I would like to own my thanks to my students Alex, Gerard and Marc for your hard work. Thanks to Armand, Jafar and Patricia for your support in Water Lab. I appreciate help from Mariska, Sabrina, Tamara and Jennifer. I would not focus on the research without your effort on organizing stuffs.

Thanks for my officemates: Dara, Jorge, Weigang, Yasmina, Ljiljana, Mona, Bayardo, Kajol, Jawairia, Liangfu and small & smart Zhe. I feel happy and safe working in room 4.44, my

home in the campus. Many thanks to my Chinese friends and colleagues in Delft: Gang, Xuedong, Hongxiao, Ying, Cuijie & Peng, Feifei & Xiaochen, Nan Nie, Zewei, Ka Leung, Guoshuai, Xuefeng & Ying, Hongbo, Wei, Ruxin, Haiyan, Max & Dayu, Lihua, Mingliang, Bin, Shuo and etc. With your accompany, I feel less lonely staying in the Netherlands. I also feel honour to work with many of my wonderful colleagues in Sanitary Engineering by lighting up the life of each other: Franca, Irene, Adrian, Amir, Lisa, Doris, Jan Peter, Jules and many of you.

I acknowledged the China Scholarship Council and Lamminga fund for their financial support.

感谢我的父母亲人在我成长中，特别是在我读博期间对我无条件的支持和理解，感谢好朋友贾曦，温馨，闫素的陪伴，感谢陈忠林老师和唐亚丽师母关心，感谢男朋友曾哲羿的包容和爱。

我爱你们。

姜楠 Nan Jiang

14<sup>st</sup> November, 2019

Delft





# **CURRICULUM VITAE**

**Personal information:**

Family name: Jiang 姜

Given name: Nan 楠

Date of birth: 4<sup>th</sup> May 1989

Place of birth: Suihua, Heilongjiang Province, China

Email: hitjiangnan@gmail.com

**Education and experience:**

2019 – present      Postdoctoral researcher at **Delft University of Technology**

*AdOx project: A next generation adsorption-oxidation process for removal of contaminants of emerging concern from municipal wastewater.*

2014 - 2019      Ph.D. researcher at **Delft University of Technology**

*Ph.D. thesis entitled: High-silica zeolites as novel adsorbents for the removal of organic micro-pollutants in water treatment.*

2012 – 2014      Master Municipal Engineering at **Harbin Institute of Technology**

*Master thesis entitled: Distribution of UV filters in Songhua River and their removal effects in advanced water treatment system.*

*Lab Assistant (GC-MS) at State Key Laboratory of Urban Water Resources and Environment.*

2008 – 2012      Bachelor Water Supply and Drainage Science & Engineering at **Harbin Institute of Technology**

*Bachelor thesis entitled: The design of wastewater treatment plants in Dalian based on cyclic activated sludge system (CASS) process.*

**Publication list:**

Jiang, N., Shang, R., Heijman, S.G., & Rietveld, L.C. (2018). High-silica zeolites for adsorption of organic micro-pollutants in water treatment: A review. *Water research*, 144, 145-161.

Jiang, N., Shang, R., Heijman, S. G., & Rietveld, L.C. (2020). Adsorption of triclosan, trichlorophenol and phenol by high-silica zeolites: Adsorption efficiencies and mechanisms. *Separation and Purification Technology*, 116152.

Jiang, N., Erdős, M., Moulton, O.A. \*, Shang, R., Vlugt, T.J.H., Heijman, S.G., & Rietveld, L.C. The adsorption mechanisms of organic micropollutants on high-silica zeolites causing S-shaped adsorption isotherms, submitted to *Chemical Engineering Journal*.

Jiang, N., Shang, R., Heijman, S.G., Rietveld, L.C., Adsorption of pharmaceuticals on high-silica zeolites affected by natural organic matters, in preparation.

